

THE DEVELOPMENT AND VALIDATION OF A MODEL FOR  
THE SPATIAL DISTRIBUTION OF SNOWMELT BASED ON  
TOPOGRAPHY AND POINT MELT MEASUREMENTS

by

Kevin Scott Williams

A thesis submitted in partial fulfillment  
of the requirements for the degree

of

MASTER OF SCIENCE

in

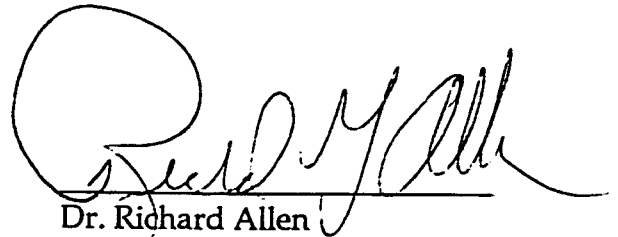
Civil and Environmental Engineering

Approved:



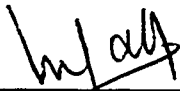
---

Dr. David Tarboton  
Major Professor



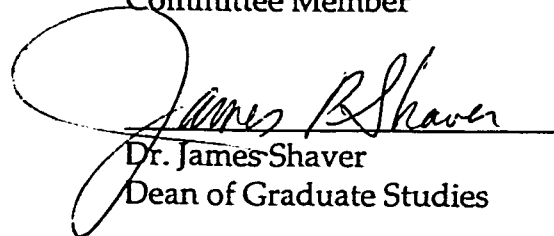
---

Dr. Richard Allen  
Committee Member



---

Dr. Upmanu Lal  
Committee Member



---

Dr. James Shaver  
Dean of Graduate Studies

UTAH STATE UNIVERSITY  
Logan, Utah

1998

## ABSTRACT

The Development and Validation of a Model for  
the Spatial Distribution of Snowmelt Based on  
Topography and Point Melt Measurements

by

Kevin Scott Williams, Master of Science

Utah State University, 1998

Major Professor: Dr. David Tarboton  
Department: Civil and Environmental Engineering

Because of the crucial role snowmelt plays in many watersheds around the world, it is important to understand and accurately quantify the melt process. As such, numerous mathematical models attempting to describe and predict snowmelt have arisen. There are two main categories of models: conceptual index models and more intricate energy balance models. The index models, like the degree-day or radiation index models, are simple and practical enough for use in large basins for operational purposes. Energy balance models, on the other hand, are generally more complicated and require large amounts of data, but they are able to represent the physics behind melt and give more accurate representations of the spatial

distribution of melt within small research basins.

The TopoFECS model (Topographically Factorized Energy Component Snowmelt model) presented here attempts to bridge the gap between these two extremes by providing a simple yet physically justifiable method that uses elevation and radiation indices together with some measurements to distribute melt over a watershed. This new model separates the energy that causes snowmelt into three components: a spatially uniform component, a component that is proportional to elevation, and one that is proportional to solar illumination (which is determined by topography). Measurements of snowmelt at several topographically unique points in a watershed allow the melt energy to be factored into its components and then adjusted to estimate the spatial distribution of melt over the whole watershed. Model results using synthetically generated data as well as real data are presented. Results from an analysis of the effects of using different time scales, spatial scales, sampling data, and weather conditions with the model are also presented. Finally, practical guidelines and recommendations for using the model are given.

(132 pages)

## ACKNOWLEDGMENTS

My deepest love and thanks go to my wife, Lesa, for her unflagging patience with me throughout my studies at USU. Lesa, you have been my life's inspiration since the day I met you. Thank you for marrying me!

My gratitude also goes to Dr. David Tarboton for the countless hours he has spent advising, encouraging, and supporting me. He has been not only an excellent thesis advisor, but a friend and a mentor as well. I will also make a special note about his patience in dealing with an arrogant master's student who thought he knew everything. Thanks for not giving up on me!

I would also like to thank Dr. Richard Allen and Dr. Upmanu Lall for their invaluable suggestions on this work. They each contributed significantly to the content of this thesis.

I am very grateful to my parents for their love and their encouragement during these last two years. If not for them, I would never have even thought about pursuing a master's degree. Thank you!

Finally, I dedicate this work to the Lord God, who gave me the opportunity, the ideas, and the endurance necessary to complete this thesis. It was He who created the complexity as well as the beautiful simplicity of snow.

*"He spreads the snow like wool, and scatters the frost like ashes." (Psalm 147:16)*

Kevin Williams

# CONTENTS

v

	Page
ABSTRACT .....	ii
ACKNOWLEDGMENTS .....	iv
LIST OF TABLES .....	vii
LIST OF FIGURES .....	ix
CHAPTER	
I.    INTRODUCTION .....	1
II.   MODEL DESCRIPTION .....	6
Intended Model Purpose .....	8
Operational Overview .....	8
III.  MODEL THEORY .....	11
IV.  MODEL TESTING .....	26
Data Used .....	26
Synthetically generated data .....	27
Upper Sheep Creek data .....	28
Smithfield Dry Canyon data .....	29
Regression Methods .....	34
Initial Model Testing .....	35
Synthetic data .....	35
Upper Sheep Creek data .....	50
Smithfield Dry Canyon data .....	58
Selection of Index Points .....	65

	vi
Location of index points .....	66
Effect of "spread" .....	68
Effect of "offset" .....	73
Comparative effect of "spread" and "offset" .....	76
Number of index points used .....	81
Effect of Weather Conditions on Model Accuracy .....	87
Effect of Spatial Scale of Application on Model Accuracy .....	89
Vertical scale .....	90
Horizontal scale .....	92
Effect of Timestep Size on Model Accuracy .....	93
V. GUIDELINES FOR USING THE TOPOFECS MODEL .....	97
VI. SUMMARY, CONCLUSIONS, AND RECOMMENDATIONS .....	100
Summary .....	100
Conclusions .....	101
Recommendations .....	102
REFERENCES .....	105
APPENDICES .....	108
Appendix A. Smithfield Dry Canyon Data .....	109
Appendix B. Upper Sheep Creek Data .....	115

## LIST OF TABLES

Table		Page
1	Statistical analysis of regressions on synthetic data for the following dates: Mar 28–30, Apr 3–5, 5–7, 7–9, 9–11, 11–13 .....	39
2	Statistical analysis of regressions on Smithfield Dry Canyon data .....	61
3	Topographic parameters for measurement sites in Smithfield Dry Canyon .....	110
4	Total height aboveground of each stake used in Smithfield Dry Canyon field study .....	111
5	Measured distance between top of stake and snow surface, and measured density at each site in Smithfield Dry Canyon, March 9, 1997 .....	112
6	Measured distance between top of stake and snow surface, and measured density at each site in Smithfield Dry Canyon, March 13, 1997 .....	113
7	Measured distance between tops of stakes and snow surface, and snow tube measurements for density calculations: Smithfield Dry Canyon, March 19, 1997 .....	114
8	Gridded values of snow water equivalence (in inches), measured at Upper Sheep Creek on March 25, 1986 .....	115
9	Gridded values of snow water equivalence (in inches), measured at Upper Sheep Creek on April 9, 1986 .....	116
10	Gridded values of melt (in inches) occurring between March 25 and April 9, 1986, calculated by subtracting SWE measured on April 9 from that measured on March 25 .....	117

11	Gridded values of snow water equivalence (in inches), measured at Upper Sheep Creek on April 30, 1993 .....	118
12	Gridded values of snow water equivalence (in inches), measured at Upper Sheep Creek on May 13, 1993 .....	119
13	Gridded values of melt (in inches) occurring between April 30 and May 13, 1993, calculated by subtracting SWE measured on April 30 from that measured on May 13 .....	120



## LIST OF FIGURES

Figure		Page
1	Operational flowchart for TopoFECS model .....	9
2	Map of Upper Sheep Creek watershed .....	30
3	Map of Smithfield Dry Canyon data collection sites .....	31
4	Smithfield Dry Canyon data: initial calculated densities .....	33
5	Smithfield Dry Canyon data: adjusted densities .....	33
6	Melt simulated by the Utah Energy Balance model vs. TopoFECS estimates .....	38
7	Plot of residuals (UEB simulations minus TopoFECS estimates) vs. UEB-simulated melt .....	43
8	Plot of residuals (UEB simulations minus TopoFECS estimates) vs. cumulative radiation: synthetic data .....	44
9	Plot of residuals (UEB simulations minus TopoFECS estimates) vs. elevation: synthetic data .....	46
10	Accumulation/ablation estimates at 8 random points: synthetically generated data .....	48
11	TopoFECS melt estimates vs. UEB-simulated melt with air temperature adjusted proportionally with incoming radiation .....	49
12	TopoFECS melt estimates vs. measured melt at Upper Sheep Creek .....	51
13	Observed melt versus incoming radiation: Upper Sheep Creek data .....	54

		x
14	Measured and modeled snow water equivalence at Upper Sheep Creek, 1986 .....	56
15	Measured and modeled snow water equivalence at Upper Sheep Creek, 1993 .....	57
16	Plot of measured melt vs. TopoFECs estimates: Smithfield Dry Canyon .....	59
17	Plot of residuals (measured melt minus TopoFECs estimates) vs. measured melt: Smithfield Dry Canyon .....	62
18	Plot of residuals (measured melt minus TopoFECs estimates) vs. cumulative radiation, Smithfield Dry Canyon data .....	63
19	Plot of residuals (measured melt minus TopoFECs estimates) vs. elevation, Smithfield Dry Canyon data .....	64
20	Median absolute modeling error vs. spread of three (3) index points: synthetic data .....	69
21	Median absolute modeling error vs. spread of five (5) index points: synthetic data .....	71
22	Median absolute modeling error vs. spread of five (5) index points: Smithfield Dry Canyon data .....	72
23	Mean absolute modeling error vs. offset of center of three (3) index points from center of data points: synthetic data .....	74
24	Mean absolute modeling error vs. offset of center of five (5) index points from center of data points: synthetic data .....	75
25	Mean absolute modeling error vs. offset of center of index points from center of data points: Smithfield Dry Canyon data .....	77

26	Loess-smoothed surface of median absolute modeling error vs. standardized spread of three (3) index points and standardized offset of index points from center of data points: synthetic data .....	78
27	Loess-smoothed surface of median absolute modeling error vs. standardized spread of five (5) index points and standardized offset of index points from center of data points: synthetic data .....	79
28	Loess-smoothed surface of median absolute modeling error vs. standardized spread of five (5) index points and standardized offset of index points from center of data points: Smithfield Dry Canyon data .....	80
29	Median absolute modeling error vs. number of index points used: Smithfield Dry Canyon data .....	82
30	Mean absolute modeling error vs. number of index points used: Smithfield Dry Canyon data .....	84
31	Mean absolute modeling error vs. number of index points used: synthetic data .....	86
32	Effect of cloud cover on model accuracy: synthetic data .....	88
33	Effect of subdividing basin into multiple elevation zones .....	91
34	Sensitivity of model accuracy to timestep size .....	94
35	Evolution of $\alpha(t)$ , $\beta(t)$ , and $\gamma(t)$ parameters with time: synthetic data .....	96

## CHAPTER I

### INTRODUCTION

Snow plays a crucial role in the hydrology of the United States as well as in many other parts of the world. In the western United States, approximately 75% of the total water budget comes from snowmelt (McManamon, Day, and Carroll, 1993), and many regions of the world rely even more heavily on snowmelt for their annual water supply. As such, snow science has been an active field of research since the turn of the century, with attention focused primarily on the practical considerations of snow as a water resource and as an avalanche danger (Colbeck, 1987). In the more recent part of the century, computers have been employed to model the complex physical processes that occur in snow and to make usable estimations concerning the state of the snowpack.

Of particular interest to hydrologists is the timing and magnitude of melt water fluxes from snow. To this end, numerous models have been suggested and implemented, ranging from simple temperature index melt models to detailed, physically based models that attempt to accurately represent all of the physical dynamics of snow accumulation, metamorphism, and melt.

In actual engineering practice, the simpler index models are generally chosen for most jobs. These models have very simple data requirements

(usually just a temperature reading, or perhaps measurements of net radiation), and are straightforward to implement. They produce somewhat reasonable results when well calibrated against prior data for a particular basin, and they are very computationally efficient. One such model, the Snowmelt Runoff Model, or SRM (Martinec, Rango, and Roberts 1994), has seen a lot of use in practical real-time snowmelt predictions. Though the model is a simple degree-day model, it has met with large success primarily due to its inclusion of real-time knowledge of the snowpack, e.g., snow-covered area (Rango and van Katwijk, 1990).

Others have tried to incorporate the significant effect of solar radiation along with air temperature index models to produce more physically realistic results. Several scientists, including Riley, Chadwick, and Bagley (1966), Cazorzi and Dalla-Fontana (1996), and Brubaker, Rango, and Kustas (1996), have presented melt models that combine air temperature with a radiation index. These models seem to provide an improvement in the spatial distribution of melt estimates over simple temperature-index methods, but they are more difficult to implement because of the need for an additional measurement of solar radiation.

These simpler index models for snowmelt are very practical for general applications where the user merely needs to know the quantity of runoff expected to appear in the river below. However, they lack sufficient

physical basis for many purposes. For instance, a simple lumped index model can give spurious predictions for runoff when the basin is subjected to climatic conditions that are outside of what the model was calibrated for (Martinec and Rango, 1986). Since index models generally do not consider the spatial patterns of melt, they cannot give reasonable inputs to other spatially explicit models to solve more complicated problems such as modeling contaminant transport, deciding the effects of land use change, modeling erosion, and determining the effects of climate alteration.

For these more complicated tasks, numerous detailed energy-balance models have been developed (Anderson, 1976; Flerchinger, 1987; Jordan, 1991; Tarboton, 1994; Tarboton, Chowdhury, and Jackson, 1995; Tarboton and Luce, 1996). These physically based models generally do a much better job of estimating melt at a point than do simpler index models. These models can also be used to simulate melt at a larger scale by dividing the area to be modeled into smaller hydrologic units and running the model again at each different unit. This provides a relatively good spatial representation of melt. However, a drawback to this type of model is that it is generally very data-intensive, requiring either much meteorological instrumentation at the point to be modeled, or interpolation and extrapolation from nearby measurement sites, introducing further uncertainty. These models also generally employ many different parameters

that need calibration and may even vary throughout the melt season.

Finally, these models can be very computationally intensive, and to model anything but a small watershed would require large amounts of computer time.

The developers of the SRM model point to the need for a compromise between the two kinds of snow models (Brubaker, Rango, and Kustas, 1996) – a new model that would be both parsimonious enough to use in practical applications for melt estimations over large areas, as well as rigorous enough to capture the fundamental physics of melt and provide spatially explicit estimations. To this end, they have recently attempted to improve their estimations by including a more physically realistic radiation component to their model (Kustas and Rango, 1994). Their new restricted degree-day model has been shown to have some benefits, but in a test using 6 years of snowmelt runoff data, it improved predictions over their old model in only 2 out of the 6 years.

The goal of this thesis was to develop a methodology for the estimation of spatially distributed snowmelt based on point measurements and topography. This was motivated by the need for a compromise between the rigorous energy-balance snow models and the less data-demanding index models (as pointed out by Kustas and Rango, 1994). The TopoFECS model (Topographically Factorized Energy Component Snowmelt model)

was the result of this work. The remainder of this thesis describes the development and testing of the TopoFECS model, which is a new method for estimating the spatial distribution of snowmelt based on point measurements and topography.

Chapter II gives a brief description of the TopoFECS model and how it could be used in a practical setting to predict snowmelt. Chapter III gives the theoretical background and derivation of the TopoFECS model. Chapter IV shows the results of using the TopoFECS model to simulate both field data and synthetically generated snowmelt data. The sensitivity of the model to weather conditions, time step size, measurement points, spatial scale, and sampling frequency are also explored in this chapter. Chapter V gives practical guidelines for using the TopoFECS model, based on the results shown in the previous chapter. Chapter VI summarizes the work, and offers conclusions as well as recommendations for future work.



## CHAPTER II

### MODEL DESCRIPTION

The TopoFECS model is based on the fact that snowmelt is an energy-driven process and that the energy available for melt is primarily dependent upon solar radiation and air temperature, which are both functionally related to topography. Solar radiation is a function of slope, aspect, and shading, while air temperature is commonly considered to be a function of elevation (Dingman, 1994). The assumption is therefore made that the spatial distribution of energy can be partitioned into components that depend on a radiation factor and an elevation factor, as well as a spatially constant factor that captures the larger scale (synoptic) weather processes that drive snowmelt, but can be considered to be constant over a region. The TopoFECS model can be stated mathematically as follows:

$$\Delta h_{mi} = \max[(\alpha(t) + \beta(t) \cdot \text{elev}_i + \text{rad}_i \cdot \gamma(t)), 0] \quad (1)$$

where  $\Delta h_{mi}$  is the depth of melt that occurs over the time step at location  $i$  expressed in snow water equivalent;  $\text{rad}_i$  is the direct, exoatmospheric radiation at  $i$ , accounting for topography (slope and aspect) and integrated over the timestep; and  $\text{elev}_i$  is the elevation of location  $i$ . The terms  $\alpha(t)$ ,  $\beta(t)$ , and  $\gamma(t)$  represent a time-dependent factorization of the melt-producing

energy during the time step.  $\alpha(t)$  is a topographically independent component quantifying the base melt rate in the watershed caused by the weather conditions during the current timestep,  $\beta(t)$  is an elevation-dependent component quantifying the effect of elevation upon melt, and  $\gamma(t)$  is a radiation-dependent component describing the transmissivity of the atmosphere to incoming solar radiation as well as the albedo of the snow. These energy factors,  $\alpha(t)$ ,  $\beta(t)$ , and  $\gamma(t)$ , are assumed spatially constant throughout the whole watershed for each time step, but they do change from one time step to the next, depending on the melt-producing effect of each of the energy terms integrated over the time step.

Ignoring the maximum operator in Equation 1 gives a linear equation with three unknown variables at each time step:  $\alpha(t)$ ,  $\beta(t)$ , and  $\gamma(t)$ . The terms  $elev_i$  and  $rad_i$  can be easily determined for every point in the watershed. Therefore, given sufficient melt observations at topographically unique points in the watershed, regression can be used to estimate effective values for  $\alpha(t)$ ,  $\beta(t)$ , and  $\gamma(t)$ . If the maximum operator is included in Equation 1, one can solve for the  $\alpha(t)$ ,  $\beta(t)$ , and  $\gamma(t)$  parameters by minimizing the error when fitting the equation to the observations. Once these three variables are established for the given time step, the melt that occurs at every point in the entire basin can be quickly calculated through Equation 1.

### Intended Model Purpose

It is worth noting here that the TopoFECS model relies on a simplification of the snowmelt energy balance that results in an interpolative approach to obtaining distributed estimates of melt. The model is shown in this thesis to be a valuable, practical method for estimating melt, but it cannot perform all of the functions that a full energy balance model can. For instance, the TopoFECS model cannot employ weather data or weather predictions in its calculations. It cannot explore the fundamental physics of snowmelt either; for these applications a full energy balance melt model is required.

### Operational Overview

Figure 1 shows a flowchart for the TopoFECS model. The model requires a digital elevation model (DEM) of the watershed as shown in the upper-left corner of the flowchart. From this DEM, elevations, slopes, and aspects are calculated for each grid cell in the watershed. The slopes and aspects are used to calculate the amount of exoatmospheric radiation that each point in the watershed receives during a given time step.

Next, Figure 1 shows that the TopoFECS model requires measurements of melt at a number of topographically unique locations

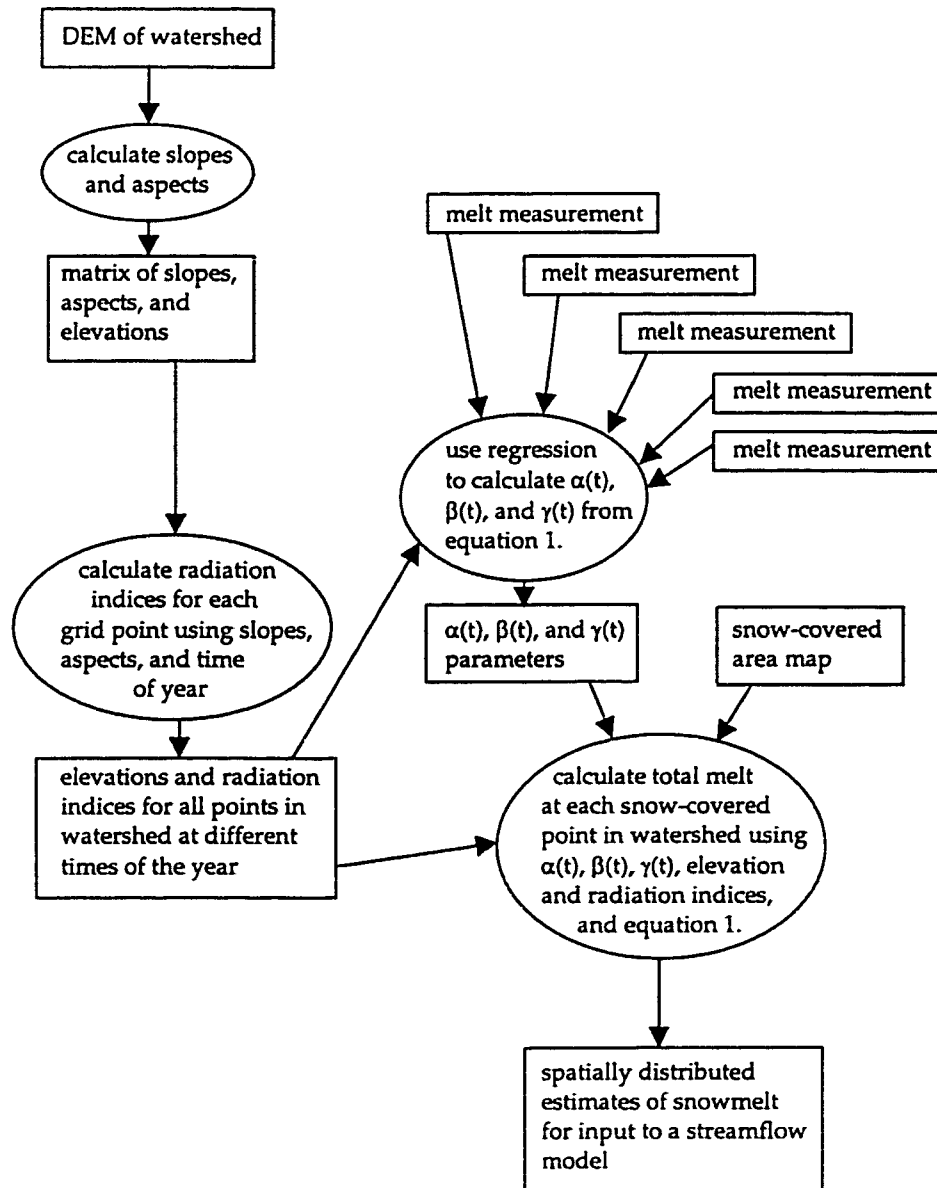


Figure 1. Operational flowchart for TopoFECS model.

throughout the watershed. These measurement sites are referred to as “index points” through the remainder of this thesis. A sufficient number of melt measurements must be collected within the watershed to obtain a sound calibration of Equation 1 at each time step. The melt at these index points would ideally be measured with automated melt collectors, and the data relayed back to a central processing station in real time. Once the central processing station has received the values for total melt occurring at each of the sampling locations over a specified time period, the model is implemented to calculate the values of  $\alpha(t)$ ,  $\beta(t)$ , and  $\gamma(t)$  for that time period. Then, using the elevations from the DEM and the calculated radiation indices, the melt is estimated from Equation 1 for all unmeasured points in the watershed that are still covered with snow, as indicated by the current map of snow-covered area.

Finally, Figure 1 shows that these estimates of melt may be used as inputs to a flow-routing module, which is used to generate a prediction for streamflow. This is the usually the quantity of interest.

## CHAPTER III

### MODEL THEORY

This section shows how to obtain Equation 1 from the physical energy balance equations relating driving meteorological variables to snowmelt. The basic theory behind all of the physically based point snowmelt models lies in balancing the energy budget for the snowpack and converting the excess energy into snowpack temperature change, metamorphism, or melt. The melt period of a seasonal snowpack begins when the net energy input starts to have a positive trend. This period can be separated into the warming phase, the ripening phase, and the output phase (Dingman, 1994).

During the warming phase, the net energy input raises the temperature of the snowpack until the whole pack reaches the melting point, as such:

$$\Delta Q = c_i \rho_w h_m \Delta T_{avg} \quad (2)$$

where  $\Delta Q$  is the total positive energy input to the snowpack during a given time interval ( $\text{J}\cdot\text{cm}^{-2}$ ),  $c_i$  is the heat capacity of ice ( $2.102 \text{ J}\cdot\text{g}^{-1}\text{C}^{-1}$ ),  $\rho_w$  is the density of water ( $1 \text{ g}\cdot\text{cm}^{-3}$ ),  $h_m$  is the depth of water equivalent of the snowpack (cm), and  $\Delta T_{avg}$  is the average change in temperature of the snowpack.

During the ripening phase and the output phase, the snowpack remains isothermal at the melting point, but the additional energy input causes some of the snow to change phase from ice to water according to the following equation:

$$\Delta Q = \lambda_i \rho_w \Delta h_m \quad (3)$$

where  $\lambda_i$  is the heat of fusion of ice at 0°C (333.7 J·g<sup>-1</sup>) and  $\Delta h_m$  is the depth of snow in water equivalence that is converted to water (cm). During the ripening phase, the liquid water is retained in the snowpack by surface-tension forces until the snow reaches its liquid holding capacity. After this, the output phase begins and melt water flows out of the snowpack. Consequently, during the output phase (which is the phase of concern for this model) the energy input is directly proportional to the amount of melt outflow.

The energy balance equation relating the meteorological driving forces to snowmelt is:

$$\Delta Q = Q_{sn} + Q_{in} + Q_p + Q_g + Q_h + Q_e \quad (4)$$

where  $Q_{sn}$  is the net shortwave energy received by the snowpack,  $Q_{in}$  is the net longwave radiation into the snow,  $Q_p$  is the energy advected by precipitation into the snow,  $Q_g$  is the ground heat flux to the snow,  $Q_h$  is the

sensible heat flux to the snow, and  $Q_L$  is the latent heat flux into the snow (Dingman, 1994).

Physically based melt models usually require measurements of driving weather variables such as air temperature, solar radiation, wind speed, etc. These variables are used as inputs for various equations to determine the quantities of the different components of the energy balance, and the sum of these energy components is used to estimate the melt occurring in a snowpack. These models have met with varying degrees of success in estimating the actual process of snowmelt. One obstacle to this method of physically modeling snowmelt is the difficulty of accurately measuring these driving variables and then appropriately using them to calculate each of the terms in the energy balance (Equation 4).

The TopoFECS model differs from most other melt models in that it uses direct, real-time measurements of melt to drive the model, rather than relying on measurements of the driving weather variables and trying to relate these back to melt rates. As such, it uses several spatially distributed measurements of actual snow melt to effectively back-calculate the driving energy terms. These inferred energy inputs are representative of how the weather in the watershed has actually affected snowmelt. These calculated energy components are then used to calculate the melt for the rest of the watershed.



The theoretical justification for this model (Equation 1) lies in recognizing melt as a linear function of available energy, and then approximating each of the components of the energy balance equation (Equation 4) as linear functions of elevation and potential solar illumination. In order to derive Equation 1, all of the energy fluxes must be expressed as linear functions of solar illumination and air temperature (and thus elevation, assuming that temperature varies linearly with elevation).

Net solar radiation at any point,  $i$ , is comprised of diffuse and direct components with the direct component related to illumination angle (the angle of the sun from the perpendicular to the land surface) as follows:

$$Q_{sni} = Q_{sndif} + \int_{\Delta t} I_o \cdot \tau \cdot (1-A) \cdot \cos(\psi) \cdot dt$$

where  $Q_{sni}$  is the net shortwave radiation received at point  $i$  over the interval  $\Delta t$ ,  $Q_{sndif}$  is the net diffuse shortwave radiation received during the timestep,  $I_o$  is the exoatmospheric solar radiation constant,  $\tau$  is the atmospheric transmissivity to direct beam radiation,  $A$  is the albedo, and  $\psi$  is the illumination angle. Now, neglecting the fact that  $A$  changes slowly with time as the surface ice crystals grow, and  $\tau$  changes with weather and sun angle,  $A$  and  $\tau$  are taken out of the integral, and the integral of  $I_o \cdot \cos(\psi)$  at location  $i$  is expressed as  $rad_i$  as such:

$$\text{rad}_i = \int_{\Delta t} I_o \cdot \cos(\psi) \cdot dt$$

Assuming that the atmospheric transmissivity,  $\tau$ , and the albedo of the snow surface,  $A$ , are unknown but spatially uniform throughout the watershed (justification for and implications of this assumption are discussed at the end of this section), the above equation for net solar radiation can be written as:

$$Q_{\text{net}} = \text{rad}_i \cdot \gamma(t) + Q_{\text{snow}} \quad (5)$$

where  $\tau$  and  $(1-A)$  are combined into the factor  $\gamma(t)$ . Dingman (1994) gives a formula for the calculation of  $\text{rad}_i$  for a given slope, aspect, and latitude at a daily time step. Dozier and Frew (1990) have presented TOPORAD, a model that can rapidly compute  $\text{rad}_i$  using digital elevation data incorporating the effects of terrain shading in its calculations. In subsequent field testing of the TopoFECS model, only local slope and aspect data was available, so the effects of terrain shading were ignored.

Net longwave radiation can be expressed as:

$$Q_{\text{lw}} = \epsilon_a \sigma \cdot T_a^4 - \epsilon_{\text{ss}} \sigma T_s^4$$

where  $\epsilon_a$  is the effective emissivity of the atmosphere,  $\sigma$  is the Stefan-Boltzmann constant,  $T_a$  is the air temperature in the basin for the given time period,  $\epsilon_{\text{ss}}$  is the emissivity of the snow surface, and  $T_s$  is the temperature of

the snow surface (all temperatures here are relative to absolute zero). Since it is desirable to write the energy fluxes as linear functions of air temperature, the above equation is approximated as a truncation of a first-order Taylor series expansion about  $Ta_{ref}$ , a constant reference temperature as follows:

$$Q_{lw} \cong \epsilon_s \sigma \cdot Ta_{ref}^4 - \epsilon_{ss} \sigma Ts^4 + 4\epsilon_s \sigma \cdot Ta_{ref}^3 \cdot (Ta - Ta_{ref})$$

Assuming that  $\epsilon_s$ ,  $\epsilon_{ss}$ , and  $Ts$  are uniform throughout the basin (again, the impacts of these assumptions are discussed at the end of this section), the terms in the last equation can be condensed to the following linear function of air temperature:

$$Q_{in} = A_{in} + B_{in} \cdot Ta \quad (6)$$

Under conditions of neutral buoyancy, turbulent mass transfer theory (Dingman, 1994) gives the sensible heat flux,  $Q_h$ , as:

$$Q_h = \frac{k^2 V}{\left( \ln \frac{z}{z_0} \right)^2} \rho_a C_p \cdot (Ta - Ts)$$

where  $k$  is the von-Karman constant,  $V$  represents the wind speed,  $z$  is the height at which the wind speed is measured,  $z_0$  denotes the effective aerodynamic roughness of the snow surface,  $\rho_a$  is the density of the air, and

$C_p$  represents the specific heat capacity of air. Thus, sensible heat flux is already a linear function of air temperature, and the above equation can be simplified to:

$$Q_h = A_h + B_h \cdot T_a \quad (7)$$

This simplification has lumped all of the variability in quantities such as wind speed ( $V$ ), roughness height ( $z_o$ ), air density ( $\rho_a$ ), and the surface temperature ( $T_s$ ) into the parameters  $A_h$  and  $B_h$ , neglecting their spatial variability. Of these, the spatial variability in wind speed is perhaps the most serious; however, it is difficult to quantify this variability in a simple way. The air density also changes significantly through space, since it is related to elevation. The impact on the model results caused by the spatial variability of these parameters is discussed at the end of this section.

Turbulent mass transfer theory (Dingman, 1994) gives the latent heat flux to the surface,  $Q_e$ , as:

$$Q_e = \frac{k^2 V}{\left(\ln \frac{z}{z_o}\right)^2} \frac{h_v 0.622}{R_d T_a} (e_a - e_s)$$

where  $h_v$  equals the latent heat of vaporization for water,  $R_d$  is the dry gas constant, and  $e_a$  and  $e_s$  are the vapor pressures of the air and surface,

respectively. These are related to temperature, relative humidity, RH, and the saturation vapor pressure versus temperature function  $e_{sat}(T)$  by:

$$e_a = e_{sat}(T_a) \cdot RH$$

$$e_s = e_{sat}(T_s)$$

Lowe (1977) provides accurate polynomial expressions for  $e_{sat}(T)$ .

Again, taking a first-order truncation of the Taylor's series expansion of this equation about a reference temperature,  $T_{a,ref}$  gives the following expression:

$$Q_e \cong \frac{k^2 V}{\left(\ln \frac{z}{z_o}\right)^2} \frac{h \cdot 0.622}{R_d T_{a,ref}} [RH \cdot e_{sat}(T_{a,ref}) - e_{sat}(T_s)] +$$

$$\frac{k^2 V}{\left(\ln \frac{z}{z_o}\right)^2} \frac{h \cdot 0.622}{R_d} \left( \frac{RH \cdot \Delta}{T_{a,ref}} - \frac{RH \cdot e_{sat}(T_{a,ref})}{T_{a,ref}^2} + \frac{e_s(T_s)}{T_{a,ref}^2} \right) (T_a - T_{a,ref})$$

where  $\Delta$  represents the derivative of  $e_{sat}$  with respect to air temperature evaluated at  $T_{a,ref}$ .

Assuming that  $V$ ,  $z_o$  and  $RH$  are uniform throughout the watershed for a given time period ( $RH$  will change with elevation, but again this is rationalized at the end of this section), the terms in the above equation can be condensed to the following:

$$Q_e = A_e + B_e \cdot Ta \quad (8)$$

Equations 4-8 can now be combined to write the following equation:

$$\begin{aligned} \Delta Q = \text{rad}_i \cdot \gamma(t) + Q_{\text{sdif}} + A_{\text{in}} + B_{\text{in}} \cdot Ta + \\ Q_p + Q_g + A_h + B_h \cdot Ta + A_e + B_e \cdot Ta \end{aligned} \quad (9)$$

Though the terms  $\gamma(t)$ ,  $Q_{\text{sdif}}$ ,  $A_{\text{in}}$ ,  $B_{\text{in}}$ ,  $Q_p$ ,  $Q_g$ ,  $A_h$ ,  $B_h$ ,  $A_e$ , and  $B_e$  may vary with time, they are (by approximation) spatially constant throughout the watershed. By condensing these terms into single constants (A and B), the above equation can be simplified to:

$$\Delta Q = \text{rad}_i \cdot \gamma(t) + A + B \cdot Ta \quad (10)$$

Next,  $Ta$  is assumed to vary linearly with elevation according to an unknown lapse rate as such:

$$Ta = a \cdot \text{elev}_i + b \quad (11)$$

Combining Equations 3, 10, and 11 gives:

$$\lambda_i \rho_w \Delta h_m = \text{rad}_i \cdot \gamma(t) + A + B[a \cdot \text{elev}_i + b] \quad (12)$$

Finally, condensing the constants in the above equation gives an expression for  $\Delta h_m$ , which is the depth of snowmelt in water equivalent:

$$\Delta h_m = \text{rad} \cdot \gamma(t) + \alpha(t) + \beta(t) \cdot \text{elev} \quad (13)$$

Equation 13 assumes a ripe snowpack (Equation 3), and as such is only valid for positive net energy contributions, i.e.,  $\Delta h_m > 0$ . Therefore, adding this necessary condition that  $\Delta h_m$  is the greatest of either the energy input or 0 (since negative energy does not result in negative melt) results in Equation 1:

$$\Delta h_{m_i} = \max[(\alpha(t) + \beta(t) \cdot \text{elev}_i + \text{rad}_i \cdot \gamma(t)), 0]$$

where the subscript “i” denotes the the form of the equation at location i.

Here  $\alpha(t)$  is an unknown energy input factor that is a function of time and is representative of the base energy input to the watershed, equal to the following:

$$\alpha(t) = (A+B \cdot b) / \rho_w \lambda_f$$

$\beta(t)$  is another unknown energy input factor that varies with time and represents the effect of elevation (or air temperature) upon snowmelt. It is equal to:

$$\beta(t) = B \cdot a / \rho_w \lambda_f$$

Finally,  $\gamma(t)$  is a time-dependent factor that takes the net incoming direct

shortwave radiation into account and is explained above. These three energy input factors vary with time, but at the end of each time step, they are assumed to be the same for every point in the whole watershed.

Because of the maximum operator, Equation 1 is a nonlinear equation with three unknown variables,  $\alpha(t)$ ,  $\beta(t)$ , and  $\gamma(t)$ . The terms  $\text{rad}_i$  and  $\text{elev}_i$  are known quantities for each point in the watershed. Therefore, given melt observations at several points in the watershed (index points), one can fit the equation to the data by minimizing either the sum of absolute errors or the sum of squared errors, and obtain unique values for the parameters  $\alpha(t)$ ,  $\beta(t)$ , and  $\gamma(t)$ . Once these three variables are established, the melt that occurs at every point in the entire basin can be quickly calculated through Equation 1. This procedure can be used at every timestep for which there are new measurements of melt to determine the amount of melt that occurred throughout the basin during that timestep.

It is interesting to note that the three terms in Equation 1 primarily describe the effects of the terrain on net radiation and turbulent transfer. Consistently in the literature, these two energy sources have been shown to dominate the snowmelt process, to the point where the other terms are usually negligible. Cline (1997) described a thorough experiment in the mountains of Colorado that quantified all of the terms of the energy balance during two melt seasons. He found that net radiation and turbulent fluxes



were of the greatest importance, but that their relative contributions to the overall energy balance varied from year to year. Kuusisto (1986) reviewed over 20 studies of snowmelt energy balances and came to the similar conclusion that net radiation and turbulent fluxes were the dominant energy components driving snowmelt.

Equation 1 clearly models only melt, not the spatial distribution of snow water equivalence. With the restriction that  $\Delta h_m > 0$ , Equation 1 is incapable of modeling the accumulation of snow. However, if desired, the TopoFECS model can be altered to keep track of the amount of water equivalence in the snowpack. In this case, the snow water equivalence needs to be maintained for each point as a state variable. The formula governing the change in snow water equivalence at each point  $i$  is:

$$\Delta w_i = \text{precip}_i - \text{melt}_i \quad (14)$$

Assuming that precipitation is approximately linearly related to elevation (Dingman, Seely-Reynolds, and Reynolds, 1988), we can write the following equation:

$$\text{precip}_i = \varphi(t) \cdot \text{elev}_i + \kappa(t) \quad (15)$$

where  $\varphi(t)$  is the unknown lapse rate for precipitation and  $\kappa(t)$  is the unknown base snowfall rate for the basin during the given time period.

Computing melt, as  $\max[(\alpha(t) + \beta(t) \cdot \text{elev}_i + \text{rad}_i \cdot \gamma(t)), 0]$ , as given in Equation 1, results in the following expression for snow water equivalence:

$$\Delta w_i = \varphi(t) \cdot \text{elev}_i + \kappa(t) - \max[(\alpha(t) + \beta(t) \cdot \text{elev}_i + \text{rad}_i \cdot \gamma(t)), 0] \quad (16)$$

This equation assumes that the advected energy from the precipitation has a negligible effect on the energy balance of the snowpack. This is a reasonable assumption in most circumstances. In his review of over 20 snowmelt energy balance studies, Kuusisto (1986) found that on average, energy advected from precipitation accounts for less than 1% of the energy budget.

If snow does indeed fall during a time step, the above equation can be simplified by dropping the maximum operator requiring that melt be greater than zero and combining the similar terms to give:

$$\Delta w_i = \alpha_{\text{swe}}(t) + \beta_{\text{swe}}(t) \cdot \text{elev}_i + \text{rad}_i \cdot \gamma(t) \quad (17)$$

where

$$\alpha_{\text{swe}}(t) = -\alpha(t) + \kappa(t)$$

$$\beta_{\text{swe}}(t) = -\beta(t) + \varphi(t)$$

$$\gamma_{\text{swe}}(t) = -\gamma(t)$$

The TopoFECS model for snow water equivalence can now be stated as follows:

If there is no precipitation

$$\text{during a timestep: } \Delta w_i = \max[(\alpha_{swe}(t) + \beta_{swe}(t) \cdot \text{elev}_i + \text{rad}_i \cdot \gamma(t)), 0]$$

If there is precipitation

$$\text{during a timestep: } \Delta w_i = \alpha_{swe}(t) + \beta_{swe}(t) \cdot \text{elev}_i + \text{rad}_i \cdot \gamma(t) \quad (18)$$

The first part of Equation 18 is simply Equation 1, while the second part of Equation 18 is a linear equation whose unknown variables can be solved for using simple linear regression. Therefore, given several measurements of the change in water equivalence at different points in the snowpack, one can use Equation 18 to model the snow water equivalence just as one would use Equation 1 to model melt.

Finally, let us examine some of the original assumptions more carefully. In the derivation of Equation 1 and subsequently Equation 18, the atmospheric transmissivity ( $\tau$ ), albedo of the snow surface ( $A$ ), snow surface temperature ( $T_s$ ), relative humidity (RH), air density ( $\rho_a$ ), and wind speed ( $V$ ) were all assumed to be spatially invariant across the watershed. The air density, atmospheric transmissivity, and the relative humidity will change across the watershed, but the gradients will probably be very strongly correlated with elevation. Therefore, the choice of elevation as a parameter

in the model will incorporate most of these effects, though only in a linearized fashion. The albedo of the snow surface and the surface temperature will most likely vary in space; however, these parameters are intimately related to the energy that the snowpack has received, which is primarily determined by the amount of radiation received and the turbulent heat exchange that has occurred over the snowpack. Therefore, the model's dependence on elevation and radiation will incorporate the effects of changing albedo and surface temperature, though again, only in a linearized fashion. Finally, though these assumptions are not completely justified in a rigorous, theoretical sense, they are all justified as pragmatic and expedient in terms of the quality of the resulting approximations, as demonstrated in the next chapter.

## CHAPTER IV

### MODEL TESTING

This chapter provides an analysis of the performance of the TopoFECS model using both synthetically generated data as well as field data. The model is shown to be capable of producing reasonably accurate distributed estimates of snowmelt. The effect of selecting different numbers of index points and different locations for those index points is investigated. The model's performance under both clear sky and cloudy conditions is analyzed. Finally, the appropriate spatial and temporal scales for applying the TopoFECS model are examined.

#### Data Used

Three data sets were used in this study. The first data set was synthetically generated by another snowmelt model and represents perfectly measured melt data. However, the model that generated the data represents a limited understanding of the physics of snowmelt, and therefore may not be completely accurate. The second set of data consists of distributed field measurements of snow water equivalence taken from the Upper Sheep Creek watershed in the Reynolds Creek Experimental Watershed. Because of the gridded nature of the data in Upper Sheep, it facilitates a visual analysis of the spatial melt patterns, something not available in the other data sets. The

last set of data comes from field measurements taken in Smithfield Dry Canyon in the spring of 1997. Each of these data sets is described in more detail in the following sections.

### Synthetically generated data

Because of limited field data, much of this research was performed on data that were synthetically generated by the Utah Energy Balance (UEB) model (Tarboton and Luce, 1996). The UEB model is a physically based energy balance model that represents the snowpack in terms of two state variables, water equivalence and energy content. A third state variable is used to quantify the snow surface age, which is used for albedo calculations. The use of only three state variables makes the model less complicated than typical energy balance melt models and therefore suitable for generating many simulations of melt at different points. The model uses a parameterization of surface heat flux into the snow based on the difference between the snow surface and average snowpack temperatures to balance external energy fluxes at the snow surface and to calculate snow surface temperature without introducing additional state variables.

In order to generate a full set of snowmelt data with which to test the TopoFECS model, a hypothetical terrain was simulated. This was accomplished by assigning randomly generated slopes, aspects, and elevations to each of the points in the hypothetical watershed. Next, the UEB

model was used with weather data recorded at the Central Sierra Snow Laboratory during the winter of 1986–1987 to calculate snow accumulation and melt at each of the hypothetical points. The incoming exoatmospheric radiation at each point was modified to account for slope and aspect, while the air temperature for each point was adjusted according to a lapse rate of 1° C for every 150 meters that the point was above the datum (Dingman, 1994). In this manner, a time series of snow water equivalence and snowmelt was generated for every point in the hypothetical watershed. This melt data could then be used to test the predictive ability of the TopoFECS model.

#### Upper Sheep Creek data

The Agricultural Research Service has collected many years' worth of snow survey data at Upper Sheep Creek Watershed, located in the Reynolds Creek Experimental Watershed, near Boise, Idaho. The Upper Sheep Creek Watershed is a small 26-ha basin varying in elevation from 1840–2036 m. It is marked off in a 100-foot (~30 meter) grid and the water equivalent at each point is periodically measured with a snow tube during the spring of each year. The melt that occurs between measurements can be calculated by subtracting the previous water equivalent from the subsequent measurement of snow water equivalent and adding any new snowfall. This provides a rare data set of spatially distributed melt measurements on rugged terrain. Data from two snow years, 1986–87 and 1993–94, were available for analysis.

Figure 2 shows the location of the Upper Sheep Creek watershed as well as a contour map of the basin.

#### Smithfield Dry Canyon data

During the 1997 melt season, melt measurements were collected at 31 locations in Smithfield Dry Canyon at approximately 5-day intervals. These locations were distributed over a range of 1200 feet (366 meters) in elevation, varied in slope from 0–38 degrees, and faced a variety of different directions. The topographical data for each of these sites are given in Appendix A, and a topographic map of the sampled area is given in Figure 3. Three graduated stakes were placed within a meter of each other at each of these sites. These stakes were painted white to decrease the effect of absorption and re-emission of radiation. Every 4 days or so the depth of snow indicated on each stake was recorded and the density of the adjacent snow was measured with a snow-tube. By this process, accurate measurements of the melt that occurred at each of the locations for each of the time steps were obtained (as an average of the melt occurring at the three stakes). The complete listing of this original data is given in Table 3 (Appendix A).

The melt that occurred between subsequent measurements at a site was calculated by subtracting the amount of snow water equivalent (SWE) measured at one time period from that of the preceding time period. No new snow fell during the melt period; thus the one negative value of melt



REYNOLDS CREEK WATERSHED

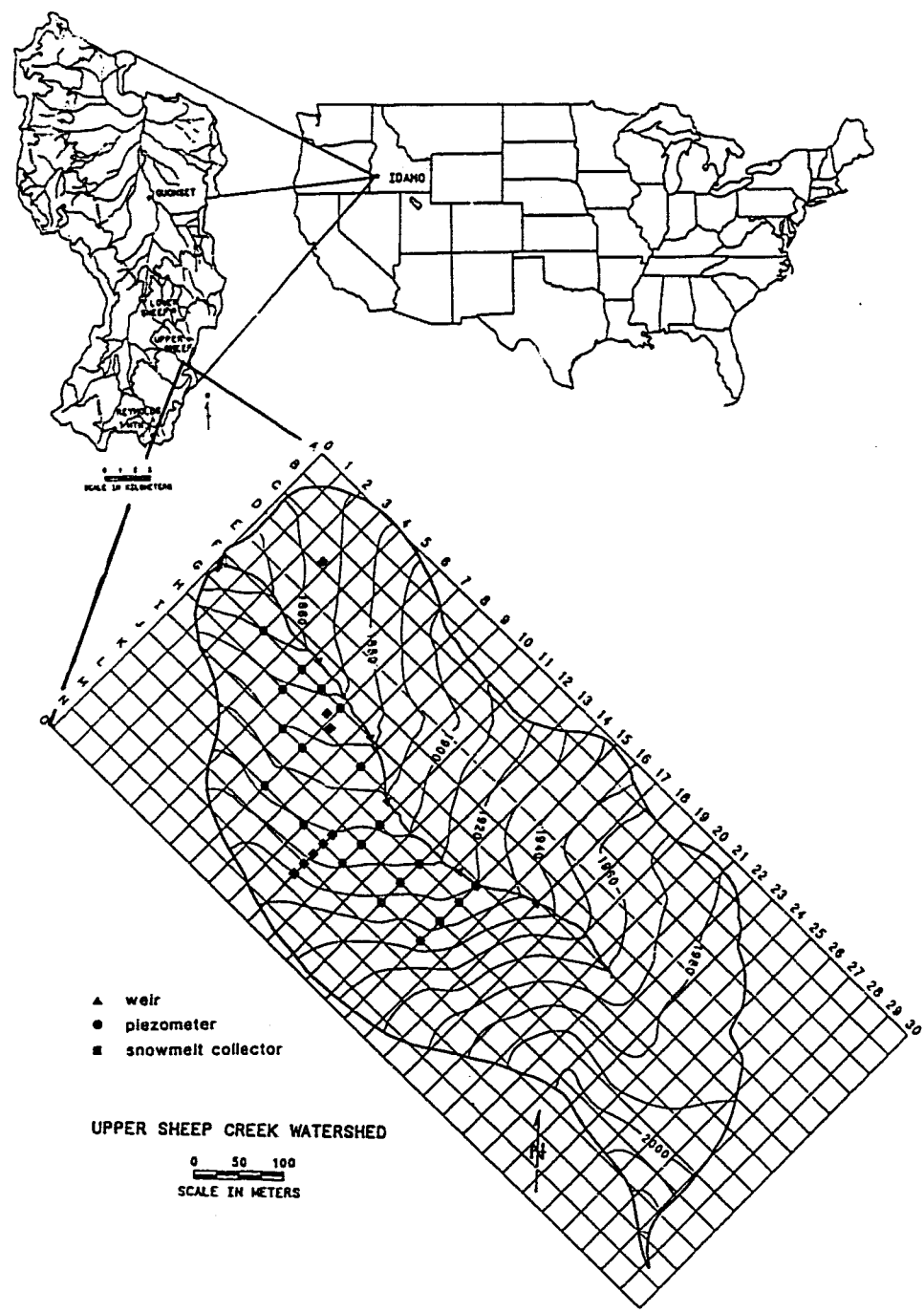
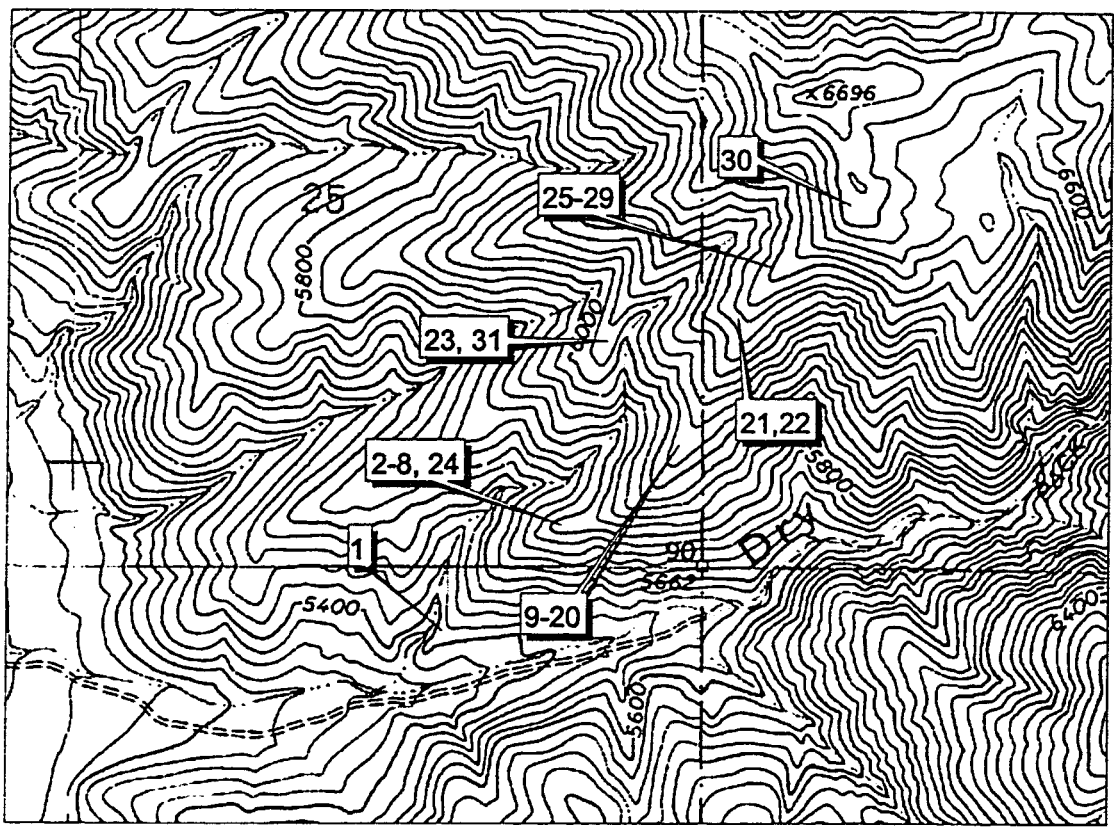


Figure 2. Map of Upper Sheep Creek watershed.



Contour Interval 40 Feet

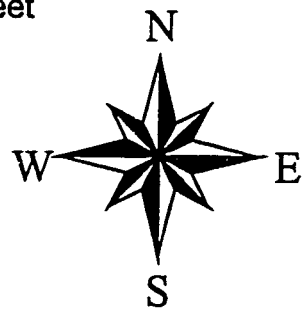
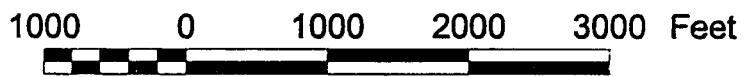


Figure 3. Map of Smithfield Dry Canyon data collection sites.

was set to zero. The SWE was calculated as the average depth of snow recorded at the three stakes multiplied by the measured density of the snow at the site.

In order to determine the density at each site, the snow tube depth was divided by the weight of snow measured. In cases where there were two such measurements of density for a single date, the two calculated densities were averaged. In cases where there was only one measurement of density, it was averaged with measurements from similar, neighboring sites to provide a more robust estimate. In some cases (on later dates), the snow was too shallow to obtain a measurement of density, so the density from the last measurement date was used. These calculated densities are plotted in Figure 4, and the adjusted densities are shown on Figure 5.

It is apparent from Figure 4 that some error remained in the density calculations for the Smithfield Dry Canyon data. In particular, points 10, 13, 14, 25, 26, 27, 28, and 30 show instances where the calculated density decreased with time. Since the entire melt period was characterized by fairly consistent melt with no accumulation of new snow, the density should only have increased. Though it is possible for snow density to decrease due to internal melting of the ice lattice causing hollow voids beneath a surface bridge of ice, this phenomenon was never observed. Therefore, these inconsistent points were modified using the following equation:

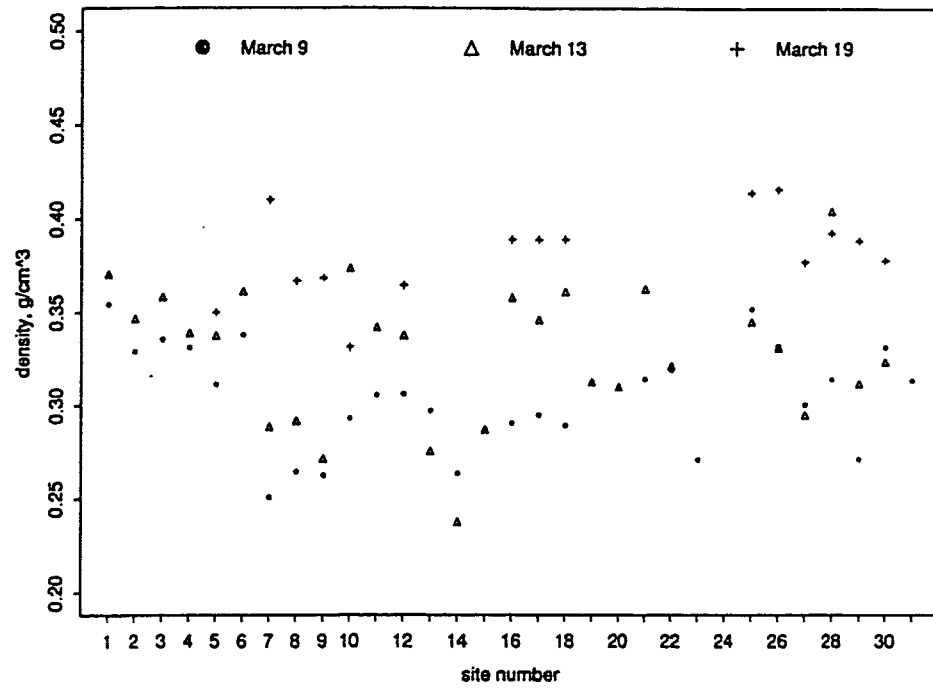


Figure 4. Smithfield Dry Canyon data: initial calculated densities.

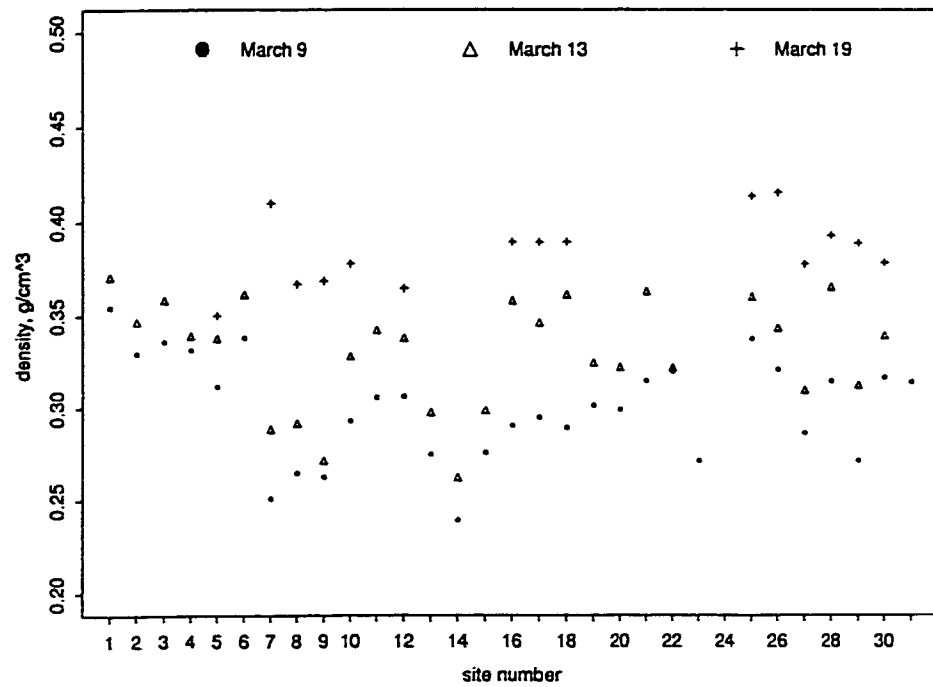


Figure 5. Smithfield Dry Canyon data: adjusted densities.

$$\rho_+ = \frac{\rho_{orig+} + \rho_{orig-}}{2} + \frac{\rho_{av+} - \rho_{av-}}{2}$$

$$\rho_- = \frac{\rho_{orig+} + \rho_{orig-}}{2} - \frac{\rho_{av+} - \rho_{av-}}{2}$$

where  $\rho_+$  is new density for the latter date,  $\rho_-$  is the new density for the prior date,  $\rho_{orig+}$  and  $\rho_{orig-}$  are the original measured density at the latter and prior dates, respectively, and  $\rho_{av+}$  and  $\rho_{av-}$  are the average measured densities of all the points in the data set before correction for the latter and prior dates, respectively. In this fashion, the average density increase for the time period was applied to each deviant density measurement. These adjusted densities are plotted in Figure 5.

Finally, the values of SWE at each point and for each measurement date were calculated by multiplying the depth of snow recorded at each of the three stakes by the adjusted densities, and averaging this product across the three stakes. Subtracting subsequent values of SWE yielded the melt that occurred at the site over the time period.

### Regression Methods

In all analyses, least-squares linear regression was employed to calculate the  $\alpha(t)$ ,  $\beta(t)$ , and  $\gamma(t)$  terms whenever the TopoFECS modeled melt with accumulation (Equation 18b). When the nonlinear form of the model was used (Equation 18a) to model solely melt with no accumulation, the  $\alpha(t)$ ,

$\beta(t)$ , and  $\gamma(t)$  terms were chosen in order to minimize the absolute error according to the following equation:

$$\text{Min} \left\{ \sum_i \left| \max \left( \alpha(t) + \beta(t) \cdot \text{elev}_i + \gamma(t) \cdot \text{rad}_i, 0 \right) - \text{measured melt}_i \right| \right\}$$

A quasi-Newton method was used in this optimization. (See Dennis, Gay, and Welsch [1981] and Dennis and Mei [1979] for details on the method.) Detailed regression diagnostics are only presented for the simpler least-squares linear regressions (Equation 18b).

### Initial Model Testing

In order to test the predictive ability of the TopoFECS model, the model was applied to all three data sets: the synthetic data, the Upper Sheep Creek data, and the data from Smithfield Dry Canyon. For each data set, a group of index points was chosen and used throughout all available melt periods to estimate the  $\alpha(t)$ ,  $\beta(t)$ , and  $\gamma(t)$  terms. Descriptions of the results for each data set are given in subsequent sections.

#### Synthetic data

For this analysis, 200 points were generated with the UEB model with slopes randomly selected from a uniform distribution over the range of 0°–60°, random aspects ranging uniformly all the way around the compass, and

random elevations selected from a uniform distribution over a range of 1500 meters. The weather conditions at each point were simulated as described in the “Synthetically generated data” section. The simulated snow water equivalence (SWE) at every point was recorded every 48 hours, and the melt during each 48-hour period was calculated as the difference in SWE between subsequent time steps. The following points were chosen as the index points to be used to determine the  $\alpha(t)$ ,  $\beta(t)$ , and  $\gamma(t)$  terms throughout the melt season:

	Elevation:	Slope:	Aspect, clockwise from North:	Characteristics:
Point 1	2650 m	57°	316°	Low radiation, med. elevation
Point 2	3420 m	59°	353°	Low radiation, high elevation
Point 3	2166 m	54°	169°	High radiation, low elevation
Point 4	3390 m	56°	72°	Med. radiation, high elevation
Point 5	2869 m	58°	116°	High radiation, med. elevation

These points are extremely varied in terms of elevation and radiation received. This wide range of variability is important for accurate melt predictions, as will be discussed in the section entitled “Selection of Index Points.”

Figure 6 shows eight plots of the UEB-generated melt versus the estimates for each of the 200 points obtained using the TopoFECS model (only those points at which the UEB model still predicts the presence of snow are shown, since the results are meaningless if the snow has completely melted). These correspond to the eight 48-hour melt periods from March 28–April 13. The solid line in each plot is the 1:1 line, representing a perfect fit. As can be seen, the TopoFECS model performed fairly well, but not perfectly. The Nash-Sutcliffe measure of predictive accuracy (or NS value) for each plot is given in the figures. Following Gupta, Sorooshian, and Yapo (1998), these NS values were calculated as follows:

$$NS = 1 - \frac{\sum (y - \hat{y})^2}{\sum (y - \bar{y})^2} \quad (19)$$

where  $y$  represents the values of melt calculated by the UEB model (or “measured” melt value),  $\bar{y}$  is the mean of all melt values calculated by the UEB model, and  $\hat{y}$  represents the values of melt predicted by the TopoFECS model.

Table 1 gives a summary of the regression diagnostics for five out of the eight time steps displayed in Figure 6. The five time steps, March 28–30, April 3–5, April 5–7, April 9–11, and April 11–13, were chosen for this analysis because precipitation fell on those dates, enabling the use of the



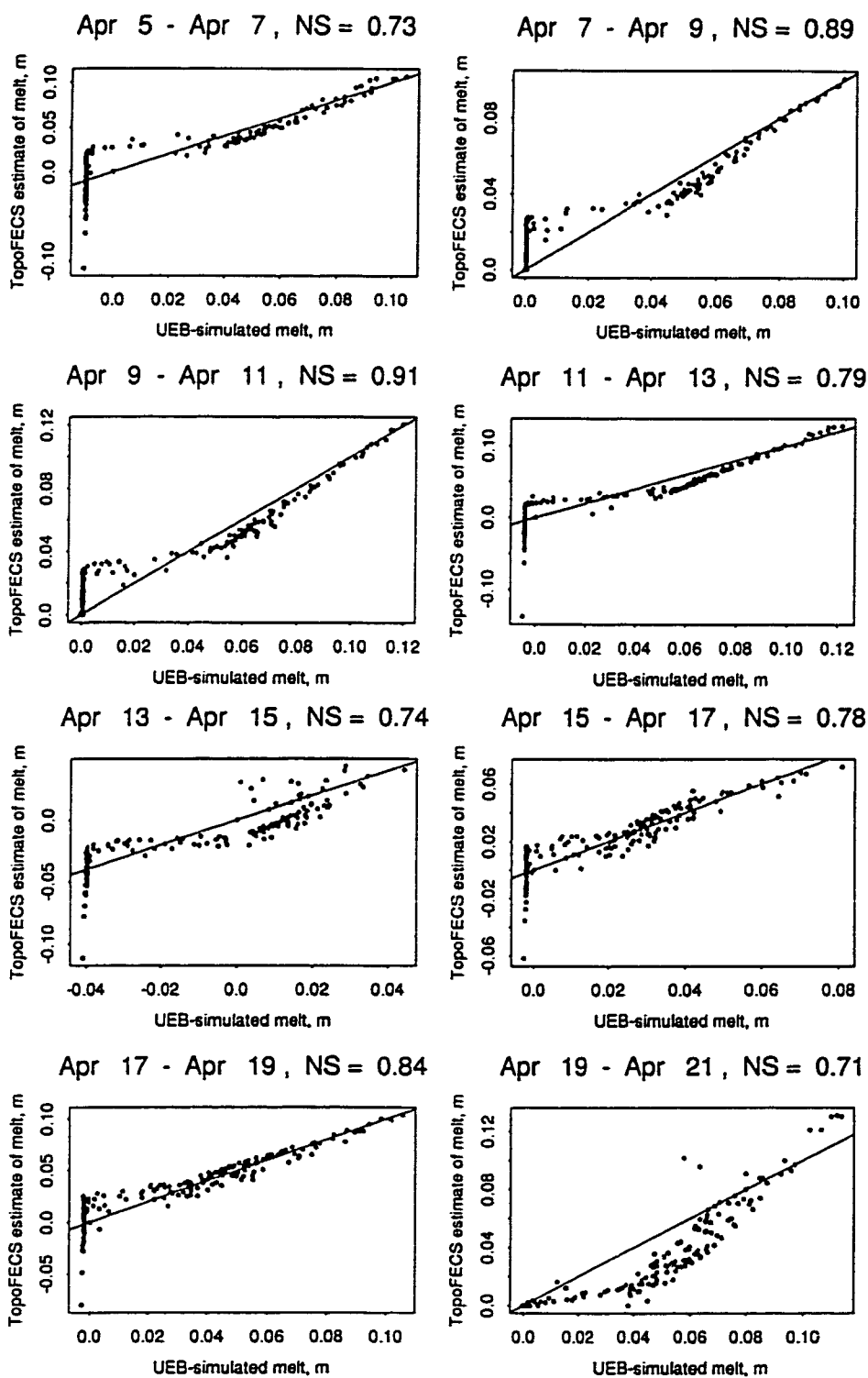


Figure 6. Melt simulated by the Utah Energy Balance model vs. TopoFECs estimates.

Table 1. Statistical analysis of regressions on synthetic data for the following dates: Mar 28–30, Apr 3–5, 5–7, 7–9, 9–11, 11–13

	p Values			
	$\alpha$	$\beta$	$\gamma$	overall
March 28–30	0.03	0.03	0.01	0.01
April 3-5	0.07	0.06	0.02	0.02
April 5-7	0.08	0.13	0.07	0.18
April 9-11	0.26	0.08	0.04	0.05
April 11-13	0.33	0.17	0.06	0.07

R2 Values	
March 28-30	0.99
April 3-5	0.99
April 5-7	0.88
April 9-11	0.97
April 11-13	0.95

F-Statistic; Significant with 90% Confidence if >54

March 28-30	89
April 3-5	55
April 5-7	5
April 9-11	19
April 11-13	13

Cook's Values – Significantly Influential if >9.16

	index point 1	index point 2	index point 3	index point 4	index point 5
March 28 - 30	0.57	0.06	1.4	2	0.69
April 3 - 5	1.1	0.44	1.5	0	0.37
April 5 - 7	0.46	0.62	1.4	0.07	0.24
April 7 - 9	0.35	3.7	0.85	0.07	0.02
April 9 - 11	0.34	3.8	0.99	0.02	0.01

linear form of Equation 18. The p-values for the regression coefficients are especially interesting. These indicate that the  $\gamma(t)$  or radiation term is the most significant term in the regression, followed by  $\beta(t)$ , and finally by  $\alpha(t)$ .

Table 1 also gives the Cook's distances for each of the index points used in the regression for each time step. The Cook's distance is a measure of the combined influence of the  $i^{\text{th}}$  point on the regression coefficients. It assumes greater values for data points with large residuals, large leverage values, or both. It has been suggested (Cook, 1977) that an observation is significantly influential if the Cook's value exceeds the lower 10<sup>th</sup> percentage point of an F-distribution. Here, the degrees of freedom in the numerator are the number of parameters used, and the degrees of freedom for the denominator are the number of observations minus the number of parameters. In this case with three parameters in the model and five index points, the lower 10<sup>th</sup> percentage point is 9.16. All Cook's values for the given index points in Table 1 are well below this value, indicating that none of them significantly altered the outcomes of the regressions.

Another point of interest in Table 1 concerns the relatively high  $R^2$  values (or adjusted multiple coefficients of determination) for some of the regressions. Following Mendenhall and Sincich (1992), these  $R^2$  values were calculated as follows:

$$R^2 = 1 - \frac{(n-1)}{n-(k+1)} \left( \frac{\sum (y - \hat{y})^2}{\sum (y - \bar{y})^2} \right) \quad (20)$$

where  $y$  represents the value of melt at each of the index points as calculated by the UEB model (or “measured” melt value),  $\bar{y}$  is the mean of  $y$ ,  $\hat{y}$  represents the value of melt at the index point as predicted by the TopoFECS model,  $n$  is the total number of index points used in the regression, and  $k$  is the number of model parameters (three).

The higher  $R^2$  values do not necessarily indicate exceptional model performance, as evidenced by the plots in Figure 6. Since the  $R^2$  value is based on a very small sample size (5 index points, leaving only 2 degrees of freedom in the regression), it is likely that some of the regression  $R^2$  values will indicate a much better fit than is actually obtained when predicting 200 points.

The regression statistics given in Table 1 should be viewed as rough estimates only, since the statistical confidence of the regression is difficult to ascertain with only five points. The F-statistics in particular show the lack of statistical confidence in the regressions. Only two of the five regressions analyzed are significant with 90% confidence (F-statistic greater than 54). However, the measure of success of the model should be judged in terms of its predictive accuracy.

In Figure 6, it is apparent that the linear TopoFECS model is not entirely appropriate for modeling this synthetic data set. Though most points fall on or near the 1:1 lines, the points on the left-hand sides of the graphs cluster into vertical lines, indicating that melt is not a continuously linear function of radiation and elevation near the points with zero melt. A possible cause for the departures in the data may be the nonlinearity of the UEB model caused by the storage of energy in the simulated snowpack. Regardless of the reason behind these errors, it is obvious that the TopoFECS model cannot reproduce the UEB results exactly.

Figure 7 shows two residual plots (UEB simulation minus TopoFECS estimates) for two different time periods: April 5–7, and April 17–19. A solid line was drawn horizontally through each plot where the residuals equaled zero. If the underlying relationship between radiation, elevation, and melt as modeled by the UEB model were really a linear function, then the residuals ought to be uniformly scattered about these lines. However, the LOESS (Cleveland and Devlin, 1988) smoothes of the data, shown by the dashed lines, show a very apparent trend in the residuals in both plots. This suggests that the linear TopoFECS model is not completely adequate to describe the behavior of the melt modeled by the UEB model.

Figure 8 shows two plots of the residuals (UEB simulation - TopoFECS estimates) versus incoming exoatmospheric solar radiation. The

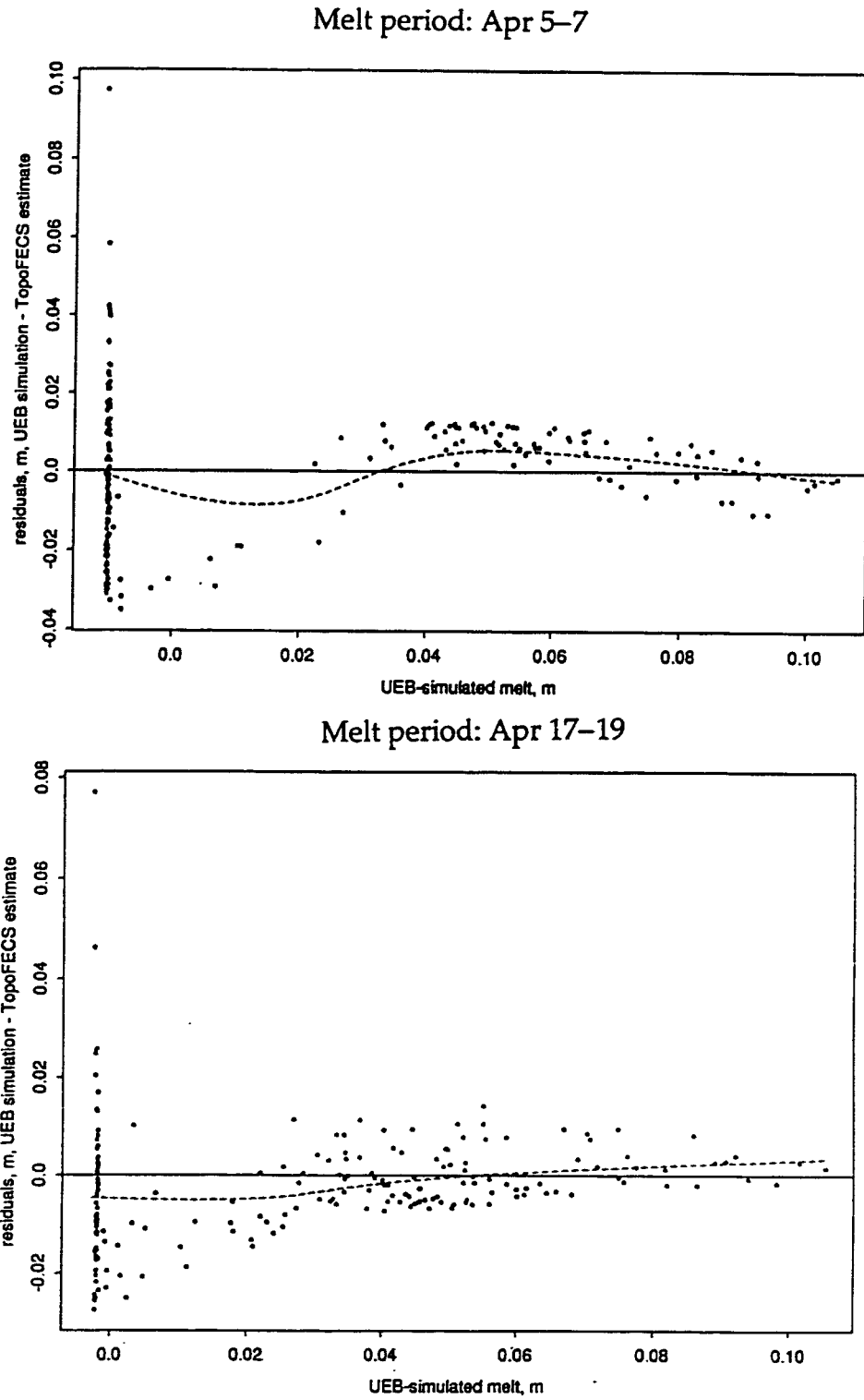


Figure 7. Plot of residuals (UEB simulations minus TopoFECS estimates) vs. UEB-simulated melt.

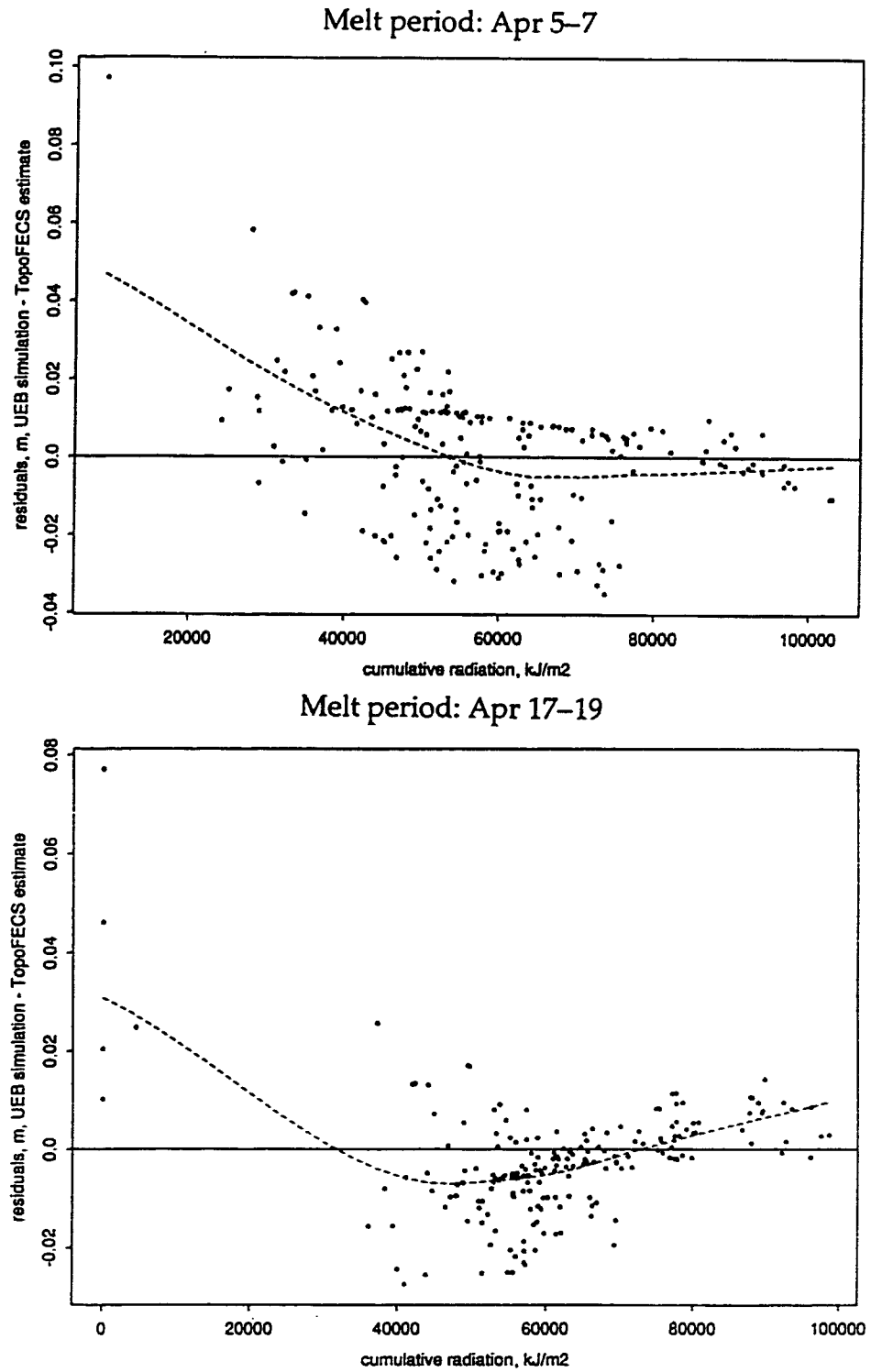


Figure 8. Plot of residuals (UEB simulations minus TopoFECs estimates). vs. cumulative radiation: synthetic data

same two time steps examined in Figure 7 are used here. Again, solid lines were drawn horizontally through each plot where the residuals equaled zero, and LOESS smoothes were plotted as dashed lines. These smoothes show a very apparent trend in the residuals in the first plot and a slightly weaker but still existent trend in the second. This indicates that the melt modeled by the UEB model is not linear with respect to radiation, and therefore the linear TopoFECS model is not completely realistic.

Figure 9 shows plots of the residuals for the same time periods (April 5–April 7 and April 27–April 29) versus elevation. Once again, a solid line was drawn across the plots where the residuals equaled zero, and LOESS regression lines were drawn through the data to show any trends. Structure can be clearly observed in the residuals of the first plot; the TopoFECS model tends to underpredict melt at both upper and lower elevations and overpredict melt at the middle elevations. The variance of the errors increases as well with increasing elevations. Weaker trends in the residuals can be observed in the second graph as well. This indicates that the assumption of melt varying linearly with elevation may not be entirely appropriate.

In this analysis of the residuals, it is important to bear in mind the nature of the data. The UEB model does not calculate melt as simply a linear function of radiation and air temperature with some Gaussian noise added. Rather, the UEB model produces melt estimates according to well-



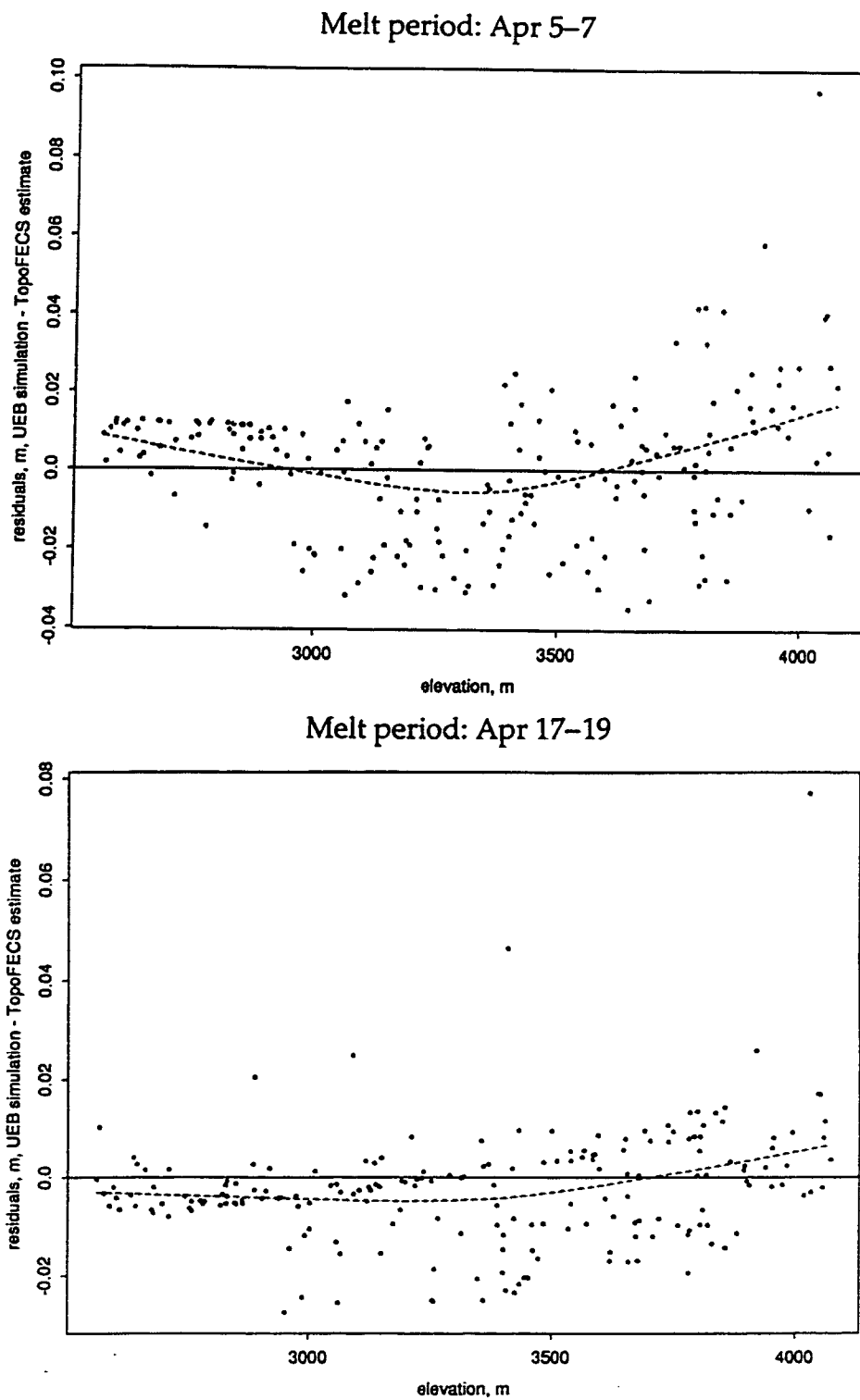


Figure 9. Plot of residuals (UEB simulations minus TopoFECS estimates) vs. elevation: synthetic data.

defined, mathematical functions. Therefore, one ought to expect highly structured residuals rather than the normally distributed, random residuals typically associated with actual field data.

A closer fit to the data could probably be obtained by using a higher-order polynomial regression, but this would require measurements from more index points. However, since the linear model obtained relatively good results for both time steps (NS values of .73 and .84, respectively), the linear model is probably sufficient for practical applications.

Figure 10 shows the cumulative melt for eight sites that were selected semi-randomly to show different extremes of accumulation and ablation. The points show the actual UEB results, while the lines show the TopoFECS estimations of the melt process using Equation 18. These figures are shown because this is a common way to display accumulation and ablation of the snowpack. The average Nash-Sutcliffe measure (NS) of predictive accuracy of the model for the eight points shown is .95, while the average NS for all of the 200 points is .94.

Since in reality radiation can affect air temperature, and since this interaction was not accounted for in the above calculations, the UEB model was also run on 40 other points in which the air temperature was modified proportionally with incoming radiation by as much as 30°. Figure 11 shows eight more plots of the UEB-generated melt under these conditions versus

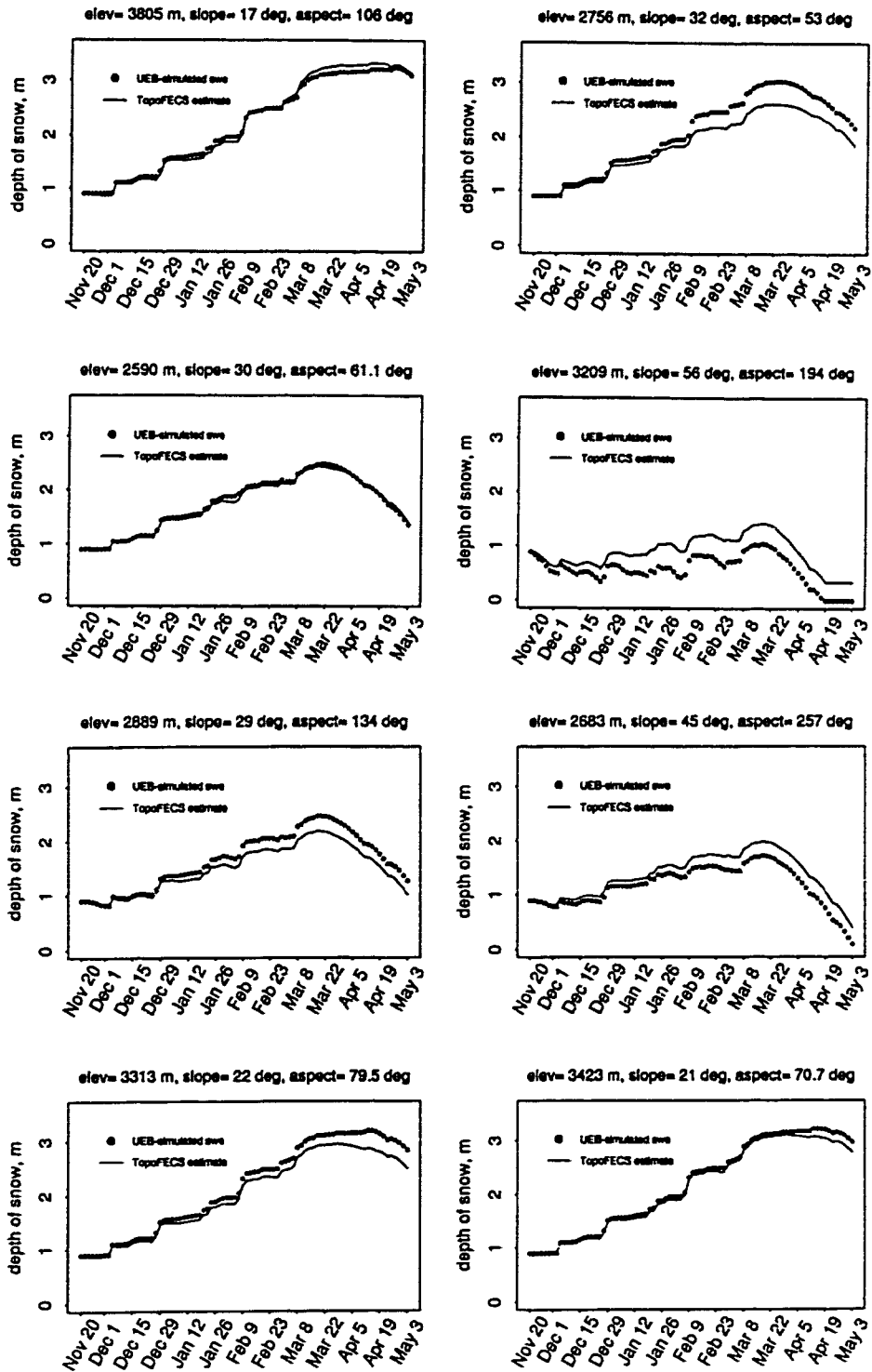


Figure 10. Accumulation/ablation estimates at 8 random points: synthetically generated data.

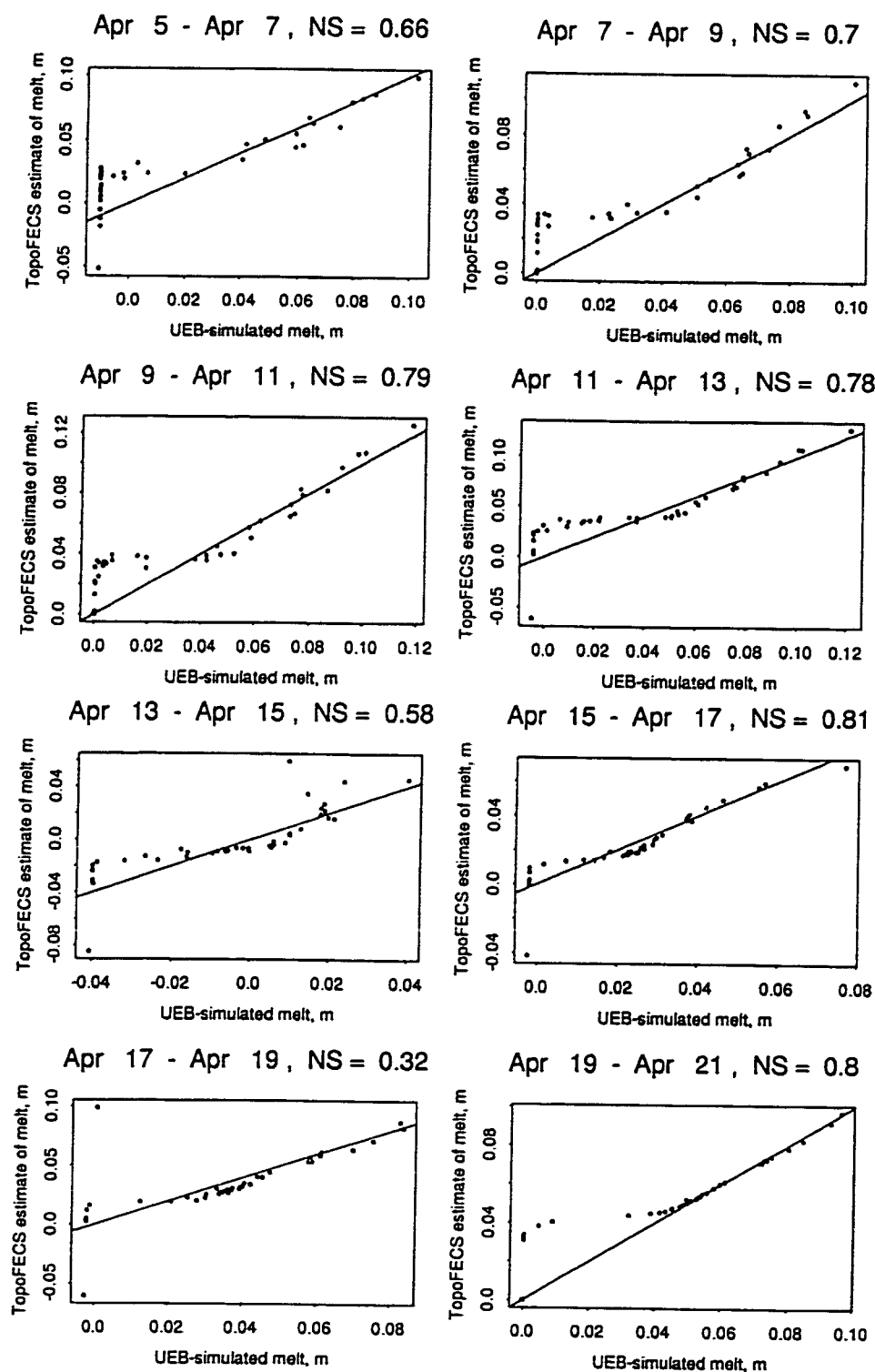


Figure 11. TopoFECs melt estimates vs. UEB-simulated melt with air temperature adjusted proportionally with incoming radiation.

the TopoFECS estimates. Again, these correspond to the same eight 48-hour melt periods, covering the time period from March 28–April 13. The NS values (calculated as in Equation 19) for these plots are given. As can be seen, the TopoFECS model's performance under these conditions seems very comparable to those under the initial conditions where air temperature was independent of radiation. Therefore, any interaction between air temperature and solar radiation can be sufficiently accounted for by the TopoFECS model.

Upper Sheep Creek data:

When the TopoFECS model was applied to the distributed melt measurements at Upper Sheep Creek, the results were extremely poor. Figure 12 shows two X-Y plots of the model's estimates versus the measurements. These two plots correspond to the two time periods March 25–April 9, 1986, and April 30–May 13, 1993. Though many index points (11 for each prediction) were used to obtain a more robust calibration of the TopoFECS equation, both sets of estimates have NS values of less than .01. To understand why the model failed, one must look at the melt data. Tables 8 and 9 in Appendix B give the measured values of snow water equivalence at each point in the watershed for March 25, 1986, and April 9, 1986, respectively. Table 10 (Appendix B) shows the melt between the two dates estimated by subtracting the April 9 values from the March 25 values.

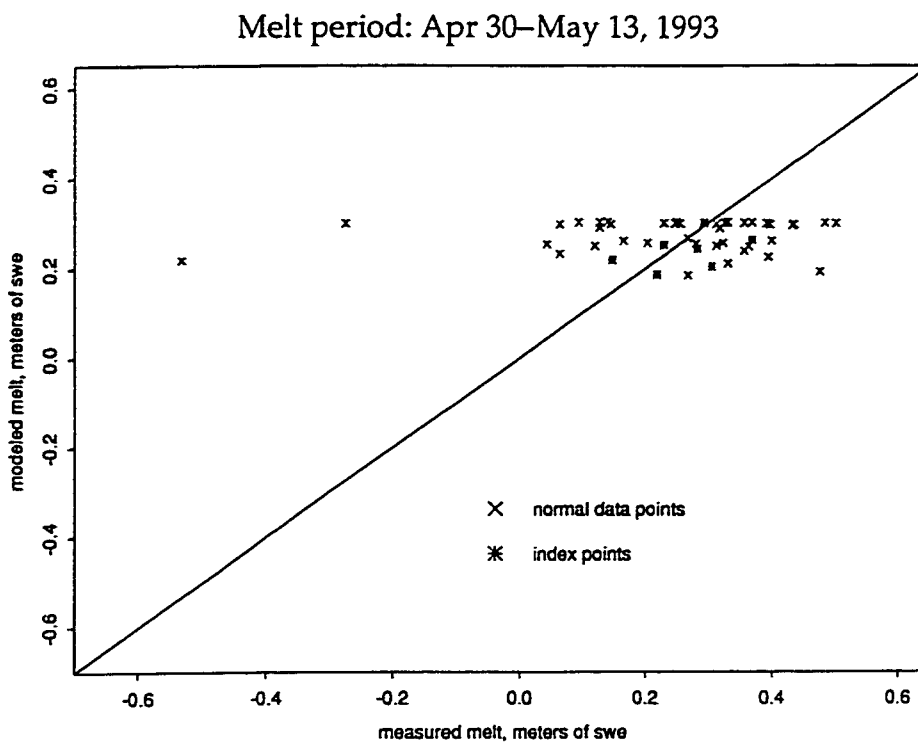
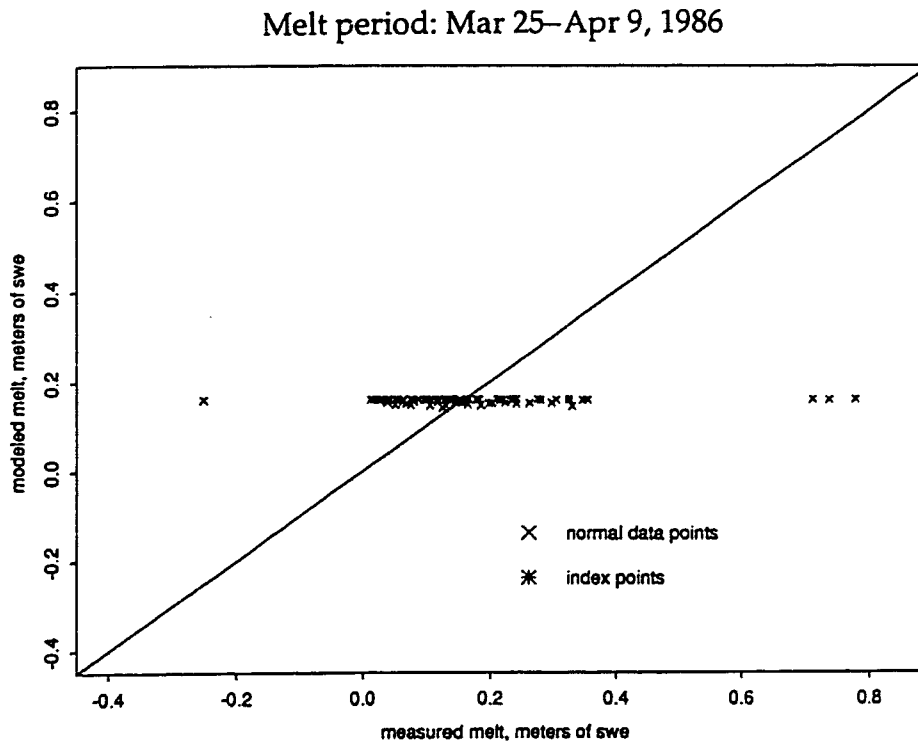


Figure 12. TopoFECS melt estimates vs. measured melt at Upper Sheep Creek.

Tables 11 through 13 (Appendix B) show the same information for April 30–May 13, 1993. Tables 10 and 13 show large discrepancies in melt values between neighboring cells. In a few instances, some cells even gained significant amounts of snow (indicated by negative melt values) while cells nearby lost large amounts.

Erratic depletion patterns such as these might be observed during periods of extreme drifting or extremely variable snowfall events. However, during the time from March 25–April 9, 1986, the average temperature in the basin was 5.3° C, and less than 3.3 inches of precipitation fell. From April 30–May 13, 1993, the average temperature was 6.3° C, and less than 1.1 inches of precipitation fell. Since the temperatures were so high, it can be assumed that the snow was consistently ripe and heavy; therefore no drifting occurred. Because of the low amounts of precipitation, these depletion patterns cannot be explained by erratic snowfall.

Differing melt conditions caused by topographic variances across the watershed could also be the culprit for these erratic depletion patterns. However, these differences cannot be due to elevation changes, because there is a range of merely 196 meters from the bottom of the watershed to the top. In order to determine whether this phenomenon could have been caused by extreme differences in melt rates caused by differing amounts of solar radiation, the values of melt for each cell were plotted versus incoming

radiation in Figure 13. As can be seen, there is no observable trend with radiation.

Instead, the reason for these discrepancies lies in the methods used to obtain the measurements of snow water equivalence. Each point was measured only once each period using a snow tube. The tube was inserted within a meter or two of the stakes that marked out the grid, so that the same spot was never measured twice. Because of the undulating nature of the ground beneath the snow, sometimes the tube would go into a pit downhill from the stake, causing a deep measurement, while at other times the tube would strike a rise in the ground or a sagebrush uphill from the stake, causing a shallow measurement. This phenomenon was observed first-hand while assisting in the collection of SWE data in 1996. Apparently, the magnitude of the measurement noise incurred by this method of sampling overwhelms the magnitudes of the melt that occurred during the intervals between measurement dates. In particular, it overwhelms the magnitude of any differences in melt that could be observed between two grid points.

Since the measurements of snow water equivalence at Upper Sheep Creek were so noisy, a point-by-point analysis of the TopoFECS model using the data is not appropriate. However, the data set was retained to demonstrate the effect of severe measurement noise upon the TopoFECS model. Also, because of the gridded nature of the Upper Sheep Creek data



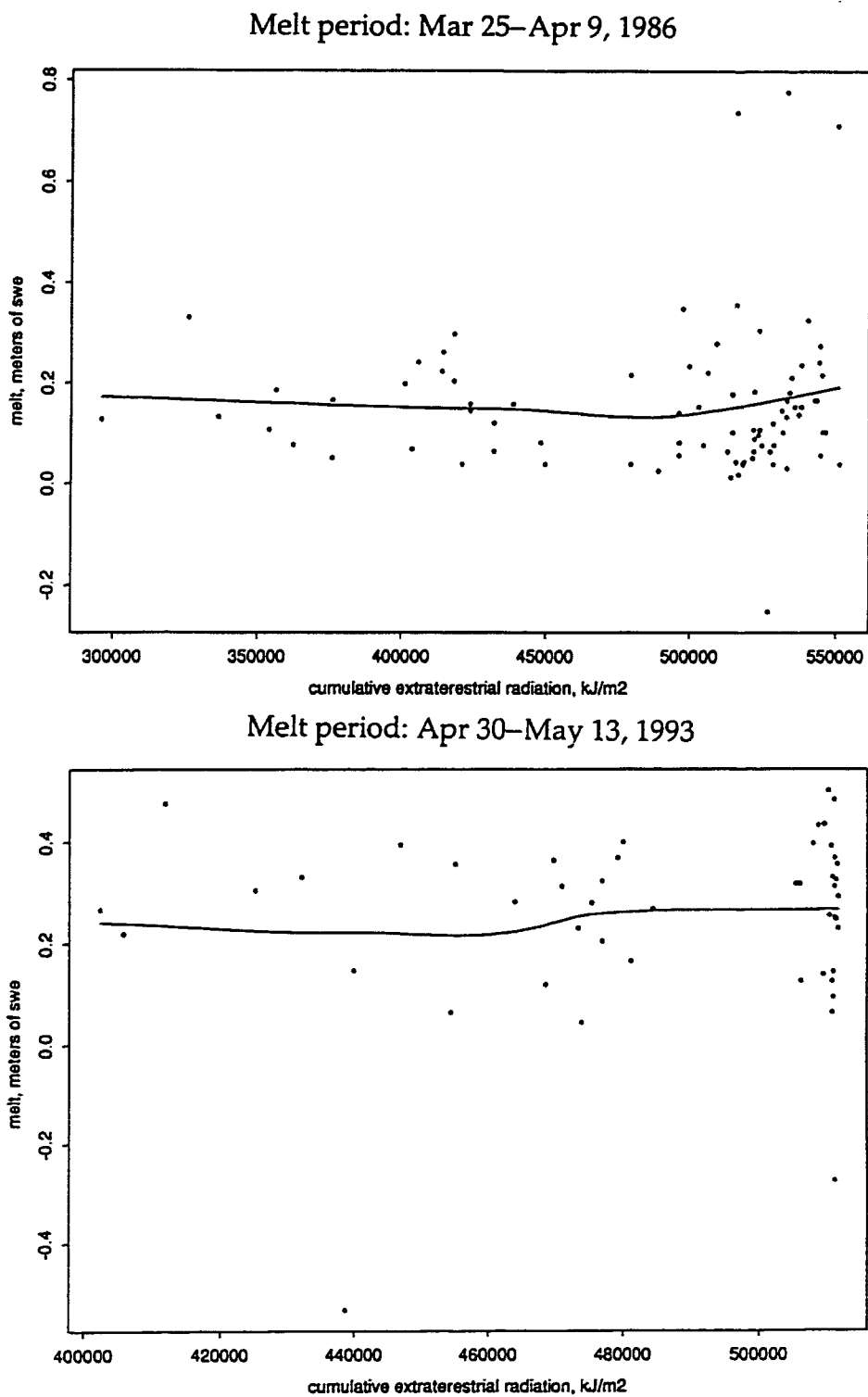


Figure 13. Observed melt vs. incoming radiation: Upper Sheep Creek data.

set, it is ideally suited to a visual analysis of the spatial patterns of melt.

Therefore, the TopoFECS model was used to estimate the melt occurring at each point in the grid, and then this was subtracted from the original snow water equivalence to arrive at an estimate of the new distribution of snow water equivalence. Figure 14 shows side-by side comparisons of the measured snow water equivalence (SWE) in meters with that predicted by the TopoFECS model for three different dates in 1986. The first graph shows the SWE that was used to initialize the TopoFECS model. Figure 15 shows the initialization snow water equivalence map and the same side-by-side comparisons for three dates during the 1993 melt season. All points with snow still remaining on them were used as index points in the TopoFECS calculations for stability. As can be seen, the patterns of SWE appear to be estimated fairly well by the TopoFECS model, even though the observed melt values do not match the TopoFECS estimates (indeed, the actual melt may be a lot closer to that predicted by the TopoFECS model than what was estimated from the observed difference in SWE, since the TopoFECS model smoothes out the large errors in the data with basically an average basin-wide melt value). Since the depth of SWE in this data set is quite often an order of magnitude larger than the depth of melt occurring, large errors in melt are not as easily recognized when comparing measured SWE to modeled SWE. This is a convincing argument for the use of melt (which

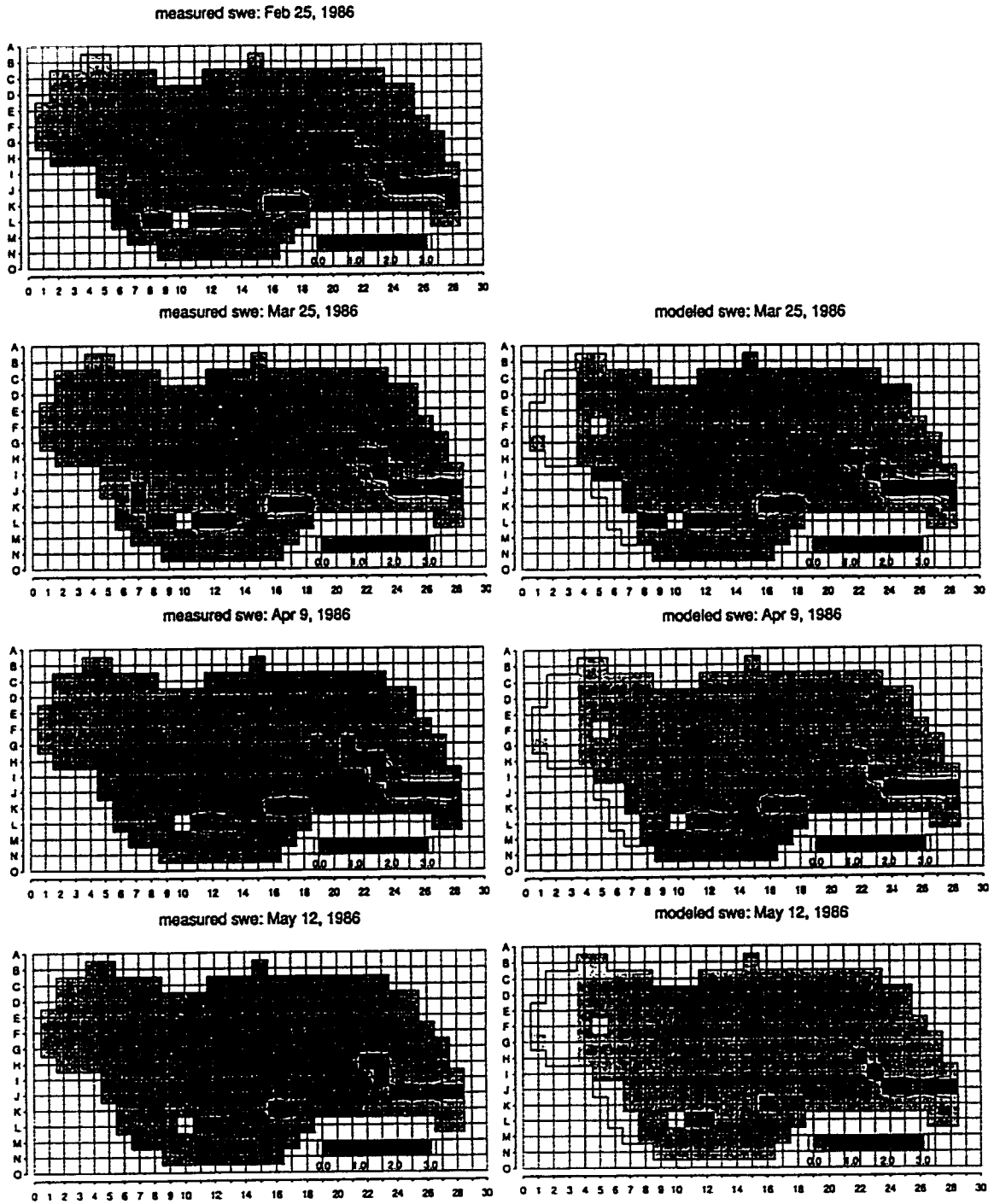


Figure 14. Measured and modeled snow water equivalence at Upper Sheep Creek, 1986.

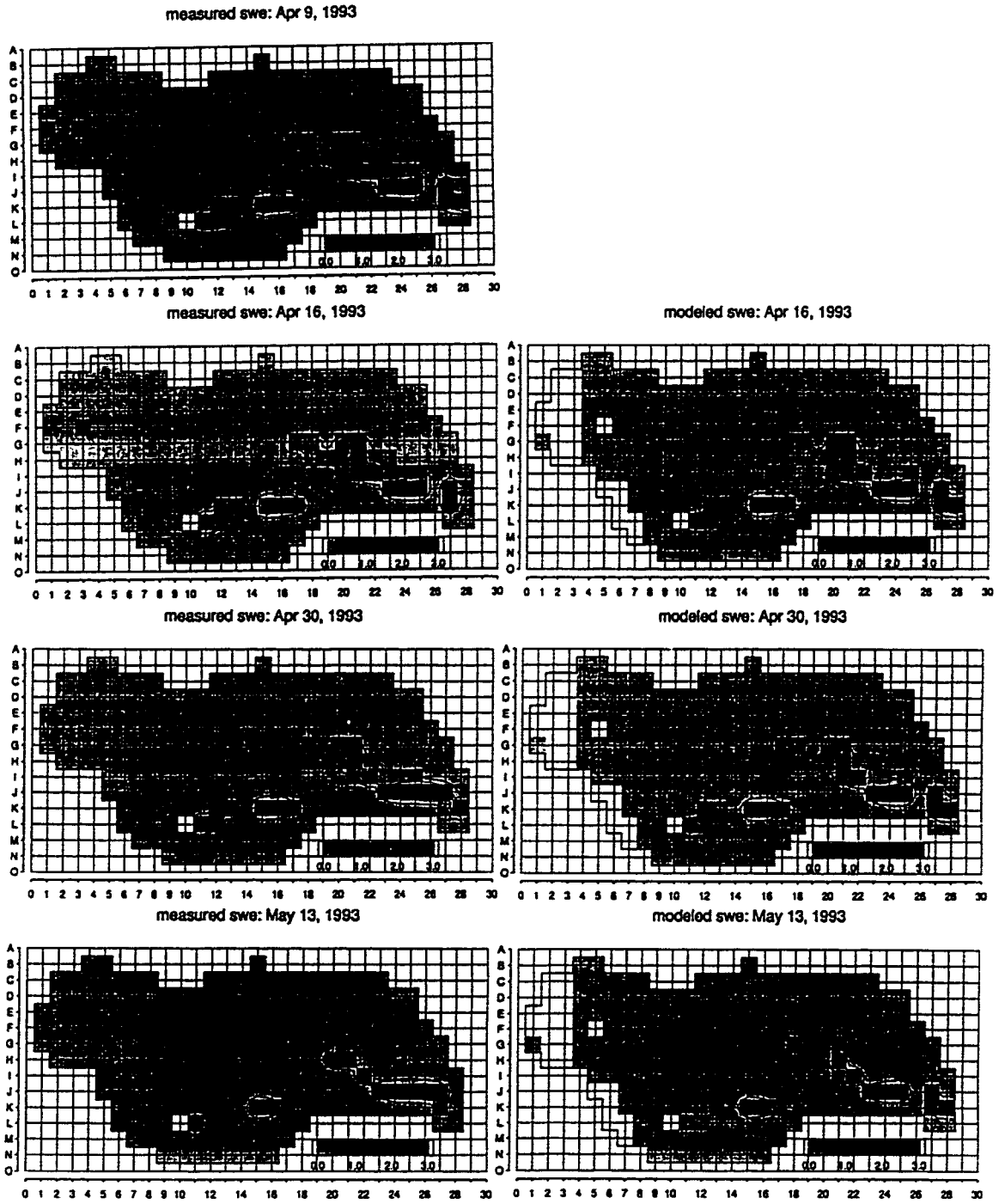


Figure 15. Measured and modeled snow water equivalence at Upper Sheep Creek, 1993.

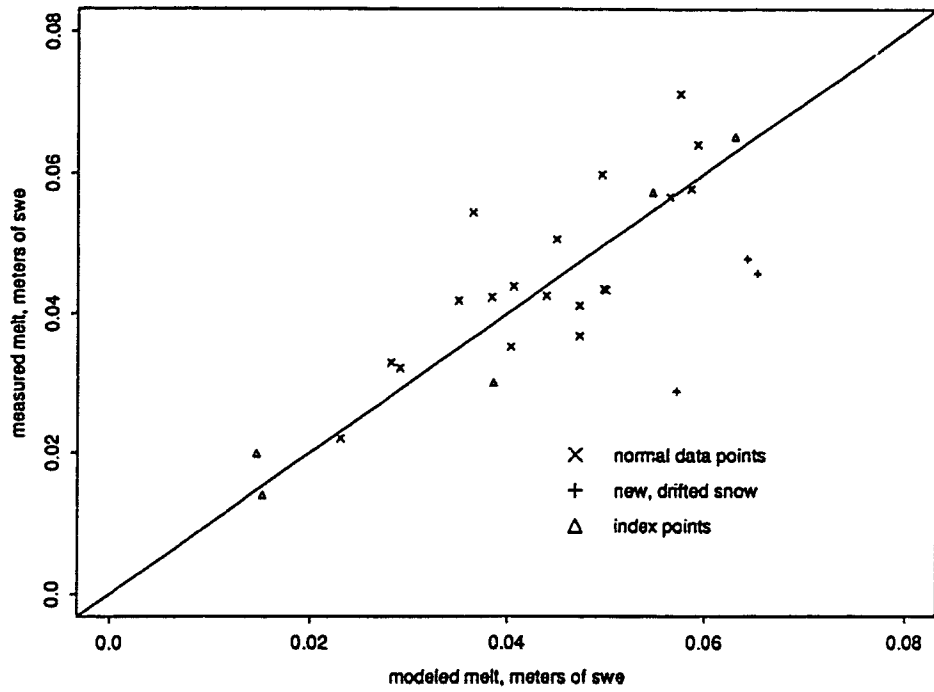
is the rate of change in SWE) rather than SWE comparisons to validate a snowmelt model.

#### Smithfield Dry Canyon data

The melt at Smithfield Dry Canyon was modeled in the same fashion with the TopoFECS model. Though no new snow fell during the study, the linear form of Equation 18 was used to predict melt for both time steps in order to simplify the analysis. This was deemed to be valid, since significant melt was recorded at all measurement points, obviating the need for the maximum term. Five index points were used: points 1, 5, 7, 26, and 29. The topographic characteristics of each are given in Table 3 (Appendix A). These points were chosen to cover a wide range of elevation and exoatmospheric radiation values.

Figure 16 shows X-Y plots of the TopoFECS model results versus the measured melt for the March 9–13 and March 13–19 melt periods. Points 1, 5, 7, 26, and 29 (see Appendix A for point characteristics) were used as index points in both cases, and are shown as triangles. The top graph (March 9–13) has an NS value of 0.51, while the lower graph has an NS value of .76. It is interesting to note the predictions for points 16, 17, and 18, which are represented as +’s in these figures. These data points were collected in a large, new drift that formed around the 7th of March. They were therefore composed of deep, fresh snow, and the energy during the first few days

Melt period: Mar 9–13, 1997



Melt period: Mar 13–19, 1997

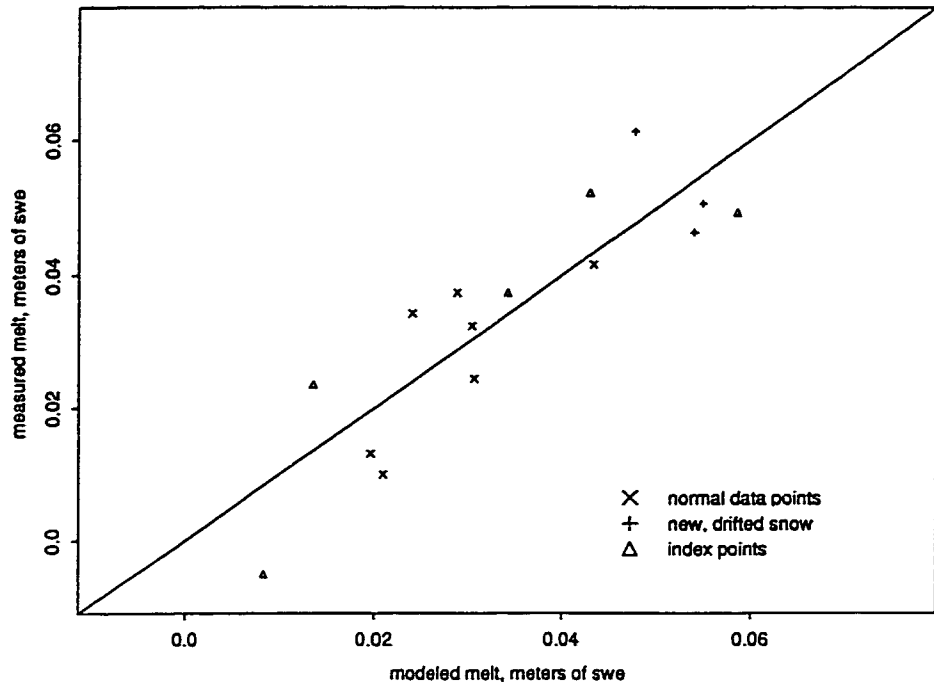


Figure 16. Plot of measured melt vs. TopoFECS estimates: Smithfield Dry Canyon.

contributed towards metamorphism or ripening of the snow rather than melt. This is evidenced by an underprediction of melt in the first period, while in the second period, after the snowpack had ripened, the predictions are more in line with observed melt. If these three points are ignored in the first graph, the calculated NS value increases significantly to 0.77.

Table 2 gives a summary of the regression diagnostics for these two time periods. Again, the p-values for the regression coefficients indicate that the radiation term,  $\gamma(t)$ , is the most important term in the regression. This term is followed in significance by the elevation term,  $\beta(t)$ , and finally by  $\alpha(t)$ . All terms are significant to at least the .19 level. It is also apparent from the computed Cook's values that none of the index points exerted undue influence on the regressions.

Again, the residuals of the modeled versus measured melt values were examined to determine the existence of any trends with respect to radiation or elevation. Figure 17 shows plots of the residuals (measured melt minus TopoFECS estimates) for each of the two time periods. Each plot has a solid, horizontal line drawn through zero, and a dotted LOESS regression line through it. In both time periods, the TopoFECS model seems to underpredict low values of melt and overpredict high melt values.

Figure 18 shows two graphs, one for each time period, of the same residuals plotted versus radiation, and Figure 19 shows the residuals plotted

Table 2. Statistical analysis of regressions on Smithfield  
Dry Canyon data

	p Values			
	$\alpha$	$\beta$	$\gamma$	overall
March 9 - March 13, 1997	0.07	0.07	0.03	0.02
March 13 - March 19, 1997	0.19	0.18	0.13	0.09

R2 Values	
March 9 - March 13, 1997	0.99
March 13 - March 19, 1997	0.94

F Statistic; Significant with 90% Confidence if >54

March 9 - March 13, 1997	52
March 13 - March 19, 1997	10

Cook's Values; Significantly Influential if >9.16

	index point 1	index point 2	index point 3	index point 4	index point 5
March 9 - March 13, 1997	0.68	0.28	0.04	0.19	0.68
March 13 - March 19, 1997	0.63	1.3	1	0.01	2.2



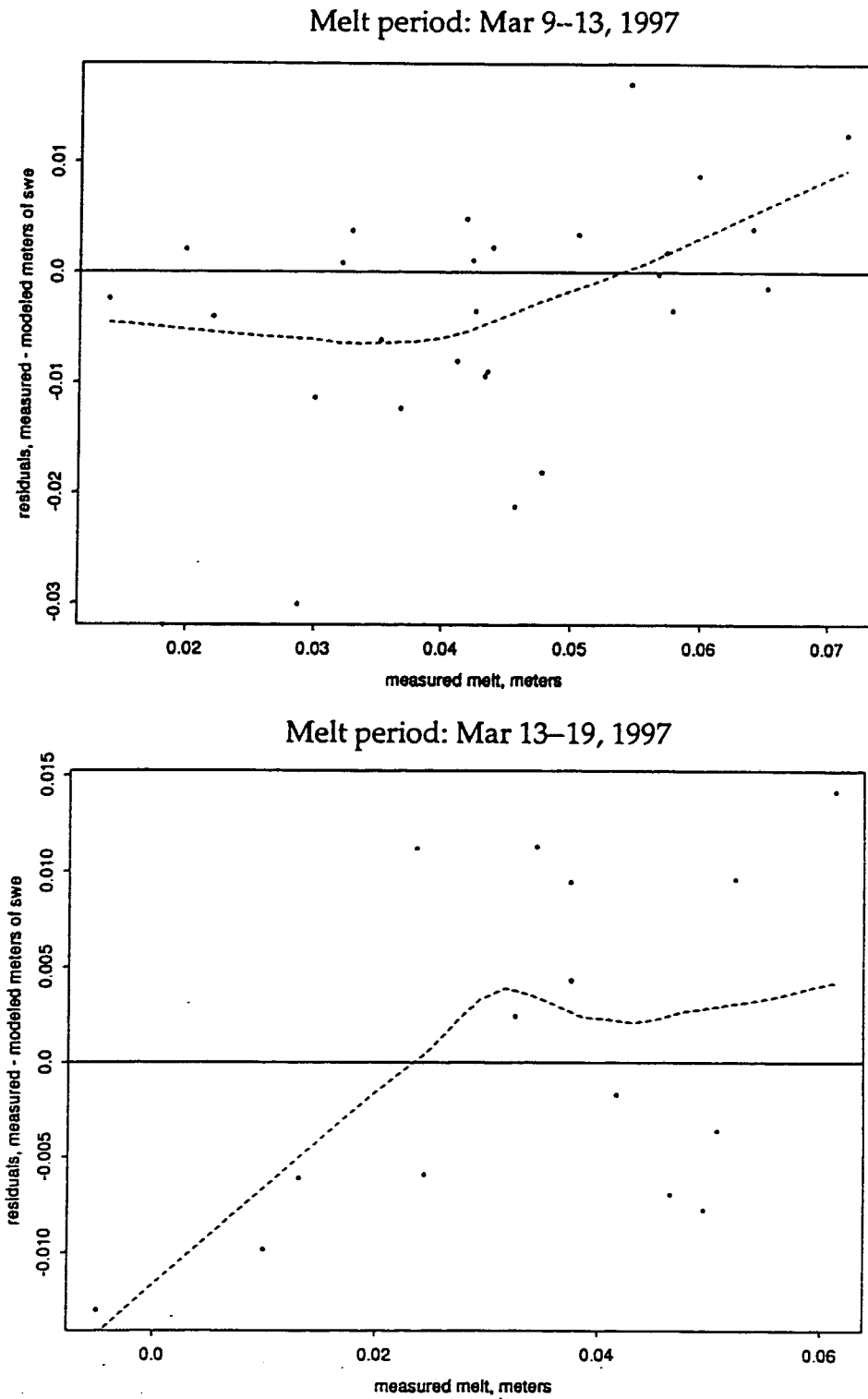


Figure 17. Plot of residuals (measured melt minus TopoFECS estimates) vs. measured melt: Smithfield Dry Canyon.

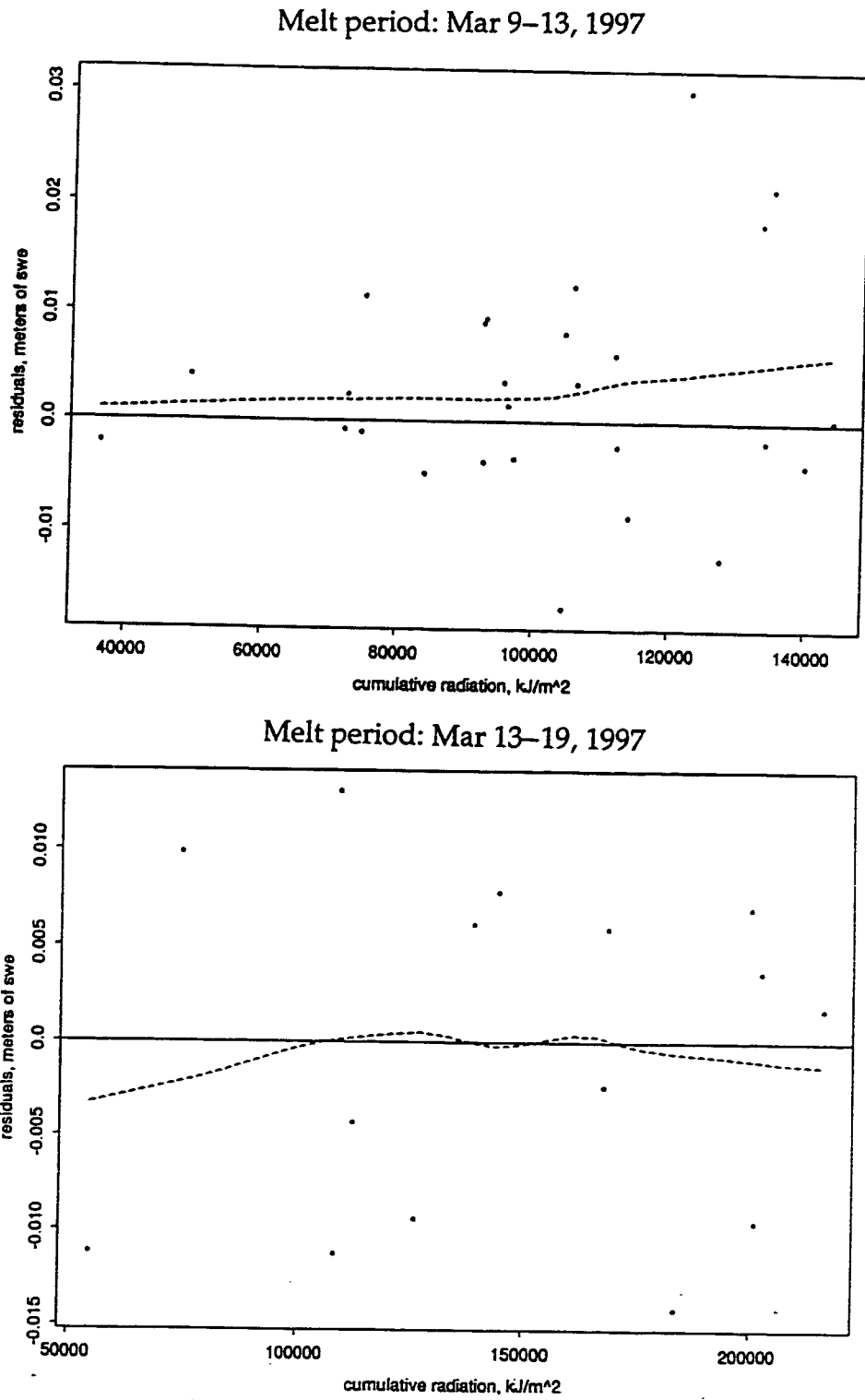
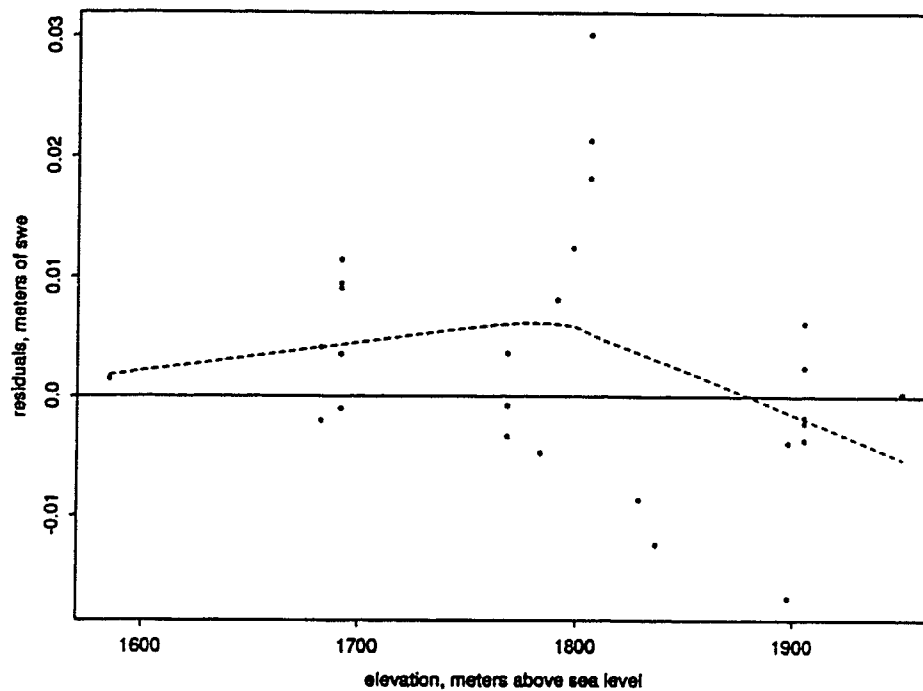


Figure 18. Plot of residuals (measured melt minus TopoFECS estimates) vs. cumulative radiation, Smithfield Dry Canyon data.

Melt period: Mar 9–13, 1997



Melt period: Mar 13–19, 1997

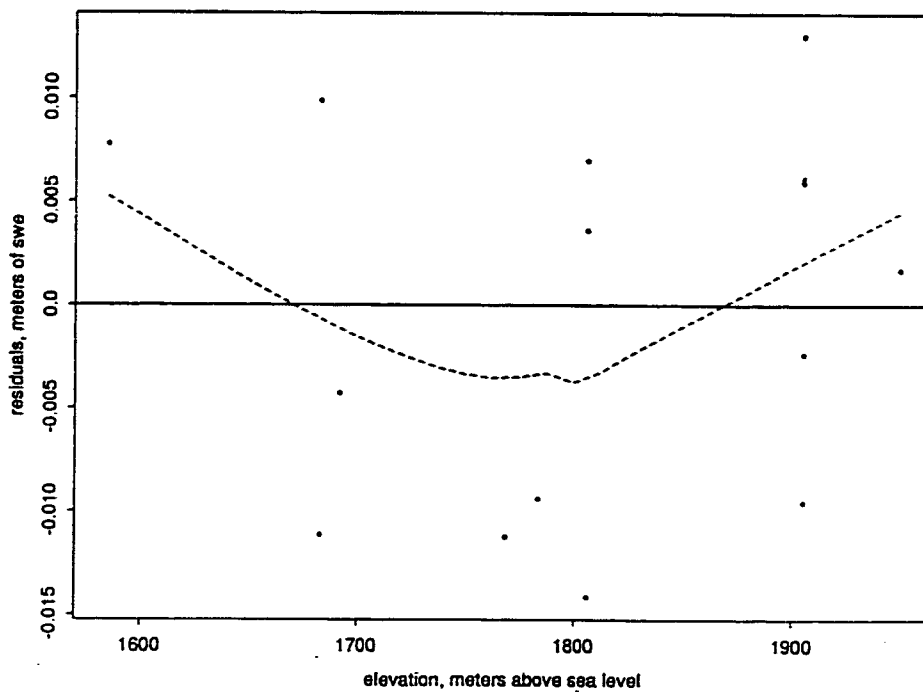


Figure 19. Plot of residuals (measured melt minus TopoFECS estimates) vs. elevation, Smithfield Dry Canyon data.

versus elevation. Again, solid lines are drawn across the plots where the residuals equal zero, and LOESS regression lines are plotted as dashed lines. There are no observable trends in either of these plots, suggesting that the linear TopoFECS model is appropriate for modeling data within the ranges of solar radiation extremes and elevation extremes encountered in this data set.

A noticeable feature of Figure 19 (particularly in the top plot) is the “clumping” of points at different elevations. This is an artificial effect created by the nature of the data collection method. As shown in Figure 3, many of the data points were located in clusters to increase the measurement efficiency. The data points within these clusters had similar elevations. Naturally, points that were clustered close together tended to melt somewhat similarly due to the effects of local topography. Therefore, the residuals tend to clump together according to elevation.

### Selection of Index Points

A crucial element for the practical application of the TopoFECS model is the proper selection of the index points at which to measure melt. Obviously, the points need to be chosen to have unique elevations and radiation indices in order to obtain a unique solution to the regression equations. But how many index points are necessary, and how dissimilar

should the points be (or where should they be located) in order to make reliable predictions? This section attempts to answer these questions by analyzing the impact of using different index points.

### Location of index points

This section examines the problem of choosing the optimal points to use as index points for modeling a watershed. For instance, is it sufficient to use only index points located on west-facing, 15° slopes and similar elevations to model other points with very different slopes, aspects, and elevations? Or instead, should one use extremely varied locations ranging across south-facing and north-facing slopes as well as from the bottom and top of the watershed?

Results from using different index points from both the synthetic as well as the Smithfield Dry Canyon data sets are used in this section to answer this question. The data from Upper Sheep Creek were not evaluated, since the data here have been shown to be too inaccurate for use with the TopoFECS model.

Two factors in the selection of the index points were hypothesized as being important to obtaining reliable results: the “spread” of the index points within the variable space (radiation-elevation space), and the distance (or “offset”) of the center of these index points in variable space from the center of the rest of the data points to be modeled.

The “spread” of the index points within the variable space is a measure of the variability of the index points. If one point is located such that it receives large amounts of solar radiation during the melt period and is at a high elevation, while another point stays mostly in the shade and is at a low elevation, then this will be defined as a large “spread” between them in variable space.

The distance of the center of the index points in variable space from the center of all of the data points (referred to as the “offset”) is a measure of how well the index points represent the average characteristics of the watershed. For instance, if five index points were chosen in the lower elevations of a watershed, and with high radiation indices, then their collective center of mass within the variable space would be offset from the center of mass of the other points in the watershed. However, if five points were chosen with an even distribution throughout the variable space, their collective center of mass would probably fall very near the center of mass for the rest of the watershed.

In order to determine how the “spread” of the index points and the “offset” of the index points affect the accuracy of the TopoFECS model, a Monte-Carlo procedure was adopted to repeatedly select a specified number of points at random to be the index points for applying the TopoFECS model. After the parameters  $\alpha(t)$ ,  $\beta(t)$ , and  $\gamma(t)$  were obtained and the estimates of

melt at the rest of the points were calculated, the median absolute error (MedAE) of the estimates was calculated and recorded. Since the radiation values were of a much larger magnitude than the elevation values, the radiation-elevation space was scaled according to the range of the radiation and elevation values of all of the points in the data set. The area in this scaled radiation-elevation space formed by the convex hull of the index points was calculated and recorded, as a measure of the “spread” of the index points. Finally, the Euclidean distance in this scaled radiation-elevation space between the center of the index points and the center of all data points was recorded as a measure of the “offset.” This process was repeated 400 times for each analysis.

Two melt periods were analyzed from both the synthetic data set and the Smithfield Dry Canyon data set. From the synthetic data set (created in the “Initial Model Testing” section), periods April 5–7 and 17–19 were chosen. Smithfield Dry Canyon melt data from March 9–13 and from March 13–19 was used.

#### Effect of “spread”

Figure 20 displays plots of the results using the synthetic data and 400 groups of three randomly selected index points. The x-axis shows the standardized area in radiation-elevation space encompassed by the index points, or the “spread,” and the y-axis shows the median absolute error

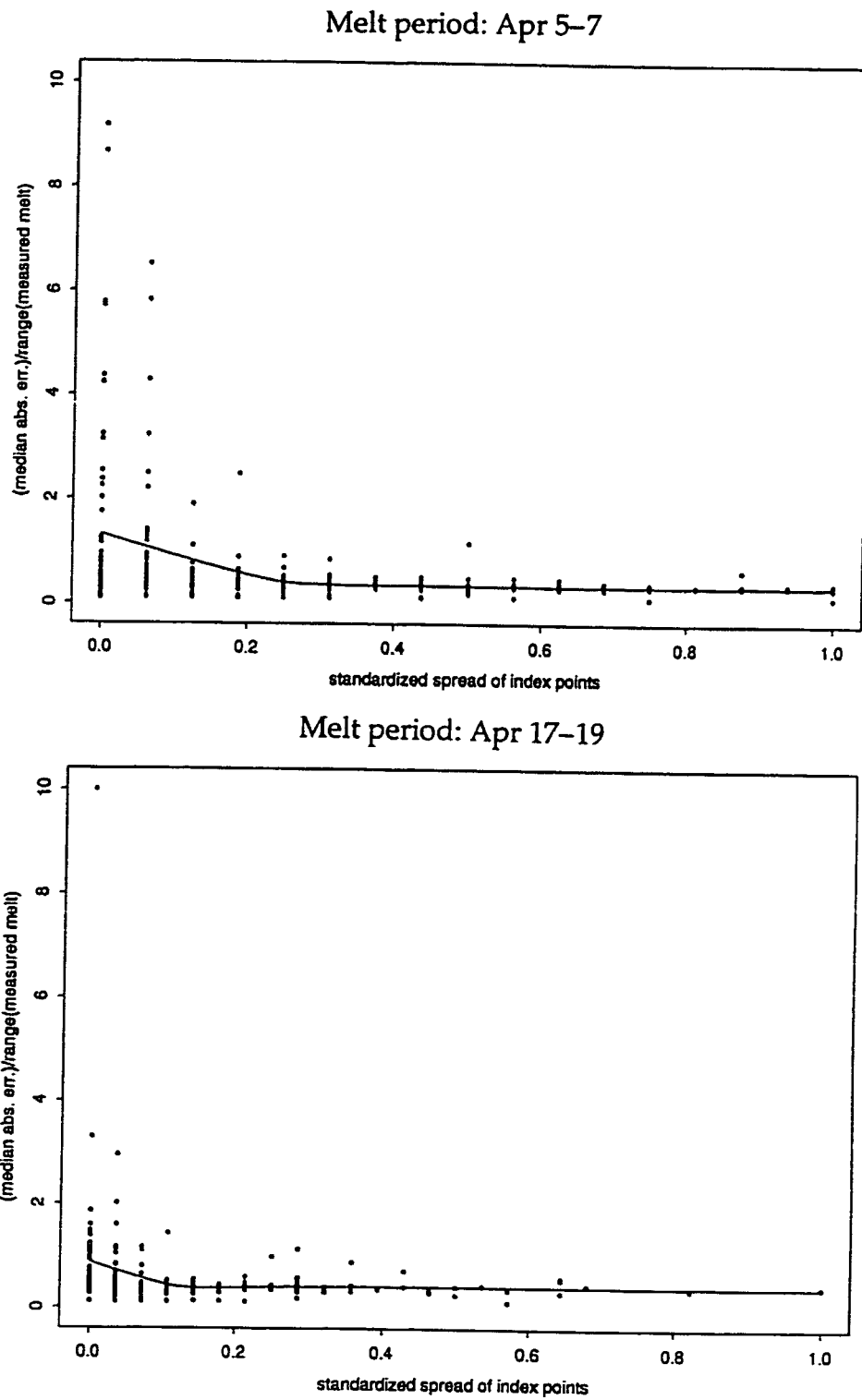


Figure 20. Median absolute modeling error vs. spread of three (3) index points: synthetic data.



(MedAE). The area was standardized by dividing by the largest recorded value of area obtained, and the MedAE values were standardized by dividing by the range of the observed melt values. The data points were very scattered, and so LOESS regression lines were drawn through the data to show the trends. These lines show a decrease in MedAE (or an increase in predictive accuracy) with an increase in "spread." This is due to the stabilizing effect of spreading out the index points in space. If the index points are too close together, the regression equations become unstable. Therefore, using highly dissimilar index points at the extremes of the elevation and radiation ranges tends to produce more reliable results.

Figure 21 shows the results of using the same data and time periods used in Figure 20, but employing five random index points instead of three. As can be seen, the trend observed in Figure 20 is missing. This is due to the stabilizing effect of adding two more index points to the regression, which enabled nearly all of the regressions to produce fairly low values of MedAE.

Figure 22 gives two more similar graphs displaying the results of using five randomly selected index points to model the Smithfield Dry Canyon data. In both of these plots, there is an obvious decrease in MedAE as the index points are spread out further in radiation-elevation space. By comparison with Figure 21, it can be inferred that the "spread" of the index

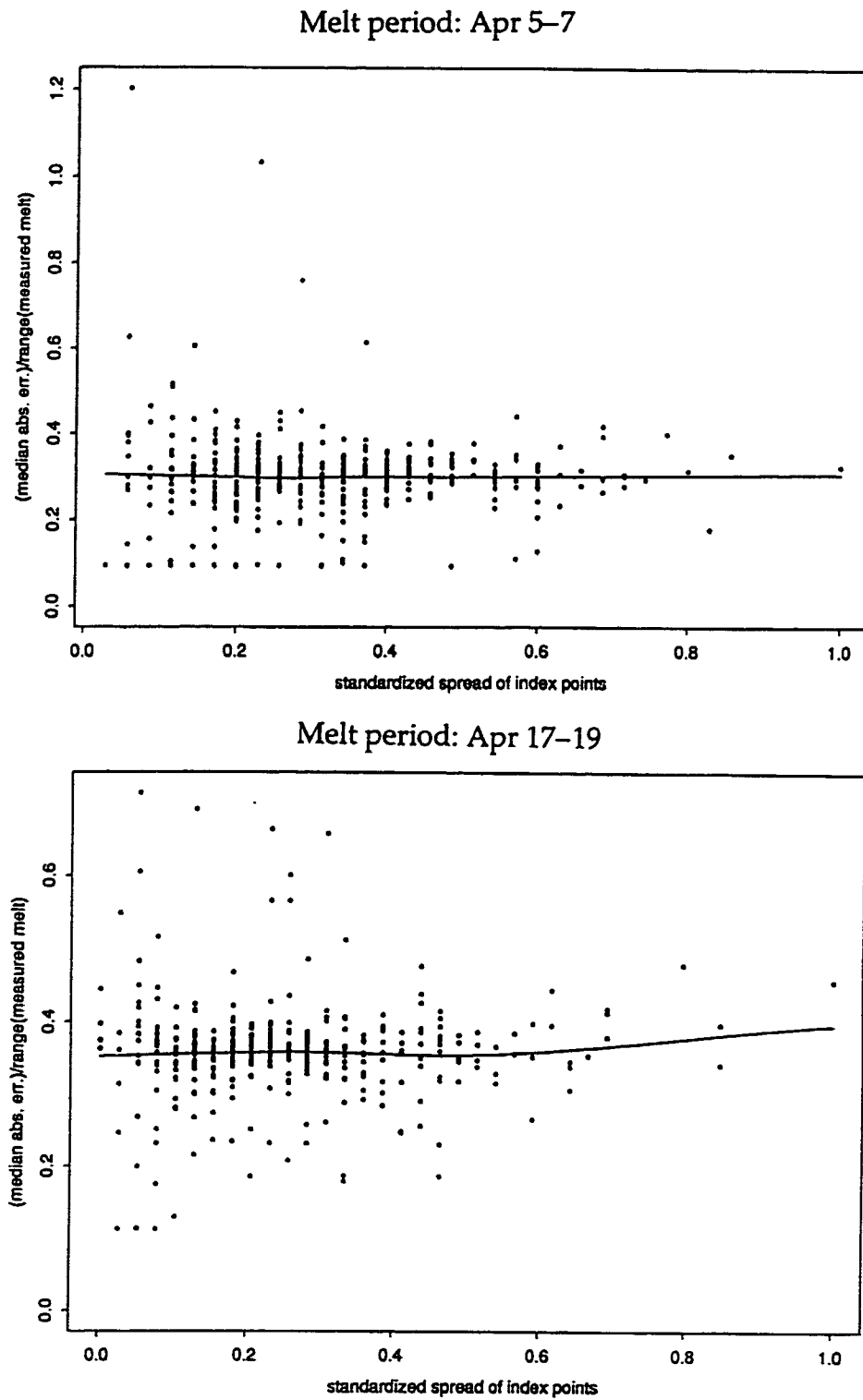
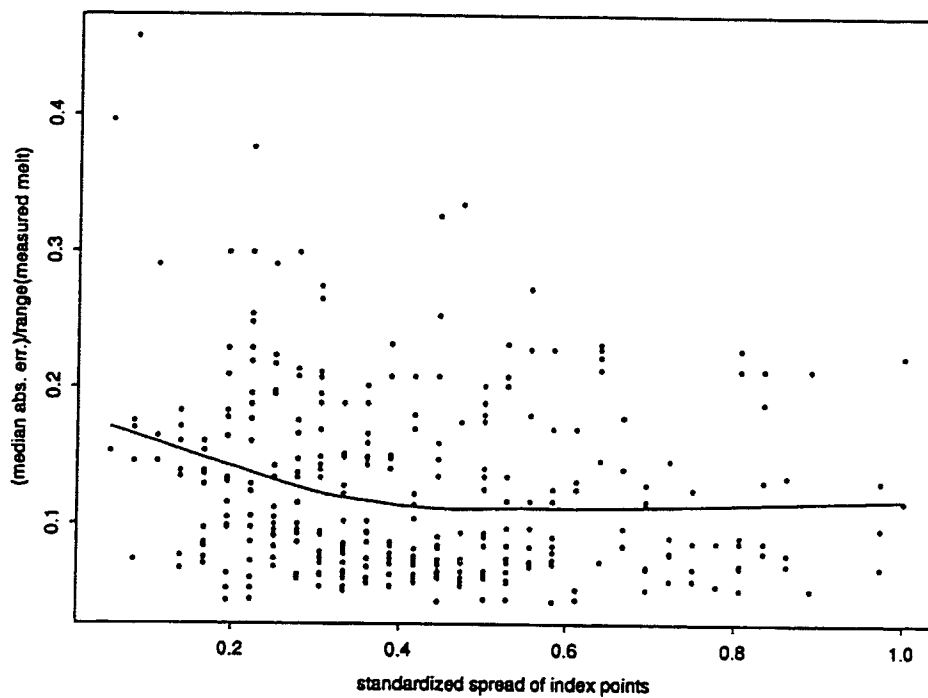


Figure 21. Median absolute modeling error vs. spread of five (5) index points: synthetic data.

Melt period: Mar 9–13, 1997



Melt period: Mar 13–19, 1997

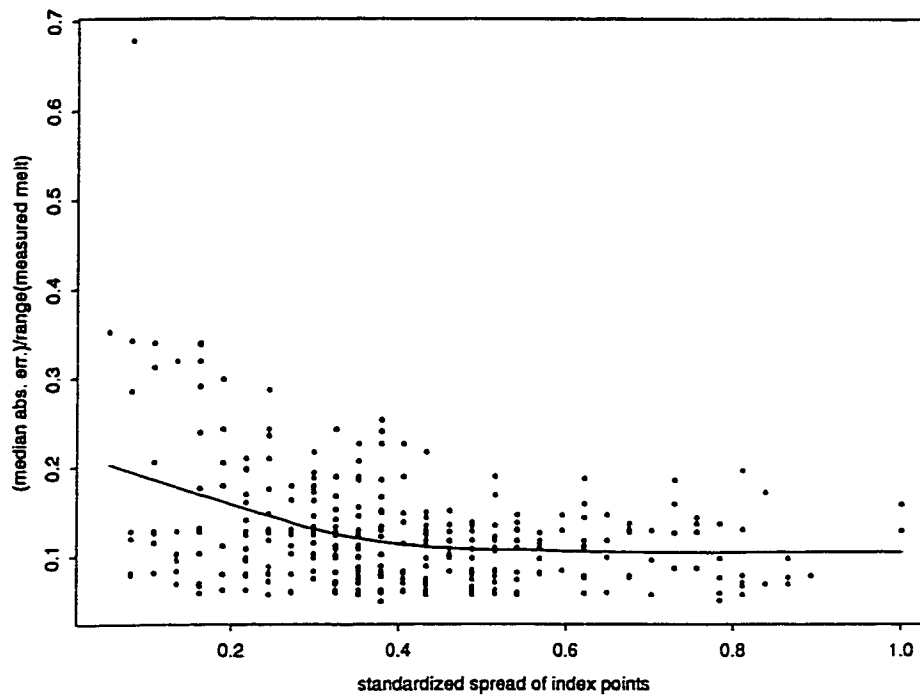


Figure 22. Median absolute modeling error vs. spread of five (5) index points: Smithfield Dry Canyon data.

points in radiation-elevation space is more crucial with real data where measurement noise is a concern.

### Effect of "offset"

Figure 23 shows the same data used in Figure 20 (synthetic data, three random index points used in the regressions), except here the standardized MedAE values are plotted against the standardized "offset" (Euclidean distance in a scaled radiation-elevation space) of the center of the index points from the center of all data points. Here, the "offset" was standardized by dividing by the largest recorded "offset" value. Again, a solid LOESS regression line was drawn through the points to show the trends. Though the first graph shows no obvious trend, the second one shows a pronounced increase in MedAE with an increase in the "offset." This is expected, since an increase in "offset" moves the index points further from the middle of the data, resulting in a less representative regression.

Similarly, Figure 24 displays the same data used in Figure 21 (synthetic data, five random index points used in the regressions), but plots the standardized MedAE against a standardized "offset" rather than "spread." The LOESS regression line shows no clear trend in either graph, due once more to the stabilizing effect of using two additional index points in the regression.

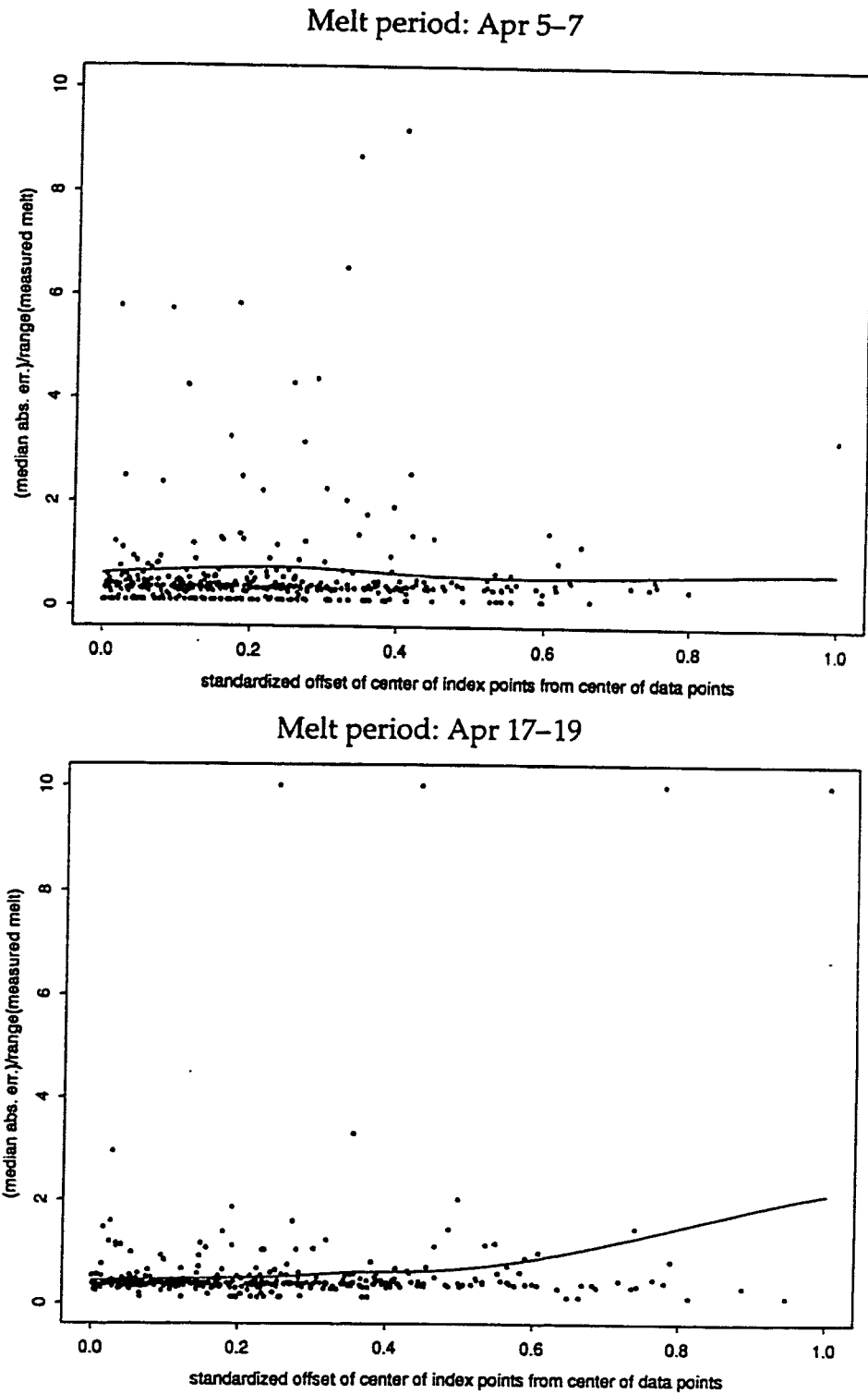
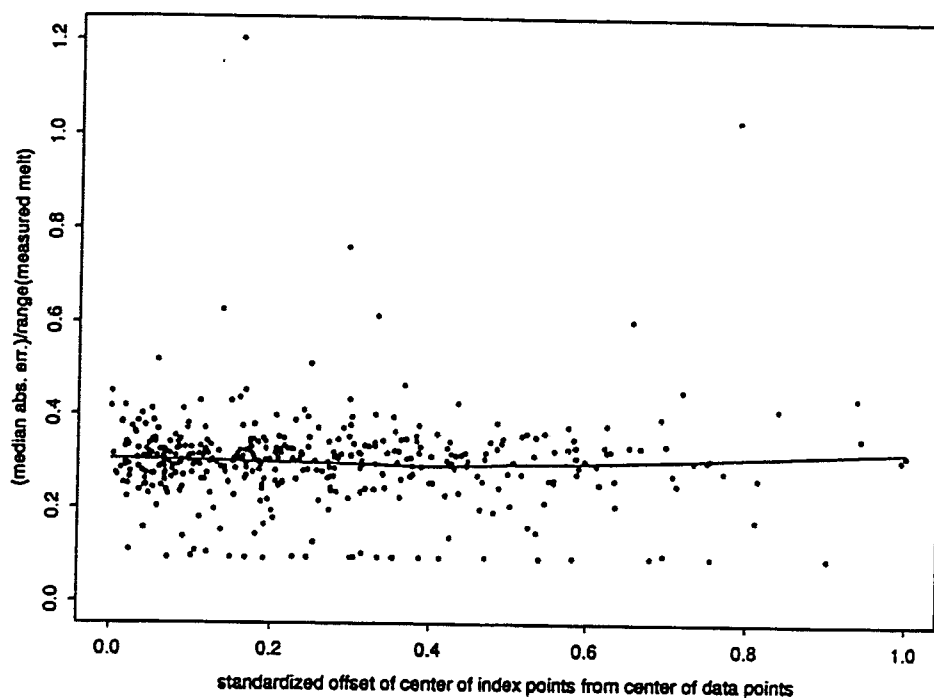


Figure 23. Mean absolute modeling error vs. offset of center of three (3) index points from center of data points: synthetic data.

Melt period: Apr 5-7



Melt period: Apr 17-19

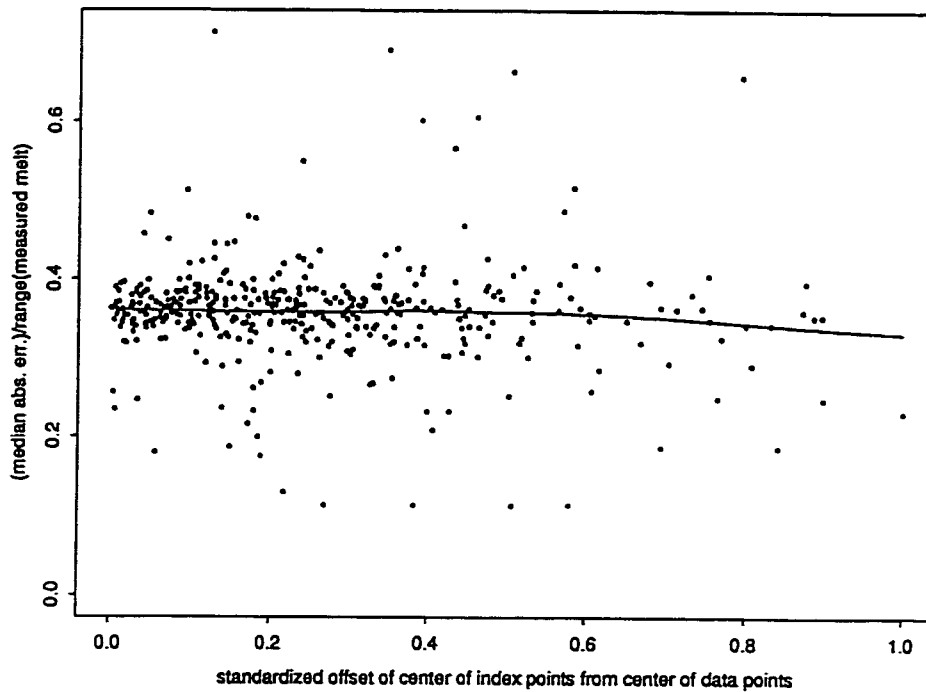


Figure 24. Mean absolute modeling error vs. offset of center of five (5) index points from center of data points: synthetic data.

Figure 25 plots the data from Figure 22 (Dry Canyon data, 5 random index points used in the regressions) against “offset.” In both of these graphs, the LOESS regression lines show clear trends towards higher MedAE values, or worse predictions, with increasing “offset.” It can be inferred by comparison with Figure 24 that the choice of index points with a low “offset” is most important when using real data with measurement noise.

#### Comparative effects of “spread” and “offset”

Finally, Figures 26–28 show 3-D perspective plots of the standardized MedAE versus the standardized distance between the centers of the index points and the rest of the points (or “offset”), and versus the standardized area in radiation-elevation space encompassed by the index points (“spread”). These plots were smoothed by LOESS regressions in order to capture the underlying trends. They basically show the same trends as revealed in the 2-D plots, but they also show the relative importance of each effect. Figures 26 and 28 show that the “spread” of the index points is the largest determining factor in the accuracy of the estimates, and the “offset” appears to play a relatively smaller role in model performance. An examination of the z-axes of the plots in Figure 27 (where 5 random index points were used to regress on the synthetic data) reveals that these surfaces are essentially flat and exhibit no real trends. This is consistent with the lack

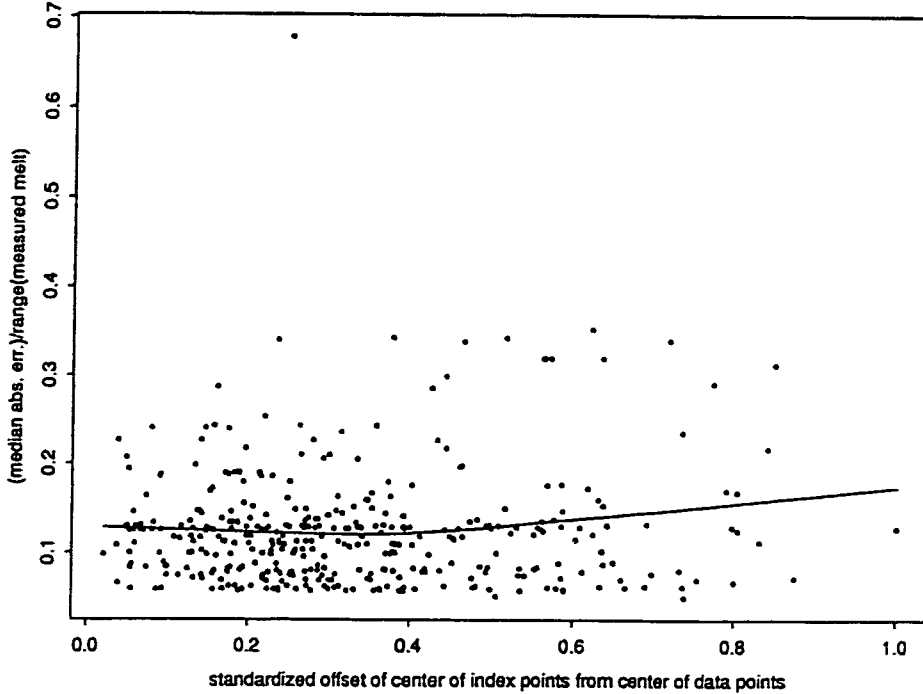
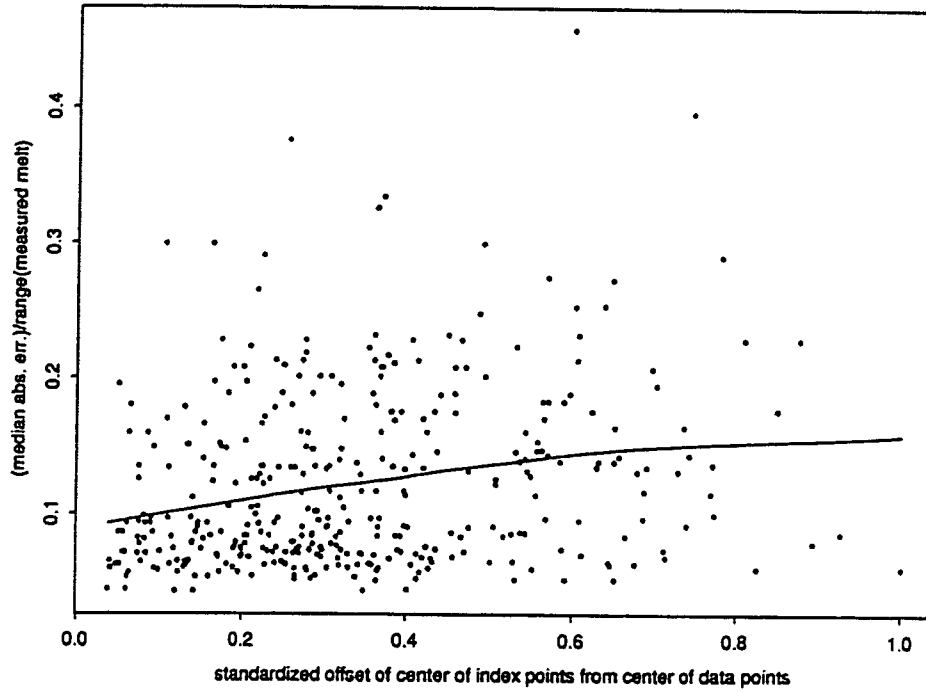
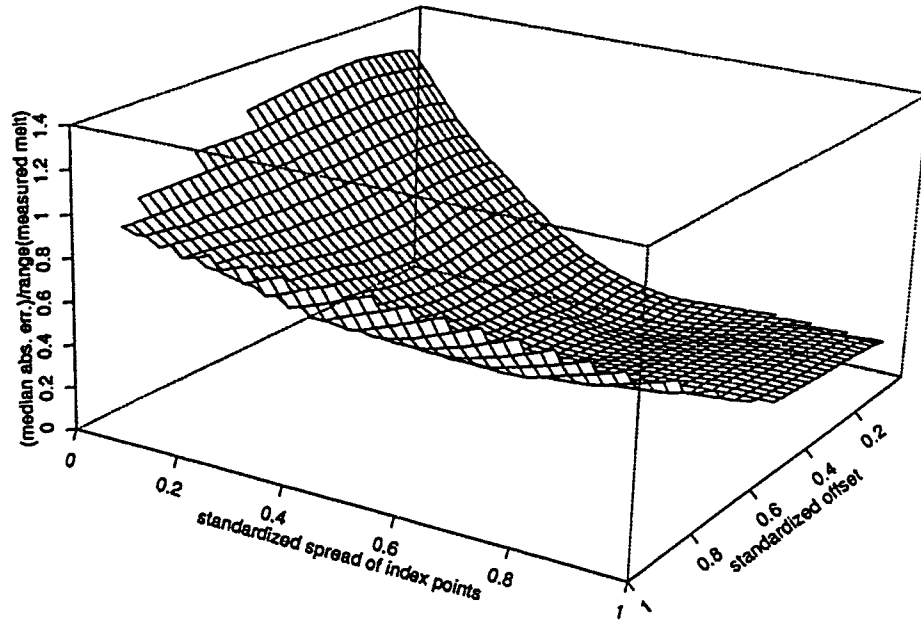


Figure 25. Mean absolute modeling error vs. offset of center of index points from center of data points: Smithfield Dry Canyon data.



Melt period: Apr 5-7



Melt period: Apr 17-19

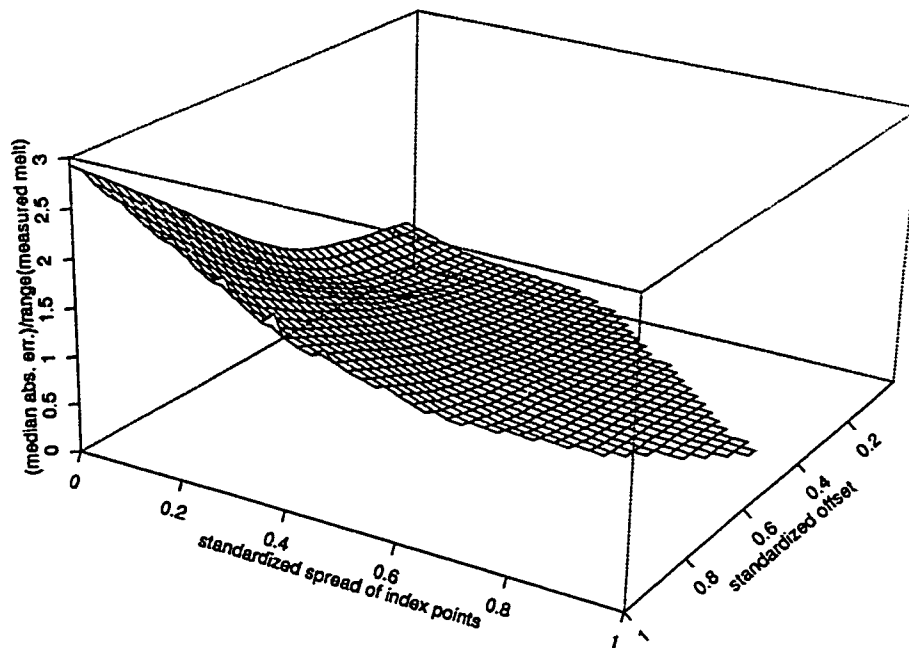
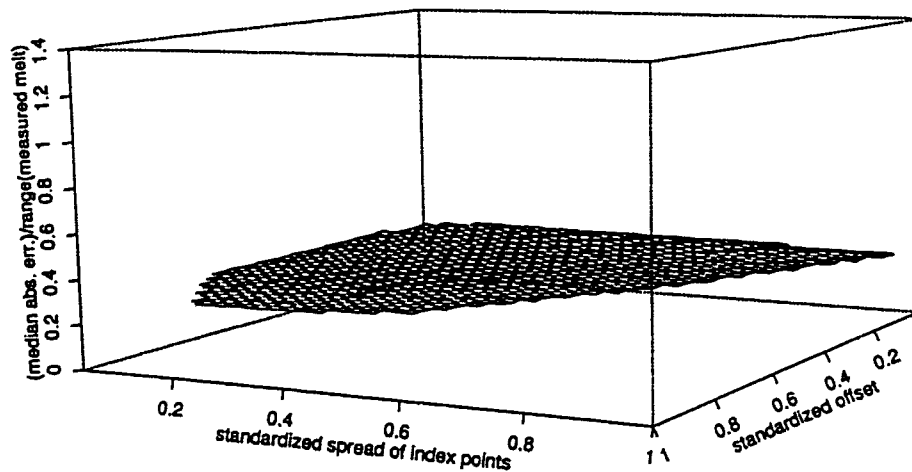


Figure 26. Loess-smoothed surface of median absolute modeling error vs. standardized spread of three (3) index points and standardized offset of index points from center of data points: synthetic data.

Melt period: Apr 5-7



Melt period: Apr 17-19

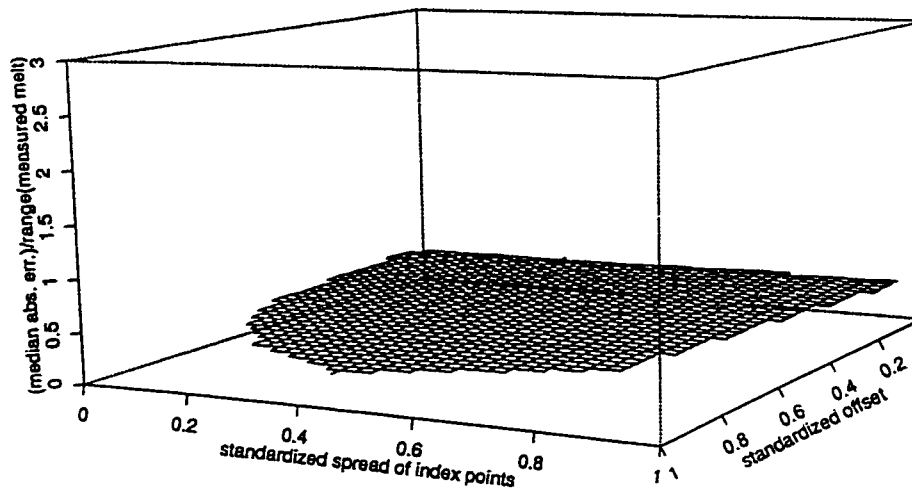
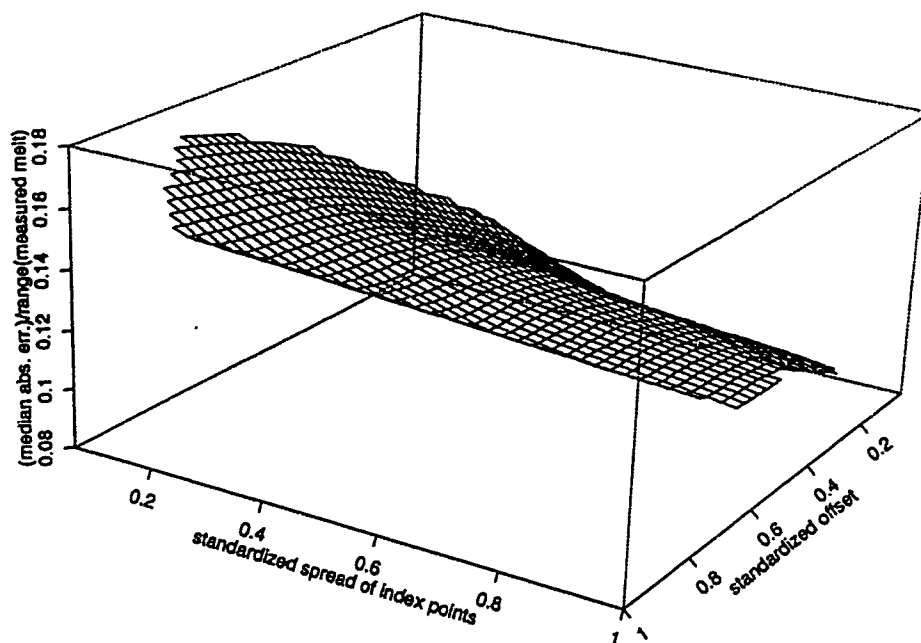


Figure 27. Loess-smoothed surface of median absolute modeling error vs. standardized spread of five (5) index points and standardized offset of index points from center of data points: synthetic data.

Melt period: Mar 9–13, 1997



Melt period: Mar 13–19, 1997

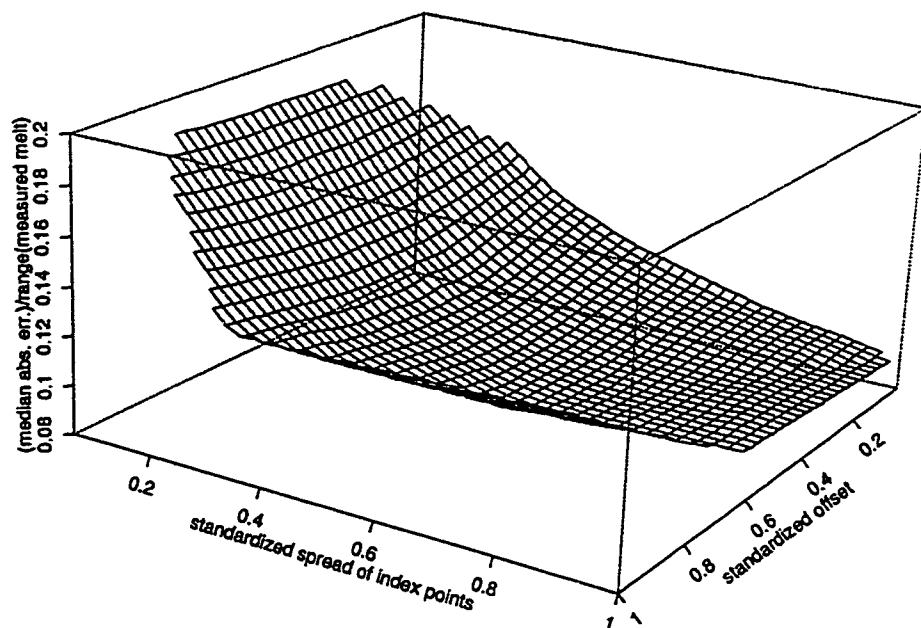


Figure 28. Loess-smoothed surface of median absolute modeling error vs. standardized spread of five (5) index points and standardized offset of index points from center of data points: Smithfield Dry Canyon data.

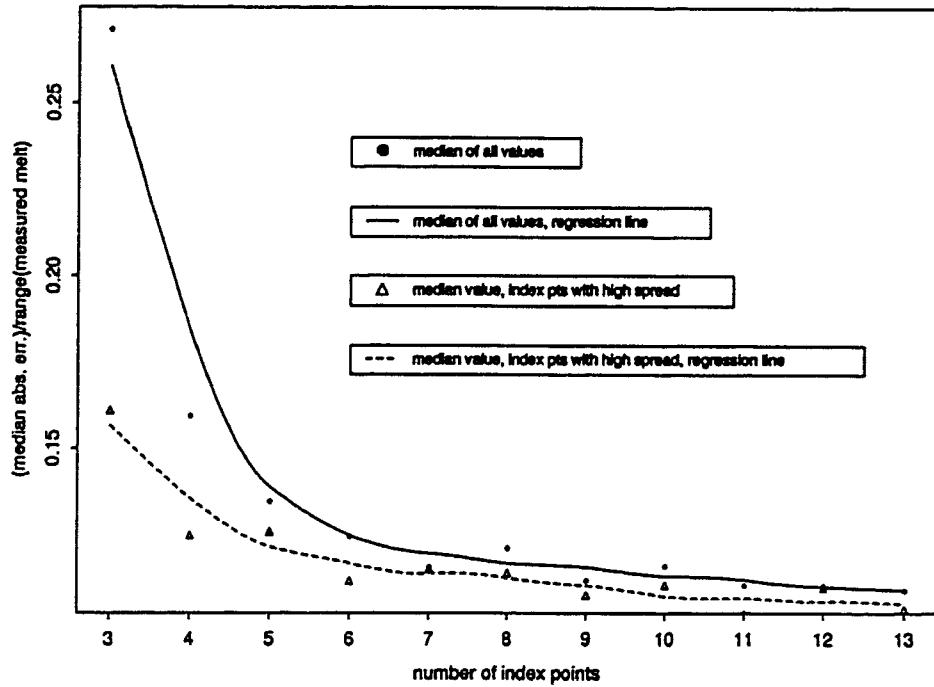
of trends revealed in the 2-D plots of Figures 21 and 24.

#### Number of index points used

In order to determine the benefits of using more index points in the TopoFECs regression, the model was applied 100 times using different sets of three randomly selected index points each time. The “spread” of the index points (measured as the area in elevation-radiation space encompassed by the convex hull of the index points) was computed, the melt estimates were calculated for all points, and the associated median absolute error (MedAE) values and mean absolute error (MAE) values for the predictions were recorded for each of the 100 iterations. This process was repeated using four index points, five index points, and so on using up to 13 random index points. This procedure was applied to each of the same time periods used in the previous section entitled “Location of index points” for both the synthetic data sets and the Smithfield Dry Canyon data.

Figure 29 shows the results of performing this analysis with the Smithfield Dry Canyon data. Here, the MedAE values standardized by dividing by the range of the measured melt values are plotted against the number of index points used. The solid points show the median of the MedAE values versus the number of index points used. The solid line through these points is a LOESS regression line spanning 40% of the data. Next, the MedAE’s of each group of 100 realizations were sorted according

Melt period: Mar 9–13, 1997



Melt period: Mar 13–19, 1997

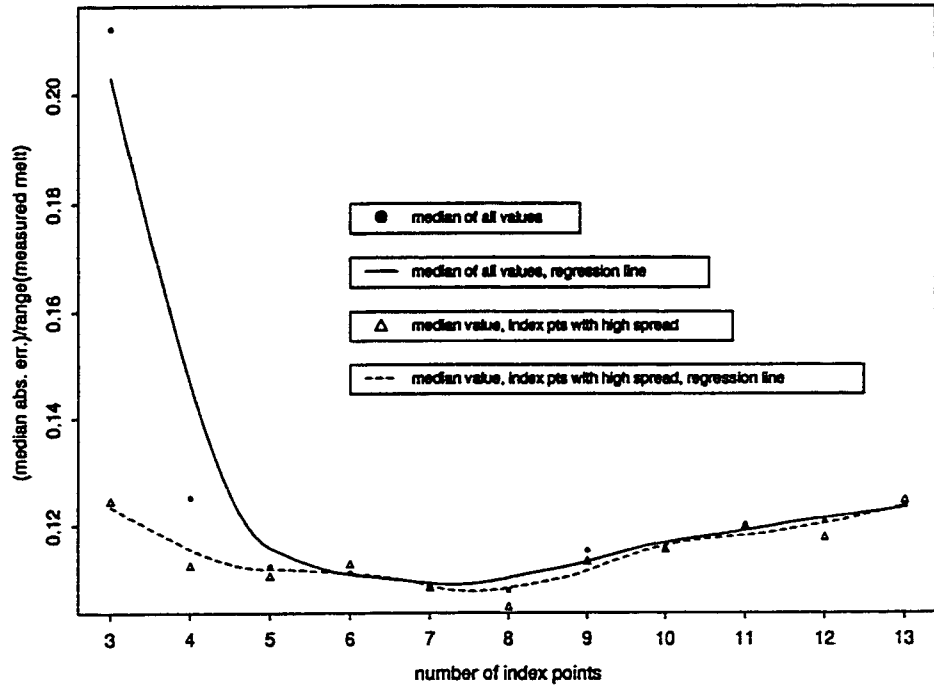


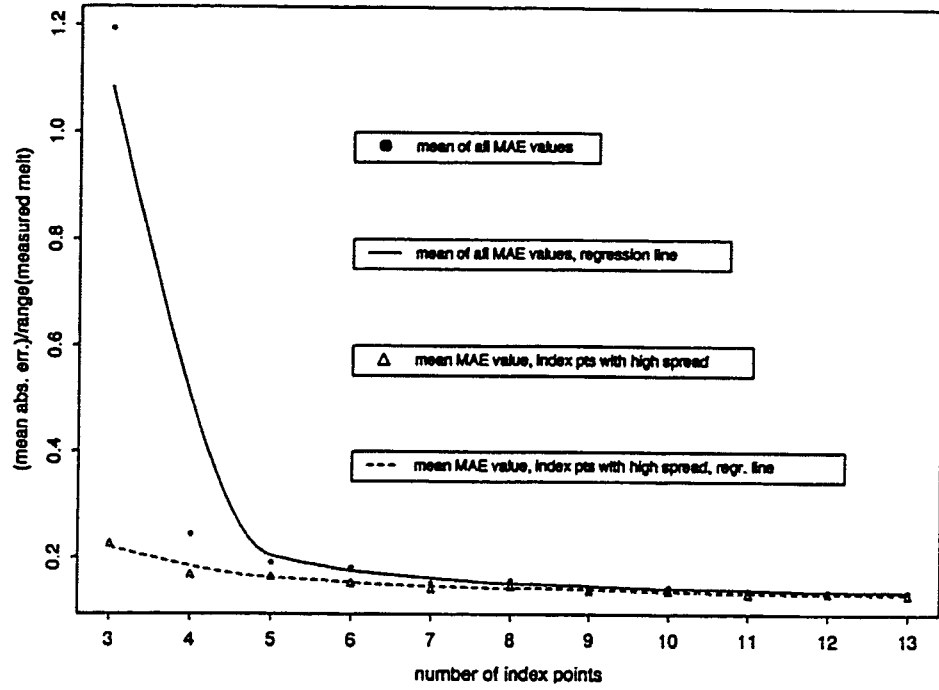
Figure 29. Median absolute modeling error vs. number of index points used: Smithfield Dry Canyon data.

to the “spread” in variable space of their associated combination of index points. The median of the MedAE values for the 34 realizations having the highest spread in each group of 100 iterations (highest third) was plotted against the number of index points used (shown as triangles in Figure 29).

The first graph in Figure 29 shows the expected decrease in modeling error associated with increasing the number of index points used in the calibration. It also shows how selecting index points with a high “spread” can increase modeling accuracy even more. However, the second graph (depicting the melt period from March 13–19) shows an eventual increase in MedAE with the use of more than eight index points. The reason for this counter-intuitive trend lies in the use of the median absolute error (MedAE) to measure model performance. Since there are only 15 available data points in the time period from March 13–19, the median value for modeling error will correspond to the eighth most accurately modeled point. Therefore, if 8 index points are used, that eighth point will be included in the regression and will be very accurately modeled. However, if all 15 points are used, the eighth point will still be included in the regression but it will not have as much influence on the regression and consequently will not be modeled quite as well.

To circumvent this problem, the mean absolute error (MAE) was used instead of the MedAE as a measure of model performance in Figure 30. Here

Melt period: Mar 9–13, 1997



Melt period: Mar 13–19, 1997

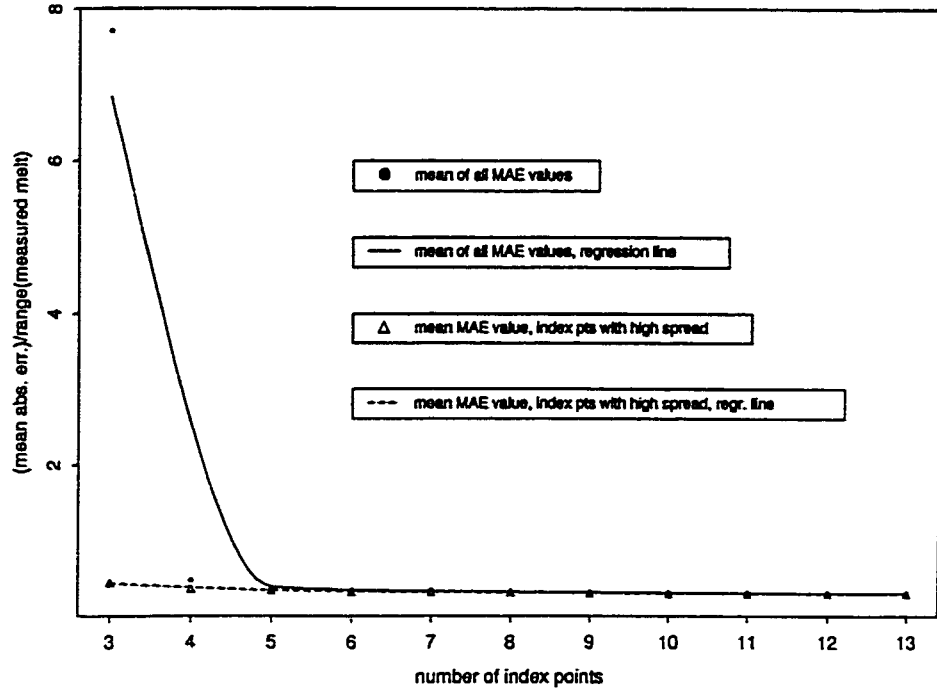


Figure 30. Mean absolute modeling error vs. number of index points used: Smithfield Dry Canyon data.

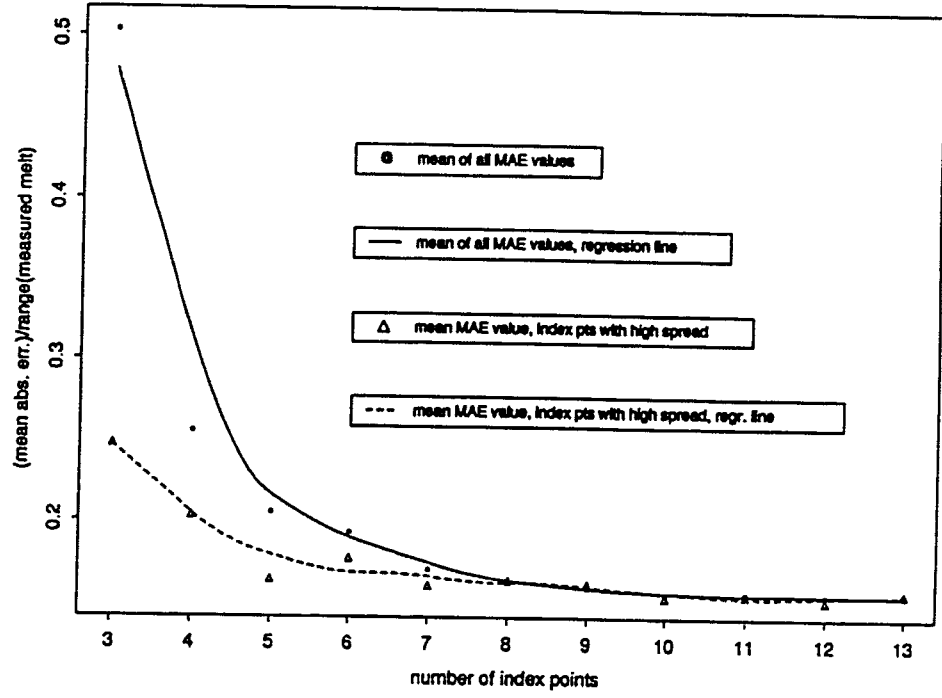
again, the solid points show the mean of the MAE values divided by the range of the measured melt values versus the number of index points used, and the solid line is a LOESS regression line spanning 40% of these points. The triangles represent the mean of the MAE values for the top 34 out of 100 realizations having the highest spread, and the dotted line is the LOESS regression line through these points. These plots conform to expectations much better than the plots in Figure 29, due to the use of the mean rather than median error as a measure of model performance.

Figure 30 shows that the improvement in modeling accuracy gained by using additional points only marginally increases after about five points. This figure also shows that if the index points were chosen to have a high degree of variability or "spread," four index points were sufficient to accurately model the melt for these two time periods.

Figure 31 shows the same analysis for the synthetic data (using MAE again as a measure of modeling performance). The top graph (April 5–7) shows a continuing, significant increase in modeling accuracy with the use of more index points up to about eight index points. However, it also shows that if the points are chosen to have a high degree of "spread," perhaps only five are needed to produce reliable results for this time period. The bottom graph (April 17–19) shows that perhaps only three or four well selected index points are necessary to reliably calibrate the TopoFECs model for



Melt period: Apr 5-7



Melt period: Apr 17-19

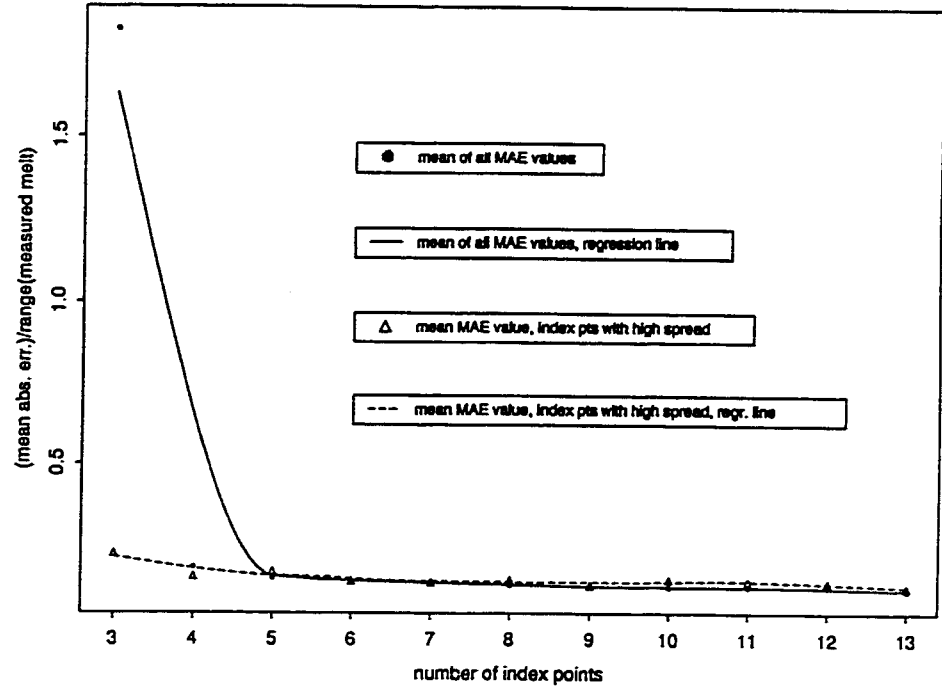


Figure 31. Mean absolute modeling error vs. number of index points used: synthetic data.

this second time period.

From this analysis, it appears that between four and six well chosen index points are required to obtain optimal results using the TopoFECS model. Obviously, if the measurements are not very accurate, more index points will be needed, though, to achieve a reliable regression.

### Effect of Weather Conditions on Model Accuracy

In this analysis, 36 new points were randomly generated within the same topographic ranges used to generate the 200 points in the “Initial Model Testing” section. The UEB model was used to simulate the accumulation and ablation of the snow at these points, and the resulting simulated SWE at each point was recorded at 24-hour intervals and used to determine the effect of cloud cover on the TopoFECS model. The 168 days during the snow accumulation/ablation season were divided into two categories: cloudy and clear days. Days in which the available solar radiation values were less than half of the clear-sky radiation were considered cloudy days, while the rest were lumped together as clear days. A global regression on all 36 points was used to estimate the  $\alpha(t)$ ,  $\beta(t)$ , and  $\gamma(t)$  parameters, and then these parameters were used to calculate estimates of melt at each of the 36 points at daily time steps throughout the snow season. Finally, the TopoFECS versus UEB modeled melt at each point was

compared for cloudy and clear days separately, and NS values for each of the 36 sites were computed. These are plotted in Figure 32. The +’s represent the NS values for each point for the cloudy days, and the triangles represent the NS values for each point for the clear days. As can be seen, the estimates for the cloudy days are consistently better than those for the clear-sky days.

There are two possible reasons for this observation:

1. The dependence of melt (as simulated by the UEB model) upon radiation is nonlinear. For days with larger radiation, the linear TopoFECs model has relatively more difficulty fitting the data.

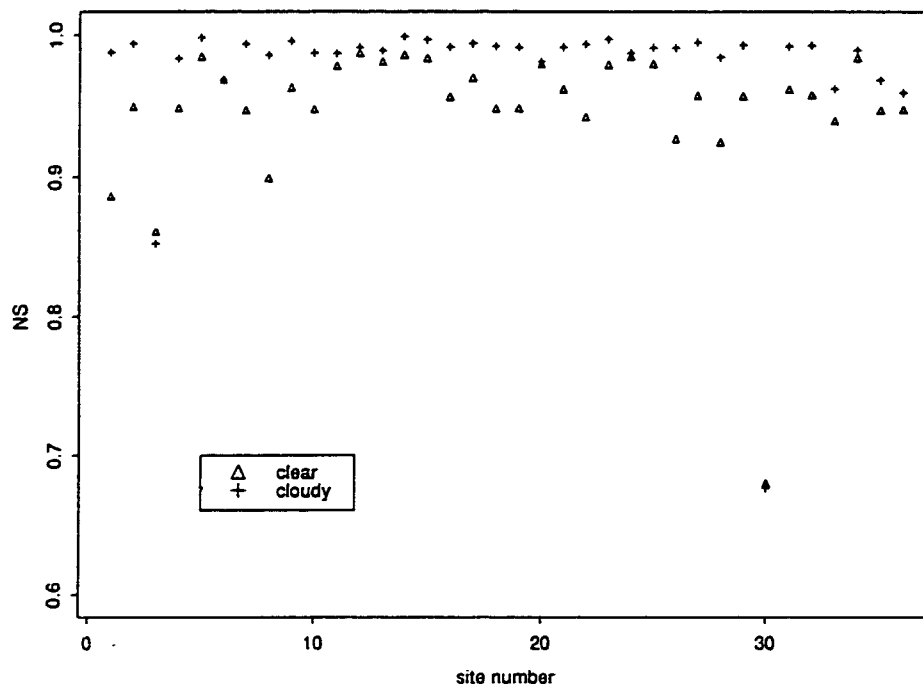


Figure 32. Effect of cloud cover on model accuracy: synthetic data.

2. The range of radiation and consequently melt values is greater for clear days than for cloudy days. The TopoFECS regression may be relatively worse for larger ranges in melt values.

### Effect of Spatial Scale of Application on Model Accuracy

In this section, the spatial scale of application for the model is defined as the spatial range over which the same  $\alpha(t)$ ,  $\beta(t)$ , and  $\gamma(t)$  parameters may be applied with an expectation of reasonable results. As the spatial scale of application increases, there will be an associated decrease in predictive accuracy. For example, if only one value for each of the  $\alpha(t)$ ,  $\beta(t)$ , and  $\gamma(t)$  parameters were used to simulate melt across the entire Rocky Mountain Range, one could not expect to obtain reasonable melt estimates everywhere. Both the elevation differences as well as the weather differences across the mountain range imply that several very different melt conditions probably exist within that large area.

There are two distinct spatial scales that are addressed in this section: the vertical scale and the horizontal scale. The vertical scale deals with the effect that elevation has on melt energy, while the horizontal scale deals with how weather changes with lateral distance across a basin. These two scale issues are discussed in detail next.

### Vertical scale

The TopoFECS model's linear regression of melt against elevation will lose accuracy with increasing ranges of elevation, since melt is not truly a linear function of elevation. However, reasonable results can be obtained over small elevation ranges, such as those obtained for the Smithfield Dry Canyon data, which had an elevation range of 366 meters. In watersheds with greater relief, the model's accuracy can be maintained by dividing the watershed into elevation zones. How great can the range in elevation be within each zone, though, if the model is still to obtain reasonable results?

In order to explore the tradeoff between elevation range and model accuracy, data from the same 200 points that were synthetically generated for the Initial Model Testing section was used. Only the days between April 5–April 21 were considered: the same time period modeled to produce Figure 6. These 200 points were divided into 75 meter zones for the first trial, then 150 meter zones for the next, 225 meter zones for the next, and so on up to the last trial with one zone covering the whole 1500 meter range of data points. For each trial, the TopoFECS model was applied to each elevation zone using a global regression on all of the points within the zone to determine the  $\alpha(t)$ ,  $\beta(t)$ , and  $\gamma(t)$  parameters. The mean absolute error for all of the points was calculated for each trial, and the results are plotted against their respective elevation zone size in Figure 33.

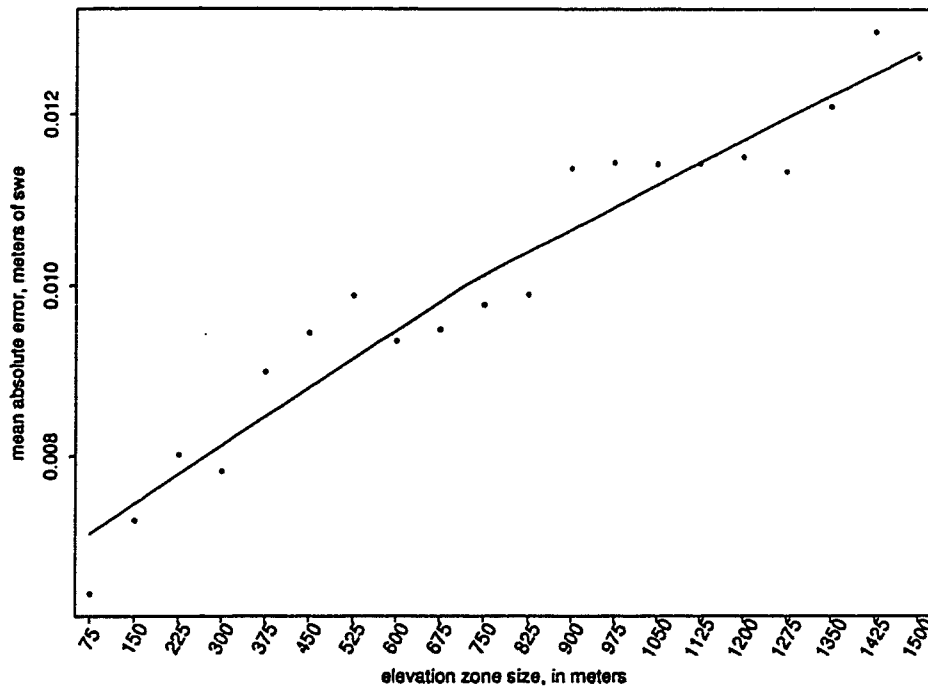


Figure 33. Effect of subdividing basin into multiple elevation zones.

Though this plot shows an obvious decrease in accuracy associated with lumping small elevation zones together into larger elevation zones, this does not mean that one should necessarily divide a basin into extremely small zones to obtain reasonable results. For each elevation zone, at least three measurements must be made to calculate the  $\alpha(t)$ ,  $\beta(t)$ , and  $\gamma(t)$  parameters for the zone. This becomes impractical quickly with more and more elevation zones. However, the magnitude of the errors obtained using the entire 1500 meters as one elevation zone was relatively small (averaging

.0125 meters over a 2-day time step) and acceptable for most applications. Upon comparison of the accuracy of the model results using only one elevation zone with the accuracy of using the model on the field data from Smithfield Dry Canyon (which has a much smaller elevation zone size; only 366 meters), it becomes apparent that the measurement error of real data far surpasses and overshadows the error incurred by not subdividing a basin into smaller elevation zones. Therefore, dividing a basin into different elevation zones is probably not worthwhile unless one is trying to model an extremely high-relief watershed where the summits are exposed to weather regimes that are markedly different from the weather in the valleys.

#### Horizontal scale

As the area of the terrain to be modeled grows, the weather across the terrain will have greater and greater variability, causing the model to err. The horizontal scale of application for the TopoFECS model will therefore be a function of the characteristic scale of variability of the weather. This will vary according to location. In order to use the TopoFECS model in basins larger than the characteristic scale of variability of the weather, the basin must be decomposed into subbasins that are modeled separately with different  $\alpha(t)$ ,  $\beta(t)$ , and  $\gamma(t)$  parameters. None of the available data sets are extensive enough to explore this horizontal scaling issue.

### Effect of Time Step Size on Model Accuracy

In order to examine the impact of different time step sizes on the model results, the TopoFECS model was used to estimate synthetic melt data at differing time steps, ranging from hourly to weekly. The data from the same 36 points used in the section entitled “Effect of Weather Conditions on Model Accuracy” were used in this analysis. Five index points with a large range of radiation and elevation values (large “spread” in radiation-elevation space) were chosen to calibrate the TopoFECS model. Once the TopoFECS estimates were obtained, the median absolute error (MedAE) between the UEB-generated results and the TopoFECS estimates was calculated for each time step length using all 36 points during the melt period from April 5–21. Figure 34 shows these MedAE values divided by the range of the measured melt during the time steps plotted versus the number of hours used in the time step.

As can be seen, the TopoFECS model performed relatively poorly for all time steps that were not multiples of 24 hours. With all time steps that were in multiples of 24 hours, though, the model appears to perform uniformly well. A possible explanation for this phenomenon lies in the TopoFECS model’s omission of a “cold-content” in the snowpack. The “cold-content” is the amount of energy required to raise the temperature of the snowpack up to an isothermal 0°C. For example, after a cold night, all of the



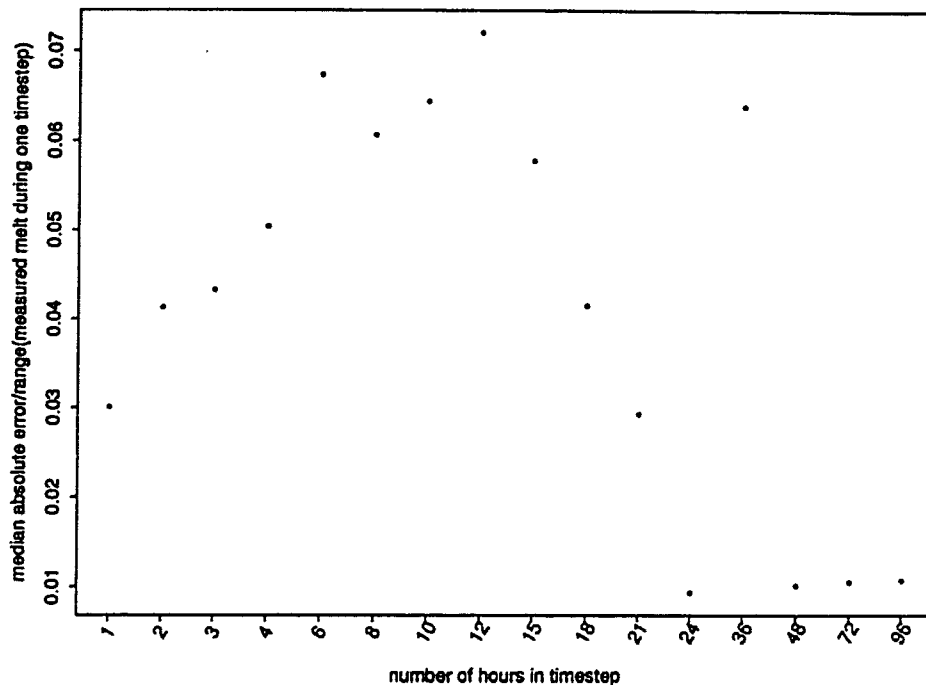


Figure 34. Sensitivity of model accuracy to timestep size.

points in the watershed that receive light early in the day will simply be warming up rather than melting. They will warm up faster than the other points in the watershed because of the sunlight, but this is not accounted for in the TopoFECS model. Later in the afternoon, after these points are in the shadows, they may start melting sooner than other points that are just coming into the bright sunlight. In this instance, the TopoFECS model would calculate melt as being negatively related to radiation. Measurements taken at any interval less than one day are susceptible to this problem. The model must aggregate all of the melt energies for an entire diurnal cycle in order to obtain robust results.

It has been suggested that perhaps the  $\alpha(t)$ ,  $\beta(t)$ , and  $\gamma(t)$  terms evolve slowly enough that the same values may be used from one time period to the next over an extended period of time. If this is true, then one needs only to sample infrequently to obtain accurate, distributed, daily melt predictions with the TopoFECS model. However, results from the UEB-generated data indicate that these parameters vary markedly from time step to time step. Figure 35 shows the values of each parameter for each 48-hour time step. If the parameters were not altered from time step to time step, the model would predict the very same melt at every time step, regardless of the weather. The primary goal of a melt model is to determine how the melt rate changes with time. Therefore, in order to meet this goal, the  $\alpha(t)$ ,  $\beta(t)$ , and  $\gamma(t)$  terms need to be recalibrated every time step. Based on findings from Figure 34, the recommended length of this time step is 24 hours in order to obtain accurate calibrations with sufficient frequency to provide input for a real-time streamflow model.

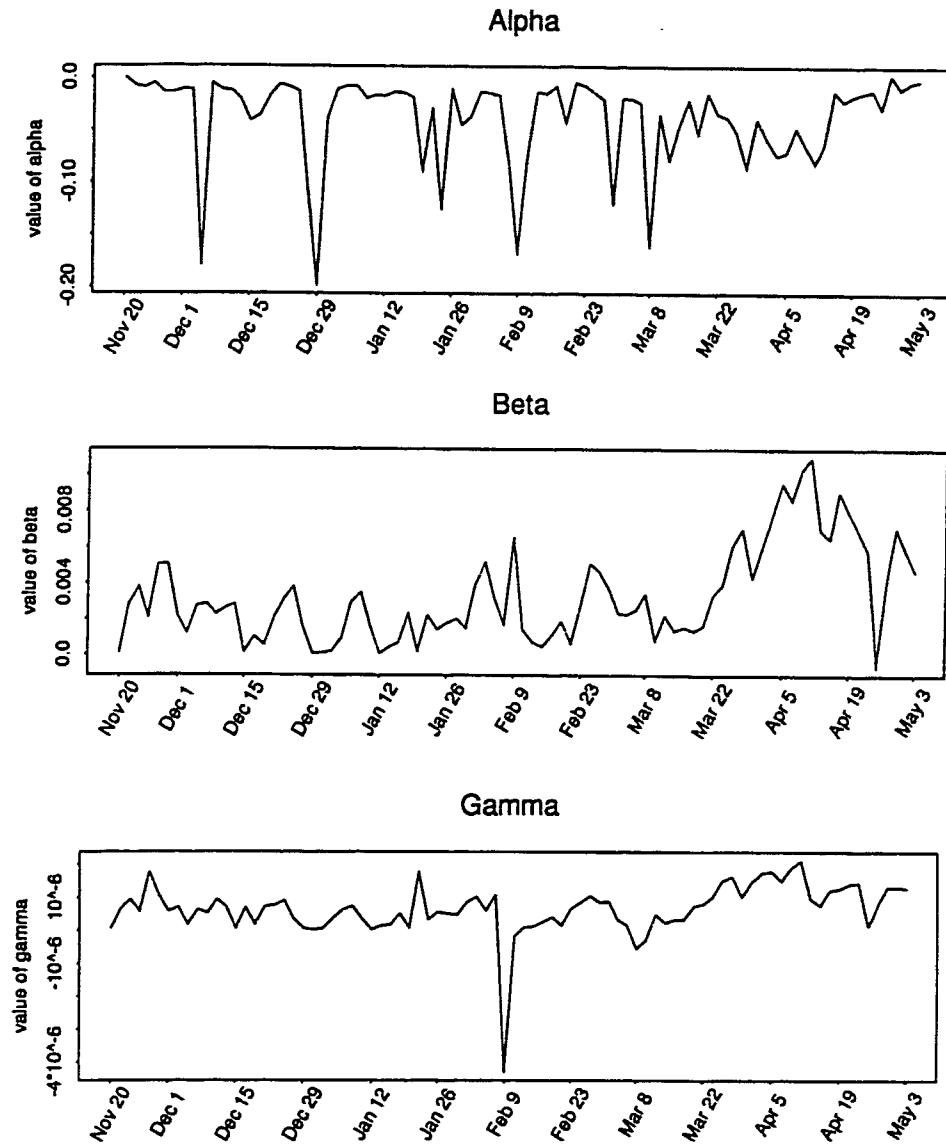


Figure 35. Evolution of  $\alpha(t)$ ,  $\beta(t)$ , and  $\gamma(t)$  parameters with time: synthetic data.

## CHAPTER V

## GUIDELINES FOR USING THE TOPOFECS MODEL

In Chapter IV, the TopoFECS model was demonstrated to be an accurate, efficient method for predicting the spatial distribution of snowmelt in high-relief, mountainous watersheds. However, before applying the model to a watershed, several questions must be considered in order to achieve reliable results. These are summarized in the following list:

1. Is a digital elevation model (DEM) available for the watershed?
2. Does the watershed have many forested areas?
3. How many index points are needed, and where should they be located?

A digital elevation model, or DEM, of the watershed is essential for the automation of the TopoFECS model. Because the model relies on topographic information (slope, aspect, and elevation) to distribute melt estimates, this must be readily available in digital form. Also, a DEM with fine resolution is preferred to one with coarser resolution, as the finer resolution would be able to distinguish smaller topographic features. However, using a DEM with finer resolution also means that it will take longer for the model to run, since there will be more points to calculate.

Forest cover plays a large role in snowmelt, since it affects all of the terms in the energy balance for snowmelt (equation 4). However, forest

cover is not yet accounted for in the TopoFECS model. In the following chapter, recommendations are made for how to deal with forest cover, but this is untested. All of the research to date has only been performed in open reaches of watersheds with no trees, and so the TopoFECS model is not recommended for use in forested areas.

As shown in the section entitled "Selection of Index Points," the locations of the index points play a large role in determining the accuracy of the model results. It was demonstrated that the use of index points with a large spread in radiation-elevation space increases the accuracy of the model estimates. Therefore, in order to select the optimal index points, the incoming radiation values midway through the melt season should be calculated for each point in the watershed, and these values should be plotted against the respective elevations of each point. The index points should be chosen from the points that fall on or near the convex hull of this scatter of points, and they should be chosen so that they encompass a maximum amount of area within this radiation-elevation space.

The section "Selection of Index Points" also shows that the number of index points used also plays an important role in the accuracy of the model results. The accuracy of the measurements will probably dictate, to a large degree, the number of index points that need to be used. With perfect measurements, only three index points are necessary, but this number grows

as the data set becomes noisier. Another factor controlling the number of index points needed for modeling larger watersheds is the characteristic scale of climatic variability in the region. This issue has not been carefully examined in this thesis, but it is one that will need to be addressed in the future if the model is to be applied to large basins. Economics is the final factor that will limit the number of index points that may be measured. Obviously, if melt collectors were extremely inexpensive, one could use hundreds of them and obtain wonderful results. However, most projects will only be able to set aside a small portion of the budget for buying, installing, and maintaining the measurement devices.

## CHAPTER VI

## SUMMARY, CONCLUSIONS, AND RECOMMENDATIONS

Summary

The snowmelt modeling literature points to the need for a model that is both simple enough to use in practical applications for melt estimations over large areas, as well as rigorous enough to capture the fundamental physics of melt and to provide spatially explicit estimations. This thesis has described the TopoFECS model, which is a new method for estimating the spatial distribution of snowmelt based on point measurements and topography. Chapter II explained how the model could be applied in a practical setting to estimate the spatial distribution of melt in a watershed. In Chapter III the model was derived from the theoretical physical equations governing snowmelt and was shown to have merit as a physically accurate model. The model was tested against three data sets in Chapter IV; a synthetically-generated data set, a noisy data set from Upper Sheep Creek, and a relatively good data set acquired from Smithfield Dry Canyon. The model performed very well with two of these three sets of data. The model's sensitivity to index point selection, weather conditions, spatial scale, and temporal scale were examined in Chapter IV. Finally, Chapter V gave explicit guidelines for applying the TopoFECS model in a practical setting.

## Conclusions

The results from Chapter IV indicate that the TopoFECS model can be an accurate, efficient way to predict the spatial distribution of snowmelt in a rugged, mountainous watershed. Because of the model's simplicity and accuracy, it could replace more traditional methods for modeling snowmelt in many applications. The advantages of the TopoFECS model include:

1. simple data requirements,
2. methodology that is easily understandable to an operator,
3. computationally efficient algorithm for rapid simulations of large basins,
4. no need for prior calibration of basin-specific parameters,
5. realistic spatial melt simulations,
6. accurate melt estimations.

Though energy balance models will always be required for some applications, there are many practical uses for the simpler TopoFECS model. Flood forecasters as well as reservoir operators, who traditionally use simpler lumped index models, would benefit from the improved accuracy over the entire range of possible weather conditions provided by a more physically realistic model. Researchers could employ the model to efficiently and accurately calculate the spatial distribution of water inputs to large watersheds. This would be useful for basin response modeling,



contaminant transport modeling, erosion modeling, etc. Developing countries with limited finances could benefit greatly from a model that required simple data, little skill from the operator, and no prior calibration of basin-specific parameters.

### Recommendations

Further research is recommended in the following areas:

1. Incorporating the effects of forest cover. The effect of forest cover is not currently accounted for in the TopoFECS model. Because forest cover has a great impact on the energy exchange processes causing melt, the model is not yet recommended for use in forested areas.

One way to incorporate forested sections of land that could be explored is the use of two sets of index points: one set of points with heavy forest cover on them, and another set of index points located in clearings. The  $\alpha(t)$ ,  $\beta(t)$ , and  $\gamma(t)$  parameters obtained from the forested points would be used to model other heavily forested parts of the watershed, while the parameters obtained from the index points located in clearings would be used to model clearings. Areas with mild to moderate forest cover would use parameters that were interpolated between the two extremes. A drawback to this approach is that it entails six unknowns to be calculated each time, rather than

three; this doubles the number of index points required. An alternative would be to extend the model to include a measure of vegetative density as a fourth predictor, in addition to elevation and radiation. These ideas need to be investigated further.

2. Using automated melt collectors. Manual collection of melt data at remote sites at a regular frequency is obviously impractical for real-time melt predictions. Therefore, the use of melt collectors should be explored to make this model feasible for practical applications. The cost, accuracy, and reliability of the automated collectors are all factors that determine whether or not they could be suitable for measuring melt at index sites for use in the TopoFECS model. Of course, it is important for the melt collectors to be on sloping sites over a range of elevations and aspects. This might create some difficulty in obtaining reliable measurements, since melt collectors are typically installed in level areas. Small plot runoff data may be easier to measure than melt data. This has infiltration losses, but may still be useful. A plastic sheet covering the ground may solve this infiltration problem. Another possible approach to measuring melt is to use sonic depth probes, installed above the surface of the snow. All of these options must be explored in order to determine the best way to collect the melt data for the TopoFECS model in a practical application.

3. Determining the spatial scale of climatic variability. In order to model a basin that is large enough to experience different weather regimes simultaneously in different regions within the basin, different values for the  $\alpha(t)$ ,  $\beta(t)$ , and  $\gamma(t)$  parameters are needed for each differing region. Therefore, the basin must be equipped with enough measurement sites to have sufficient index points to make reliable estimates of the  $\alpha(t)$ ,  $\beta(t)$ , and  $\gamma(t)$  parameters for each region. The number of measurement sites in a basin is therefore a function of the spatial scale of climatic variability of the region to be modeled. This must be determined in order to properly select the index points.
4. Determining the applicability of remotely sensed data. Though equation 18 provides a method for modeling the accumulation of snow, it is overly simplified and cannot model the erratic snowfall and drifting patterns found in complex terrain. Therefore, in order to correctly predict melt runoff from a basin, the model must, at a minimum, be supplied with current maps of snow-covered area. Otherwise, it will be susceptible to predictions of melt at locations where snow no longer remains. If available, other information such as remotely sensed maps of SWE should be incorporated into the model. This will be an area of much future research.

## REFERENCES

- Anderson, E. A. 1976. A point energy and mass balance model of a snow cover. U.S. National Oceanic and Atmospheric Administration NOAA Technical Report NWS 19. 150 p.
- Brubaker, K., A. Rango, and W. Kustas. 1996. Incorporating radiation inputs into the Snowmelt Runoff Model. *Hydrological Processes* 10:1329-1343.
- Cazorzi, F., and G. Dalla-Fontana. 1996. Snowmelt modeling by combining air temperature and a distributed radiation index. *Journal of Hydrology* 181(1-4):169-187.
- Cleveland, W. S., and S. J. Devlin. 1988. Locally weighted regression: an approach to regression analysis by local fitting. *Journal of the American Statistical Association* 83(403):596-610.
- Cline, D. W. 1997. Effect of seasonality of snow accumulation and melt on snow surface energy exchanges at a continental alpine site. *Journal of Applied Meteorology* 36(1):32-51.
- Colbeck, S. C. 1987. History of snow-cover research. *Journal of Glaciology, Special Issue* 60-65.
- Cook, R. D. 1977. Detection of influential observations in linear regression. *Technometrics* 19:15-18.
- Dennis, J. E., Gay, D. M., and Welsch, R. E. (1981). An adaptive nonlinear least-squares algorithm. *ACM Transactions on Mathematical Software* 7: 348-383.
- Dennis, J. E. and Mei, H. H. W. (1979). Two new unconstrained optimization algorithms which use function and gradient values. *Journal of Optimization Theory and Applications* 28, 453-483.
- Dingman, S. L. 1994. *Physical hydrology*. Prentice-Hall, Englewood Cliffs, New Jersey. 575 p.

- Dingman, S. L., D. Seely-Reynolds, and R.C. Reynolds III. 1988. Application of kriging to estimating mean annual precipitation in a region of orographic influence. *Water Resources Bulletin* 24:329-339.
- Dozier, J., and J. Frew. 1990. Rapid calculation of terrain parameters for radiation modeling from digital elevation data. *IEEE Transactions on Geoscience and Remote Sensing* 28(5):963-969.
- Gupta, H. V., S. Sorooshian, and P. O. Yapo. 1998. Toward improved calibration of hydrologic models: multiple and noncommensurable measures of information. *Water Resources Research* 34(4):751-763.
- Flerchinger, G. N. 1987. Simultaneous heat and water model of a snow-residue-soil system. Unpublished Ph.D dissertation. Washington State University, Pullman, Washington. 307 p.
- Jordan, R. 1991. A one-dimensional temperature model for a snow cover. Technical Documentation for SN THERM.89. U.S. Army Corps of Engineers, CRREL, Special Report 91-16. 43 p.
- Kustas, W. P., and A. Rango. 1994. A simple energy budget algorithm for the Snowmelt Runoff Model. *Water Resources Research* 30(5):1515-1527.
- Kuusisto, E. 1986. The energy balance of a melting snow cover in different environments. In E. M. Morris (Ed.). *Modeling snowmelt-induced processes*. IAHS, Wallingford, United Kingdom.
- Lowe, P. R. 1977. An approximating polynomial for the computation of saturation vapor pressure. *Journal of Applied Meteorology* 16:100-103.
- Martinec, J. and A. Rango. 1986. Parameter values for snowmelt runoff modeling. *Journal of Hydrology* 84:197-219.
- Martinec, J., A. Rango, and R. Roberts, 1994. *The Snowmelt Runoff Model (SRM) users manual*. Updated Edition 1994, Version 3.2. Department of Geography, University of Berne, Berne, Switzerland.
- McManamon, A., G. N. Day, and T. R. Carroll. 1993. Snow estimation – a GIS application for water resources forecasting, p. 856-861 in C. Y. Kuo (Ed.). *Engineering hydrology*.

- Mendenhall, W., and T. Sincich. 1992. *Statistics for engineering and the sciences*, third edition. Dellen Publishing Company, San Francisco. 963 p.
- Rango, A., and V. van Katwijk. 1990. Development and testing of a snowmelt-runoff forecasting technique. *Water Resources Bulletin* 26(1):135-144.
- Riley, J. P., D. G. Chadwick, and J. M. Bagley. 1966. Application of electronic analog computer to solution of hydrologic and river basin planning problems: Utah Simulation Model II. Utah Water Research Lab., Utah State University, PRWG32-1.
- Tarboton, D. G. 1994. Measurement and modeling of snow energy balance and sublimation from snow. *Proceedings, International Snow Science Workshop, October 31 - November 2, 1994, Snowbird, Utah.* pp. 260-279.
- Tarboton, D. G., T. G. Chowdhury, and T. H. Jackson. 1995. A spatially distributed energy balance snowmelt model. *In* K. A. Tonnessen et al. (Ed.) *Biogeochemistry of Seasonally Snow-Covered Catchments. Proceedings of a Boulder Symposium, July 3-14, IAHS Publication no. 228:141-155.*
- Tarboton, D. G. and C. H. Luce. 1996. Utah Energy Balance snow accumulation and melt model (UEB): computer model technical description and user's guide. Utah Water Research Laboratory and USDA Forest Service Intermountain Research Station, Logan, Utah. 42 p.

APPENDICES

## Appendix A

### Smithfield Dry Canyon Data

This appendix gives the raw data obtained from Smithfield Dry Canyon. Chapter 4 describes the data collection process. Each of the stakes used was marked in inches, starting from the top of the stake and continuing to the bottom. The total height from the ground to the top of each stake was recorded after the snow melted, since there was no way to tell how far into the ground the stake penetrated when the snow was still there. Table 4 gives this distance for each stake. Tables 5, 6, and 7 give the field measurements recorded on March 9, 13, and 19, respectively. These measurements include stake readings and snow tube readings which were used to determine the average SWE still remaining at each site. Though measurements were also made on many different earlier dates, significant melt did not occur until March 9, and so these three dates (representing two melt periods) are the only ones presented. One more measurement was obtained after March 19, but so few sites had snow remaining that the results were not worth showing.



Table 3. Topographic parameters for measurement sites in Smithfield Dry Canyon

Site	Slope	Aspect (from N)	Elevation	Latitude	Longitude
1	20°	295°	1646 m	41° 49.77' N	111° 47.01' W
2	30°	290°	1753 m	41° 49.91' N	111° 46.86' W
3	36°	304°	1753 m	41° 49.91' N	111° 46.86' W
4	5°	310°	1753 m	41° 49.94' N	111° 46.78' W
5	18°	0°	1753 m	41° 49.94' N	111° 46.78' W
6	16°	310°	1753 m	41° 49.94' N	111° 46.78' W
7	38°	340°	1743 m	41° 49.94' N	111° 46.78' W
8	30°	346°	1743 m	41° 49.94' N	111° 46.78' W
9	22°	300°	NA	41° 50.02' N	111° 46.62' W
10	31°	312°	1829 m	41° 50.02' N	111° 46.62' W
11	24.5°	291°	1829 m	41° 50.02' N	111° 46.62' W
12	30°	300°	1844 m	41° 50.02' N	111° 46.62' W
13	31°	276°	1852 m	41° 50.00' N	111° 46.57' W
14	19°	280°	1859 m	41° 50.00' N	111° 46.57' W
15	30°	285°	1829 m	41° 50.00' N	111° 46.57' W
16	15°	158°	1867 m	41° 50.01' N	111° 46.57' W
17	15°	178°	1867 m	41° 50.01' N	111° 46.57' W
18	6°	174°	1867 m	41° 50.01' N	111° 46.57' W
19	22°	265°	1890 m	41° 50.01' N	111° 46.57' W
20	31°	245°	1897 m	41° 50.01' N	111° 46.57' W
21	28°	218°	1958 m	41° 50.20' N	111° 46.52' W
22	26°	278°	1958 m	41° 50.20' N	111° 46.52' W
23	28°	128°	NA	NA	NA
24	16°	160°	1753 m	41° 49.94' N	111° 46.81' W
25	0°	0°	1966 m	41° 50.26' N	111° 46.47' W
26	20°	140°	1966 m	41° 50.26' N	111° 46.47' W
27	22°	298°	1966 m	41° 50.26' N	111° 46.47' W
28	26°	268°	1966 m	41° 50.26' N	111° 46.47' W
29	26°	320°	1966 m	41° 50.26' N	111° 46.47' W
30	26°	198°	2012 m	41° 50.40' N	111° 46.48' W
31	15°	164°	NA	NA	NA

Table 4. Total height (in inches) aboveground of each stake used in Smithfield Dry Canyon

Site	Stake 1	Stake 2	Stake 3
1	23	22	21
2	24	23	22.5
3	21.5	22	23
4	24	24.5	23
5	19	17	22
6	24	24	25
7	22	22	15
8	24	23	21.5
9	NA	NA	NA
10	21	23	16
11	23	19.5	20
12	22	22	20.5
13	32.5	23	20.5
14	32	21	18.5
15	30	20	22
16	20.5	21.5	32
17	32	33	33.5
18	33	32	32
19	22.5	32	20
20	28.5	33.5	27
21	30	32.5	22
22	32.5	31	21.5
23	NA	NA	NA
24	45.5	45	42
25	45.5	45.5	45.5
26	44.5	46.5	45
27	45	48	44
28	44	45	41
29	45.5	44.5	45
30	45.5	44	45.5
31	NA	NA	NA

Table 5. Measured distance between tops of stakes and snow surface, and snow tube measurements for density calculations: Smithfield Dry Canyon, March 9, 1997

Site	1st Tube		2nd Tube		Stake Depth 1 (inches)	Stake Depth 2 (inches)	Stake Depth 3 (inches)
	1st Tube Depth (inches)	Weight (inches of SWE)	2nd Tube Depth (inches)	Weight (inches of SWE)			
1	15	5.9	14	4.8	13	8	8.5
2	9	3.1	NA	NA	16	15.5	11
3	8	2.5	12	4.8	9	11	10
4	13.7	4.7	13.5	4.7	NA	10	10.5
5	13	3.7	NA	NA	3	1.8	6.8
6	12	4.7	NA	NA	11	10.6	10
7	15	3.5	16	4.7	4	5	covered
8	19.5	5.5	NA	NA	6	1.5	1
9	19	5.2	NA	NA	6	1.25	9.7
10	16.3	4.4	NA	NA	5.2	9.5	covered
11	14	4.2	NA	NA	9	5.6	3.25
12	15	4.5	NA	NA	2.5	3.5	0.75
13	15	4.2	NA	NA	18.5	10	6
14	15	3.8	15	4.5	18	3.25	8
15	13.5	3.5	NA	NA	19	9	NA
16	23	6.8	NA	NA	3	2.5	10.5
17	21	6.6	NA	NA	9	10	14
18	19.5	5.7	NA	NA	15	10	11
19	9	3.2	12	3.7	9	19	8
20	10	3.4	10	3.2	18	22	17
21	11	3.6	16	5.3	17.5	15	6
22	25	8.1	23	7.6	7.5	6	covered
23	12	3.3	12	3.6	10	9.5	11.5
24	NA	NA	NA	NA	NA	NA	NA
25	31	11	31	11.2	15	15.5	13
26	20	7	21	7	24.5	24	25
27	24	7.3	21	6.6	22.5	28	19.5
28	26	7.6	21	7.4	23.2	21.5	18
29	27	7.6	28	7.7	17	18	20.5
30	22	7.1	19.5	7	24	24	24
31	15	4.6	15	5.2	10	10.5	10

Table 6. Measured distance between tops of stakes and snow surface, and snow tube measurements for density calculations: Smithfield Dry Canyon, March 13, 1997

Site	1st Tube		2nd Tube		Stake Depth 1 (inches)	Stake Depth 2 (inches)	Stake Depth 3 (inches)
	1st Tube Depth (inches)	Weight (inches of SWE)	2nd Tube Depth (inches)	Weight (inches of SWE)			
1	7	2.5	8	3.5	NA	16	15.5
2	5	2	6	2.2	NA	NA	16.5
3	6	2.2	6	2.5	16	16.25	14
4	7	3	9	2.7	18	12	17.5
5	10.5	3.7	12	4.3	7.5	6.7	11.5
6	9	3.6	9	3.3	16	16.5	16
7	13	3.8	10	3.2	9	10	4.5
8	19	5.2	15	5	10.5	6.5	6
9	11	3.5	14	3.6	12.8	14.7	15.2
10	9	3.8	9.5	3.5	10.5	15	5
11	7	2.8	8	2.7	15.75	11.75	9.8
12	12	4.4	12	4.1	8.5	10.3	8
13	9	3	10	2.6	25	17	12
14	8	2	6	1.7	24	15.5	10
15	NA	NA	NA	NA	26.5	16.5	NA
16	13	5.2	14.5	5	12.5	12	18.2
17	13	4.7	13	4.7	18.5	17	22.8
18	16	6.2	15	5.4	21.8	17	18.75
19	NA	NA	NA	NA	27	18	15.5
20	NA	NA	NA	NA	NA	32	26
21	8	3.2	8	3	26.5	24	15
22	17	5.6	16	5.4	14.5	12.7	5
25	28	10.4	27	9	22	21.8	20
26	14	4.8	15	5.2	31.7	32.7	33
27	16.5	4.1	15	5.5	28.7	33.3	25.5
28	15	6.6	16	6.3	29.5	28	26
29	23	7.3	20	6.5	22	23.2	26
30	17	6.1	13	4.1	32	32	32

Table 7. Measured distance between tops of stakes and snow surface, and snow tube measurements for density calculations: Smithfield Dry Canyon, March 19, 1997

Site	1st Tube		2nd Tube		Stake Depth 1 (inches)	Stake Depth 2 (inches)	Stake Depth 3 (inches)
	1st Tube Depth (inches)	Weight (inches of SWE)	2nd Tube Depth (inches)	Weight (inches of SWE)			
1	NA	NA	NA	NA	NA	22+/-2	20+/-2
5	8	2.6	5	2.2	13	11	15.5
7	6	2.6	5	2.3	14.3	16.5	10
8	12	4.7	12	4.5	14	11	10.5
9	8	3	7.5	3.1	NA	19.5	21
10	6	2.3	8	2.7	15.5	NA	10
11	NA	NA	NA	NA	NA	18	15.3
12	7	2.6	7	2.9	13.2	15.5	13
16	9	3.6	7	3	NA	NA	24
17	9	3.6	7	3	26	23	NA
18	9	3.6	7	3	28	24	27
25	22	9.2	22	9.4	27	27.2	26
26	6	2.7	7	3.1	39	40	40
27	13	4.9	13	5.3	32	38	30.5
28	13.5	5.5	12.5	5.1	33.6	22.6	NA
29	18	7.2	16	6.4	25.7	27.5	29
30	11	4	10	4.3	38	37	38

## Appendix B

## Upper Sheep Creek Data

Table 8. Gridded values of snow water equivalence (in inches),  
measured at Upper Sheep Creek on March 25, 1986

	A	B	C	D	E	F	G	H	I	J	K	L	M	N	O
1					0	0	0								
2			0	0	0	0	3	0.8							
3			0	0	0	0	4	6							
4		0	0	0	0	0	0	4							
5		0	0	0	0	0	0	4	17	0					
6			0	0	0	0	3.2	0	24	7	1.5	0			
7			0	0	0	0	0	1.5	1.2	29	27	0	0		
8			0	0	0	0	0	2.5	3	1.7	8.7	31	0		
9				0	0	0	0	2.5	1.5	0	6	31	0	0	
10				0	0	0	0	0.5	2	0	4.2	41	0	0	
11				0	0	0	0	1	0	1.5	2.5	49	0	0	
12			0	0	0	0	0	0	7.2	0	3	57	0	0	
13			0	0	0	0	0	0	2.2	1.7	5.5	37	4	0	
14			0	0	0	0	0	0	4.7	4	9.7	24	0	0	
15		0	0	0	0	0	0	0	12	6.5	14	17	0	0	
16			0	0	0	0	0	6.2	5.2	3	67	11	0	0	
17			0	0	0	0	0	1.5	1.5	3	53	0	0		
18			0	0	0	0	17	0	0	0	48	0			
19			0	0	0	0	29	9.5	0	0	2				
20			0	0	0	0	17	13	0	0	0				
21			0	0	0	0	28	29	0	0	0				
22			0	0	0	0	11	59	16	0	0				
23			0	0	0	0	2.7	35	75	4.2	0				
24				0	0	0	0	6.5	36	65	0				
25				0	0	0	0	1.5	17	69	0				
26						0	0	0	13	49	0				
27							0	0	8.5	79	0	0			
28									2.5	63	26	0			

Table 9. Gridded values of snow water equivalence (in inches),  
measured at Upper Sheep Creek on April 9, 1986

	A	B	C	D	E	F	G	H	I	J	K	L	M	N	O
1					0	0	0								
2			0	0	0	0	0	0							
3			0	0	0	0	0	0							
4		0	0	0	0	0	0	0							
5		0	0	0	0	0	0	0	5.2	0					
6			0	0	0	0	0	0	13	0	0	0			
7			0	0	0	0	0	0	0	0	13	0	0		
8			0	0	0	0	0	0	0	0	0	22	0		
9				0	0	0	0	0	0	0	0	17	0	0	
10				0	0	0	0	0	0	0	0	33	0	0	
11				0	0	0	0	0	0	0	0	42	0	0	
12			0	0	0	0	0	0	0	0	0	51	0	0	
13			0	0	0	0	0	0	0	0	0	27	0	0	
14			0	0	0	0	0	0	0	0	4	15	0	0	
15		0	0	0	0	0	0	0	0	0	5.7	7.5	0	0	
16			0	0	0	0	0	0	0	0	36	3.5	0	0	
17			0	0	0	0	0	0	0	0	47	0	0		
18			0	0	0	0	6.2	0	0	0	37	0			
19			0	0	0	0	23	0	0	0	0				
20			0	0	0	0	7.7	5.2	0	0	0				
21			0	0	0	0	25	24	0	0	0				
22			0	0	0	0	3	31	3	0	0				
23			0	0	0	0	0	33	63	0	0				
24				0	0	0	0	0	29	61	0				
25				0	0	0	0	0	11	64	0				
26					0	0	0	9.2	43	0					
27						0	0	0	73	0	0				
28							0	0	73	14	0				

Table 10. Gridded values of melt (in inches), occurring between March 25 and April 9, 1986, calculated by subtracting SWE measured on April 9 from SWE measured on March 25

	A	B	C	D	E	F	G	H	I	J	K	L	M	N	O
1					0	0	0								
2			0	0	0	0	3	0.8							
3			0	0	0	0	4	6							
4		0	0	0	0	0	0	4							
5		0	0	0	0	0	0	4	12	0					
6			0	0	0	0	3.2	0	11	7	1.5	0			
7			0	0	0	0	0	1.5	1.2	29	14	0	0		
8			0	0	0	0	0	2.5	3	1.7	8.7	9.2	0		
9				0	0	0	0	2.5	1.5	0	6	14	0	0	
10				0	0	0	0	0.5	2	0	4.2	8.3	0	0	
11				0	0	0	0	1	0	1.5	2.5	7.1	0	0	
12			0	0	0	0	0	0	7.2	0	3	5.4	0	0	
13			0	0	0	0	0	0	2.2	1.7	5.5	9.3	4	0	
14			0	0	0	0	0	0	4.7	4	5.7	8.5	0	0	
15		0	0	0	0	0	0	0	12	6.5	7.8	9.5	0	0	
16			0	0	0	0	0	6.2	5.2	3	31	7	0	0	
17			0	0	0	0	0	1.5	1.5	3	6.5	0	0		
18			0	0	0	0	10	0	0	0	11	0			
19			0	0	0	0	6.2	9.5	0	0	2				
20			0	0	0	0	8.8	7.3	0	0	0				
21			0	0	0	0	3.2	5	0	0	0				
22			0	0	0	0	8	28	13	0	0				
23			0	0	0	0	2.7	2.2	13	4.2	0				
24				0	0	0	0	6.5	6.5	4.2	0				
25				0	0	0	0	1.5	6	4.7	0				
26					0	0	0	0	3.8	5.7	0				
27						0	0	0	8.5	5.2	0	0			
28									2.5	-9.9	12	0			



Table 11. Gridded values of snow water equivalence (in inches),  
measured at Upper Sheep Creek on April 30, 1993

	A	B	C	D	E	F	G	H	I	J	K	L	M	N	O
1					0	7.3	0								
2			0	0	0	0	0	2.9							
3			0	0	0	5.4	0	0							
4		0	0	0	0	0	0	0							
5		0	0	0	0	0	0	0	0	0					
6			0	0	0	0	0	0	0	3.7	0	0			
7			0	0	0	0	0	0	0	0	13	4.9	0		
8			0	0	0	0	0	0	0	0	0	5	0		
9				0	0	0	0	0	0	0	0	17	0	0	
10				0	0	0	0	0	0	0	0	0	0	0	
11				0	0	0	0	0	0	0	0	63	0	0	
12			0	0	0	0	0	0	0	0	21	24	0	0	
13			0	0	0	0	0	0	0	0	33	14	0	0	
14			0	0	0	0	0	0	6.5	0	8	5	0	0	
15		0	0	0	0	0	0	0	1.7	2.5	74	3.7	0	0	
16			0	0	0	0	0	0	13	16	53	0	0	0	
17			0	0	0	0	16	11	11	0	34	0	0		
18			0	0	0	0	23	18	0	0	0	0			
19			0	0	0	0	13	21	0	0	0				
20			0	0	0	0	26	26	11	0	0				
21			0	0	0	0	33	50	24	0	0				
22			0	0	0	0	4.7	20	59	0	0				
23			0	0	0	0	0	14	18	40	0				
24				0	0	0	0	0	18	74	0				
25				0	0	0	0	0	25	76	0				
26					0	0	0	0	5.7	98	0				
27						0	0	0	0	57	20	0			
28								0	0	12	99	0			

Table 12. Gridded values of snow water equivalence (in inches),  
measured at Upper Sheep Creek on May 13, 1993

	A	B	C	D	E	F	G	H	I	J	K	L	M	N	O
1					0	0	0								
2			0	0	0	0	0	0							
3			0	0	0	0	0	0							
4		0	0	0	0	0	0	0							
5		0	0	0	0	0	0	0	0	0					
6			0	0	0	0	0	0	0	0	0	0			
7			0	0	0	0	0	0	0	0	0	0	0		
8			0	0	0	0	0	0	0	0	0	0	0		
9				0	0	0	0	0	0	0	0	0	0	0	
10				0	0	0	0	0	0	0	0	0	0	0	
11				0	0	0	0	0	0	0	0	44	0	0	
12			0	0	0	0	0	0	0	0	8.7	5	0	0	
13			0	0	0	0	0	0	0	0	21	0	0	0	
14			0	0	0	0	0	0	0	0	0	0	0	0	
15		0	0	0	0	0	0	0	0	0	63	0	0	0	
16			0	0	0	0	0	0	0	0	42	0	0	0	
17			0	0	0	0	0	0	0	0	20	0	0		
18			0	0	0	0	11	3.2	0	0	0	0			
19			0	0	0	0	0	7	0	0	0				
20			0	0	0	0	17	47	0	0	0				
21			0	0	0	0	18	41	5	0	0				
22			0	0	0	0	0	14	47	0	0				
23			0	0	0	0	0	1	8.2	34	0				
24				0	0	0	0	0	8	57	0				
25				0	0	0	0	0	12	60	0				
26					0	0	0	0	0	82	0				
27						0	0	0	0	48	31	0			
28							0	0	0	2	0.6	0			

Table 13. Gridded values of melt (in inches) occurring between April 30 and May 13, 1993, calculated by subtracting SWE measured on May 13 from SWE measured on April 30

	A	B	C	D	E	F	G	H	I	J	K	L	M	N	O
1					0	7.3	0								
2			0	0	0	0	0	2.9							
3			0	0	0	5.4	0	0							
4		0	0	0	0	0	0	0							
5		0	0	0	0	0	0	0	0	0					
6			0	0	0	0	0	0	0	3.7	0	0			
7			0	0	0	0	0	0	0	0	13	4.9	0		
8			0	0	0	0	0	0	0	0	0	5	0		
9				0	0	0	0	0	0	0	0	17	0	0	
10				0	0	0	0	0	0	0	0	0	0	0	
11				0	0	0	0	0	0	0	0	20	0	0	
12			0	0	0	0	0	0	0	0	12	19	0	0	
13			0	0	0	0	0	0	0	0	13	14	0	0	
14			0	0	0	0	0	0	6.5	0	8	5	0	0	
15		0	0	0	0	0	0	0	1.7	2.5	11	3.7	0	0	
16			0	0	0	0	0	0	13	16	12	0	0	0	
17			0	0	0	0	16	11	11	0	15	0	0		
18			0	0	0	0	12	14	0	0	0	0			
19			0	0	0	0	13	14	0	0	0				
20			0	0	0	0	9	-21	11	0	0				
21			0	0	0	0	15	8.6	19	0	0				
22			0	0	0	0	4.7	5.5	12	0	0				
23			0	0	0	0	0	13	9.8	5.8	0				
24				0	0	0	0	0	10	17	0				
25				0	0	0	0	0	13	16	0				
26					0	0	0	0	5.7	15	0				
27							0	0	0	9	-11	0			
28									0	9.7	98	0			